AIRFLOW LIMITATION IN CROUP

BY
M. L. JAROSLAWSKI

Thesis prepared in partial fulfillment of the requirements for the degree of Msc in Biomedical Engineering

I, the undersigned, hereby declare that the work contained in this thesis, is my own original work, and has not previously in its entirety, or part, been submitted at any university for a degree

..... Date.....

Acknowledgments

I wish to thank Dr. W. Capper for his invaluable advice and enthusiasm in the supervision of this thesis. Equally, I stress my thanks to Dr. A. Argent for not only supervisory work but also for allowing me to use the data which he collected over many years.

I also would like to thank Dr. B. Van Geems and Professor L. Adams for their involvement in developing techniques for analysing videos made during laryngoscopic procedures. I also greatly appreciate the assistance of Dr. D. Wensley who helped me with clinical aspects during the absence of Dr Argent.

Synopsis

This thesis investigates a mechanism for air flow limitation in children with croup. Croup is a common condition affecting many young children. Infection (usually viral) causes swelling of the mucosa in the subglottic region of the airway with consequent narrowing of the airway. Although researchers have investigated croup for the past sixty years, there is still very little information available on how croup affects air flow dynamics. The current theory assumes that the stenosis formed by croup in the subglottis of infants leads to a dynamic collapse of the extrathoracic trachea (Chernick, 1990). According to this literature, the dynamic collapse of the extrathoracic trachea will limit the inspiratory flow. It was believed that in severe cases of croup, the dynamic collapse may even temporarily block the airways.

In order to investigate the mechanism for air flow limitation in croup the author used the intrathoracic pressure - flow traces from twenty patients with croup, four patients who had been intubated for croup and five normal subjects. Laryngeal X-rays from another twenty patients with croup were analysed as well as five videos, made during laryngoscopy, of the subglottic cross sectional area of an additional five patients with croup requiring intubation. All data used in this project was collected by an experienced paediatrician from the Red Cross War Memorial Children's Hospital who is also the supervisor of this thesis.

Both the video and the X-ray data showed that the dynamic collapse of the trachea contributes much less to airflow obstruction than the subglottic swelling itself. The hypothesis investigated in this thesis is that air flow becomes restricted due to wave speed limitation. According to the theory of wave speed limitation, an increase in driving pressure (the intrathoracic pressure) does not increase the flow

if the speed of the air particles exceeds the wave speed. In our case the wave speed is the speed of sound within the lumen of the compliant, narrowed airway. In order to test that theory, it was necessary to obtain the flow, the driving pressure in the subglottis and the cross sectional area of the subglottis of patients with croup. Unfortunately, the measurement of subglottal cross sectional areas from videos made during laryngoscopies, proved to be impossible due to both ethical and practical constraints. The measurement of the subglottal cross sectional areas from X-rays was also difficult in practice. Therefore, the cross sectional area is calculated. The general orifice equation is modified in order to calculate the subglottal cross sectional areas in patients with croup.

Two methods are used to test the hypothesis of wave speed limitation:

i) *The wave speed limitation formula.* The wave speed limitation formula directly calculates the maximum flow from the pressure - flow data. Hereafter the calculated maximum flow is compared with the measured flow.

ii) *A lumped component model.* A non linear, lumped component model has been used to calculate the flow from the driving pressure (intrathoracic pressure). Flow is not limited in this model and an increase in driving pressure will result in a corresponding increase in flow. The flow which is calculated using this model has also been compared to the measured flow.

It was found that, in children with croup, there is a good correlation ($r=0.82$) between calculated and measured values of maximum flow using the wave speed limitation model. The slope of the linear fit using a least square's approximation is 0.98 and this linear relationship is valid for a 0.05 level of significance for Conover's nonparametric test (Daniel and Terrell, 1989).

The lumped component model was able to fit the inspiratory flow data with a small sum of square error in the case of both normal ($(7.56 \pm 0.86) \cdot 10^{-9} (\text{ml} / \text{s})^2$) and intubated patients ($(3.2 \pm 0.75) \cdot 10^{-9} (\text{ml} / \text{s})^2$). However, the error rose dramatically in patients with croup ($(2.04 \pm 0.5) \cdot 10^{-8} (\text{ml} / \text{s})^2$) thus indicating that the lumped component model is no longer valid in these patients.

It is concluded that the measured flow velocities in patients with croup approach the calculated velocity of sound in the region of the subglottic swelling, and that the wave speed theory accurately describes the flow limitation. Further support of this is the fact that the lumped component model, which does not incorporate a flow limiting mechanism, breaks down in patients with croup.

Table of contents

Glossary

A	general cross sectional area
Ao	cross sectional area of the constriction
Ag	subglottal/glottal cross sectional area
AC	alternating pressure or flow
β	damping constant
Baseline	line which indicates reference point - either a zero flow or the ambient pressure
c, Vp	sonic speed
C	general compliance
Cw	wall compliance
Cd	discharge coefficient of an orifice
D	diameter of a tube/airway
DC	steady pressure or flow
Δ	in front of a variable it indicates large changes
d	in front of a variable it indicates infinitesimal changes
E	Young's Modulus
Effort dependence (negative)	decrease in flow beyond the flow limitation point
Effort dependence (positive)	increase in flow beyond the flow limitation point
Endotracheal tube	In infants this tube is about 7 mm^2 in cross sectional area and is of varying length (typically 12 cm). It is inserted into the subglottis and often down to the trachea in order to open occluded airways

Intubation	insertion of an endotracheal tube into subglottis
Isentropic	process which is reversible and adiabatic (if adiabatic processes are considered)
k	ratio of specific heats
Kl	laminar flow constant
Kt	turbulent flow constant
l	length of tube/airway
L	general inertance
Lw	wall inertance
M	Mach number
$\mathbf{N_R}$	Reynolds number
P	transmural pressure
Pc, Pe	recoil pressure
Pca	kinetic pressure
Pd	driving pressure
Pg	static/lateral subglottic pressure
Pl	static/lateral pressure
$\mathbf{P_P}$	pressure to overcome the resistance to gas flow
Po, Pt	general total pressure
$\mathbf{P_T}$	intrathoracic pressure
$\mathbf{P_V}$	pressure to overcome the frictional resistance caused by a movement of tissues
ρ	density of fluid/gas
r	radius of a circular tube/airway
R	general resistance
Ra	resistance to airflow
Rb	coefficient of inertial pressure losses

Subglottal losses	pressure losses in the subglottis
t	wall thickness
T	sampling interval
μ	viscosity of fluid/gas
v	anterior posterior length of the airway
V,v	speed of the fluid
$\dot{\mathbf{V}}$, $\dot{\mathbf{V}}_{\mathbf{max}}$	fluid/gas flow (subscript max indicates maximum)
ω	resonant angular frequency
W	width of the airway in the transverse view
∇	vector differential operator. It is defined as $\mathbf{i}\frac{\partial}{\partial x}+\mathbf{j}\frac{\partial}{\partial y}+\mathbf{k}\frac{\partial}{\partial z}$ where **i**, **j** and **k** are unit vectors in three dimensional coordinate system

List of figures

List of tables

1. Introduction

The viral infection which causes croup (see definition of croup in section 2.1) produces swelling of the subglottic mucosa and hence it leads to obstruction to air flow through the upper airways. The ring formed by the signet shaped cricoid cartilage around the subglottis (see description of anatomy in section 2.1.1) prevents outward expansion of the airway and thus the swelling compresses the airway lumen. Ventilation becomes more difficult because of increased subglottal pressure losses. As high-velocity air particles pass through the region, stridor appears. Initially stridor is low pitched, loud and inspiratory. However, as the obstruction progresses, the stridor becomes softer, higher pitched and extends into exhalation. With severe obstruction wheezing and coughing appear (Chernick, 1990).

Patients with croup attempt to maintain sufficient flow by increasing intrathoracic pressure change. Further narrowing of the subglottis during the inspiratory cycle may cause a saturation phenomenon, in which further lowering of the downstream pressure does not increase the flow. In severe croup it may become impossible for the patient to maintain flow through the high resistance portion by increasing driving force further. This flow limiting mechanism during inspiration is not understood and requires further investigation. The literature does not describe the flow limitation in croup but it refers mainly to the flow limitation in the intrathoracic airways during expiration (Dawson and Elliot, 1977); (Hyatt, 1983); (Bertram and Raymond, 1991). Here, airways are collapsible during expiratory manoeuvers. The subglottis on the other hand is fully bounded by the cricoid cartilage which resists collapse during inspiratory manoeuvers. Although there might be a difference between the causes of flow limitation during expiration and

inspiration, the basic mechanism of flow limitation should be the same. Two causes of flow limitation have been reported in the literature:

- flow limitation caused by wave speed and

- flow limitation caused by viscosity.

In this thesis, two further possibilities are considered, the first being that the flow could be limited by the simultaneous effect of both wave speed and viscosity (see Appendix E), and the second that flow may be attenuated rather than limited. The second possibility was investigated using a lumped component model.

For the flow to be limited by the wave speed the airway must be compliant (Section 2.2.5 (a)). This may seem to be contradictory to the fact that the area of subglottic swelling is surrounded by a cartilage which has a very limited radial movement. However, tissue lining the airway lumen in the subglottis has its own compliance which may influence the inward and outward movement of the wall tissue, subject to pressure changes inside the subglottis. The fact that the medical practitioner is able to insert an endotracheal tube, whose cross sectional area is greater than the cross sectional area of the subglottis in patients with croup, suggests that the compliance of the tissue lining the subglottis is significant. In addition, Duncan (1978) found that there was a significant improvement in the condition of children with croup when density of air was lowered using helium-oxygen mixture. This suggests that if there is a flow limitation in croup then it is likely to be caused by wave speed and not viscosity.

The author was able to analyse measurements of the flow and the intrathoracic pressure in twenty children with croup. In addition laryngeal X-rays were also

available in a separate group of another twenty children with croup. Videos were made during laryngoscopies on five patients. All measurements were performed by an experienced paediatrician, who is also the project supervisor, as part of a study approved by the University of Cape Town Ethics and Research Committee.

Unfortunately, measurements of the subglottal cross sectional areas in children with croup proved to be ethically and practically difficult because the patients are not adults but infants whose subglottic apertures are very small. In healthy infants the cross sectional dimensions in the subglottis are on average 7 mm in the anterior-posterior direction and 4 mm in width (Wolfsdorf and Swift, 1978). Therefore, the increase in the thickness of mucous membrane that occurs in croup causes a significant area reduction which is life threatening for the child with croup. This means that the time available for measurements is very limited.
In this study pressure and flow data collected from patients with croup have been used to calculate, from the orifice formula, the cross sectional area of the subglottic swelling (see Chapter 4). In another approach X-rays of the subglottic region of patients with croup were used to calculate the cross sectional area of the subglottic swelling, assuming that the geometry of the airways under investigation is elliptical.

The thesis investigates the hypothesis that inspiratory airflow obstruction in patients with severe croup is caused by wave speed limitation and that this limitation occurs at the swollen subglottic region.

2. Literature review

The anatomical structures affected by croup and the pathologic condition itself are described first. Next, the basic aspects of airflow are investigated followed by a description of flow limitation. Finally, lumped component models of the airways are described.

2.1 Croup

Viral croup is a common illness affecting the airway in children and a common cause of upper airway obstruction in children (Fried, 1996).
In this case the laryngeal mucosa becomes swollen (Rabe, 1941). This leads to airway obstruction which may be lethal when the diameter of the airway is small, such as in the subglottic area of infants. It is not the infection which is life threatening but the location of the disease in the airways. In our case the location is in the subglottic region of an infant's larynx.

The incidence of viral croup over all ages has been estimated at 1% to 2% per year. Boys are affected more commonly than girls, in a ratio 2:1. The majority of patients are between the ages of six months and four years (Fried, 1996). Older children and even adults are not immune to croup but because these patients have larger airways the effect of croup on these patients is seldom life threatening.

In the following subsection the anatomical structures of the larynx are described and the effect which some of these structures may have on the flow dynamics in a child with croup are discussed. A brief paragraph on croup diagnosis is also

included. However, the reader must note that the methods of croup diagnosis introduced in this project are those practiced at the Red Cross War Memorial Children's Hospital in Cape Town, South Africa.

2.1.1 Anatomy of the larynx

The larynx is situated below the oropharynx and above the trachea. The primary function of the larynx is to separate the respiratory tract from the alimentary tract and the adaptation of the larynx for phonation is a secondary feature (Hall-Craggs, 1990). The larynx consists of a skeleton of cartilages and membranes lined by mucosa. There is also an important group of muscles in the larynx which control the processes of respiration and phonation. The skeleton of the larynx has been well investigated using cadavers. The architecture of the laryngeal skeleton provides important information from which the behaviour of flow and pressure in the larynx of a living person can be calculated. This is used in various models to simulate the action of the larynx (Rosler and Strube, 1989); (Van Den Berg et al 1957). Figure 2.1 shows the exploded view of the laryngeal cartilages, while figure 2.2 shows a coronal section through the larynx.

A word of caution should be said about figure 2.2. The anatomy of the larynx in infants differs from that of adults (Chernick, 1990) and it will not be as developed as the larynx presented in the anatomy textbooks. Generally, the larynx of the infant is situated high in the neck and the epiglottis is narrow. In addition the infant's larynx is funnel shaped as compared to the adult's cylindrical larynx (figure 2.3).

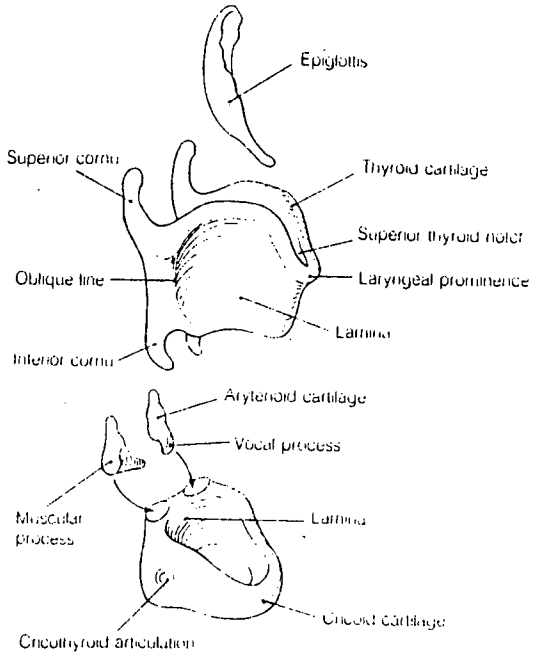

Figure 2.1 The laryngeal cartilages separated from each other (Hall-Craggs, 1990)

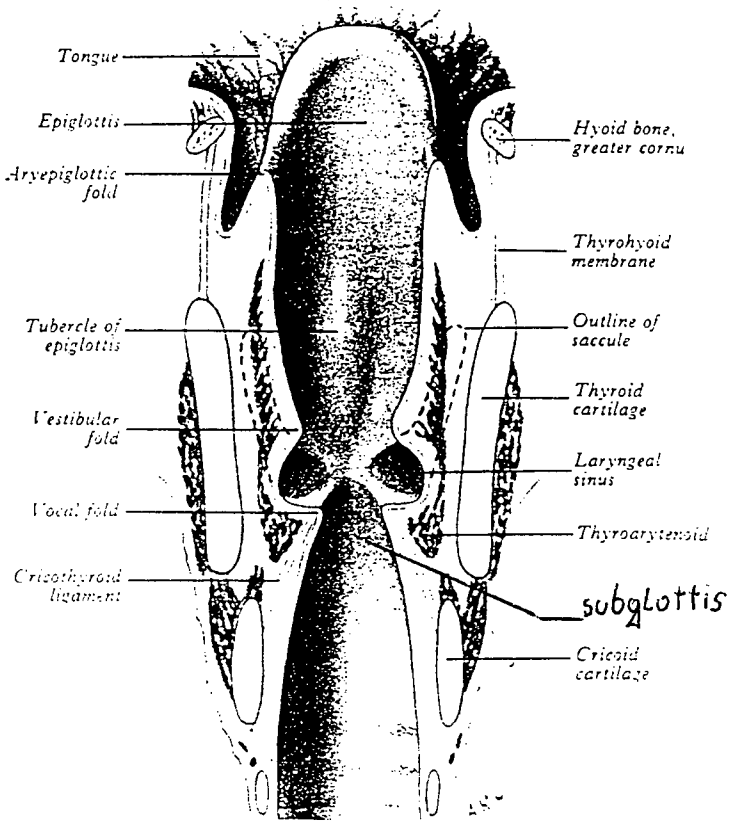

Figure 2.2 A coronal section through the larynx (Warwick and Williams, 1973). The subglottic region is surrounded by the cricoid cartilage.

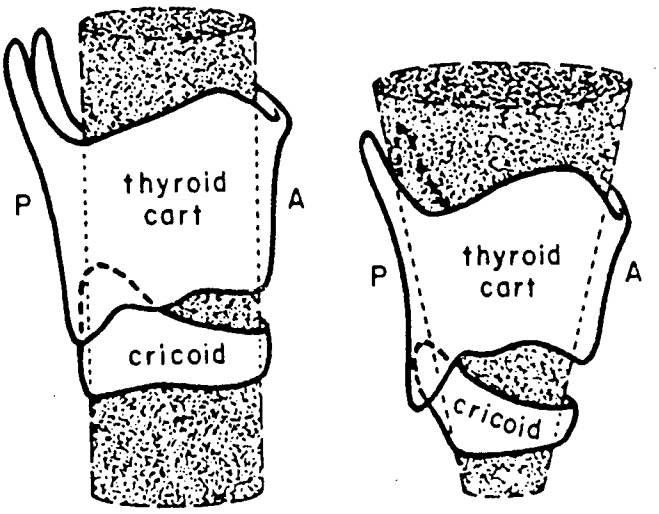

Figure 2.3 The adult's cylindrical larynx (left hand graph) and the infant's funnel shaped larynx (right hand graph) (Warwick and Williams, 1973).

However, the most important feature is the size of the airways. The subglottis is the narrowest airway segment of an infant while the vocal cords are the narrowest airway section of an adult (Chernick, 1990). Benjamin (1990) clearly shows that the opening of the vocal cords in an adult is much wider than the opening of the subglottis in an infant. The typical aperture of a healthy infant's larynx is 7 mm in the anterior posterior direction and 4 mm in width (Wolfsdorf and Swift, 1978). The author stresses again that the size of the airways is a feature which distinguishes the upper airways of a very young child from those of an older child or an adult and this feature renders the infant at special risk for the development of life threatening upper airway obstruction.

2.1.2 Pathology

Pathologically, croup forms a swelling of the mucosa and submucosa of the subglottis situated below the vocal cords. At the vocal fold the submucosa of infants and adults is thin, thus this region has little chance for swelling. The subglottis on the other hand has a well defined submucosa (Warwick and Williams, 1973) and significant swelling may occur. In infants with croup, the submucosa in the subglottic area is loosely attached to the mucous membrane which may lead to the accumulation of fluid (Chernick, 1990). Local cellular defenses become impaired and inflammatory cell infiltration follows. Thick secretion may further compromise the airway. As the illness progresses mucus plugging of the airway and the swelling of the tissue lining the subglottic lumen will further obstruct the airway, and abnormalities of gas exchange may develop (Fried, 1996). Since the infants' subglottis is very small, the secretion of mucus as well as the swelling of the submucosa place these patients at much greater risk than it would in older individuals.

2.1.3 Diagnosis

The flow obstruction during the initial stages of viral croup is most significant during inspiration but as the disease progresses expiratory flow is also obstructed. According to the Red Cross War Memorial Children's Hospital, the usual method to diagnose croup is by observing certain clinical signs. Initially, a patient has a runny nose, a red throat and produces a barking cough. Eventually the stridor develops. Typically, the stridor softens as the obstruction becomes more severe. In the case of extreme obstruction a soft expiratory wheeze may replace the inspiratory stridor.

2.1.4 Mechanics of croup

The primary difficulty in analysing the effect of croup in an infant's larynx is the size of the airways. It is impossible to introduce a transducer into the subglottic area to measure the pressure without interfering with the airflow. Although optical technology is gradually emerging (Goodyer et al, 1996), the smallest pressure transducers would produce significant obstruction.

Chernick (1990) believes that the increased resistance due to croup in the subglottis results in a dynamic collapse of the extrathoracic trachea. Figure 2.4 illustrates this theory by showing that the subglottal obstruction causes a dramatic pressure drop across this obstruction during inspiration. Since the region just downstream from the obstruction is surrounded by the same pressure as the region upstream, the membranous walls of the extrathoracic trachea collapse, resulting in what is known as dynamic collapse.

Patients with croup who are in demand of more air will produce a greater negative intrapleural pressure. This increases the flow which, according to the Bernoulli principle, results in a larger pressure drop across the obstruction, further reducing its cross sectional area by dynamic collapse. Therefore, the child will show positive feedback where the increased airflow increases the dynamic collapse. At the same time, the reduction of the cross sectional area of the airway by the dynamic collapse, forces the patient to increase the driving pressure in order to increase the airflow.

During expiration the positive pressure created below the obstruction will assist in ventilation because these airways will now expand radially outwards. In this case there will not be a dynamic collapse in the extrathoracic trachea (Chernick, 1990).

Researchers (Chernick, 1990; Wood et al, 1976; Peslin and Fredberg, 1986; Duncan, 1978) believe that the airflow through the upper airways is turbulent. According to Chernick the obstruction of the glottis and the subglottic area results in flow with increased turbulence. This has an important consequence because the increased turbulence due to the obstruction characterises the effect of the orifice. Duncan in his study with Helium shows that the condition of patients with croup improves with decreased air density.

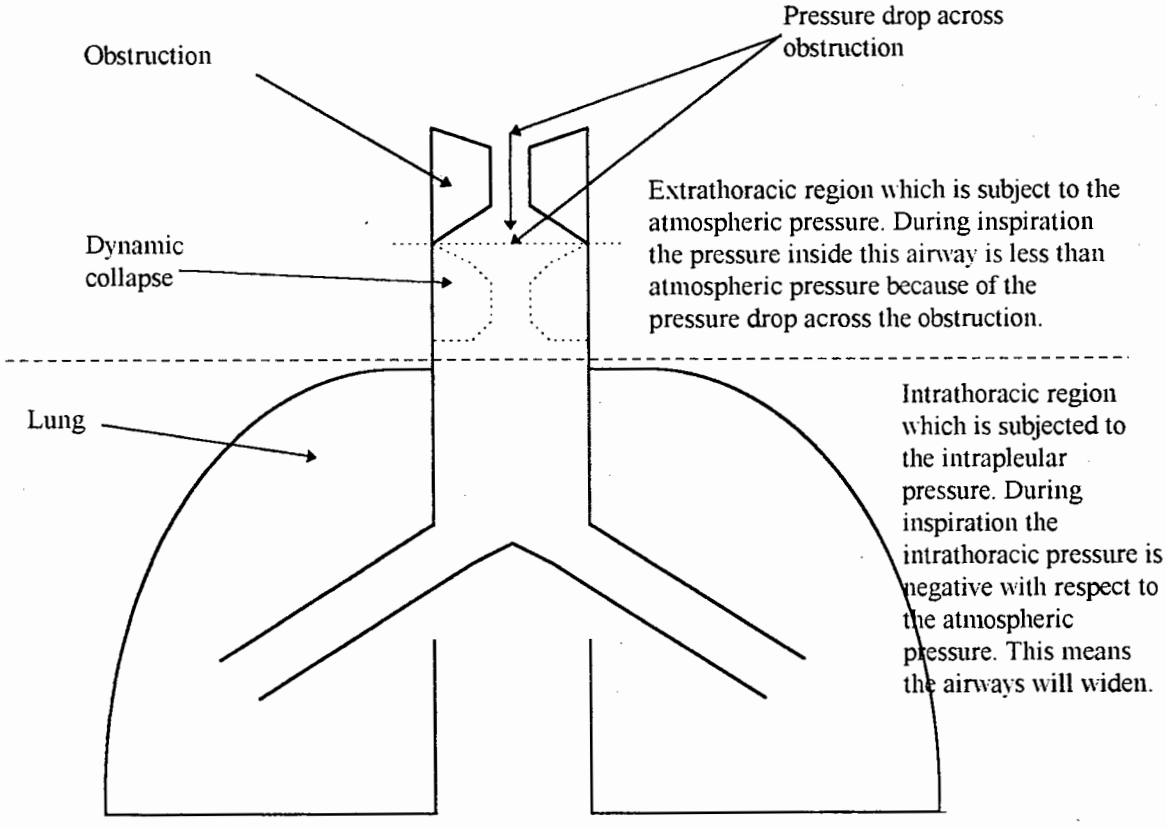

Figure 2.4 A simplified model of the croup mechanics during inspiration. The pressure drop across the obstruction (swelling of the mucosa in the subglottic ring) causes a negative pressure below the lesion. This negative pressure (relative to the atmospheric pressure) results in the dynamic collapse. It is important to note that the dynamic collapse does not occur on all sides of the extrathoracic trachea but only at the membranous posterior side.

2.2 Mechanics of air flow in airways

Fluids are divided into two groups - gases and liquids. The laws which govern the dynamics of gases are generally applicable to liquids. The major difference between gases and liquids is that gases are much easier to compress than liquids. However, if the pressure changes in gases are very small, such as under subsonic flow, then the behaviour of gases will resemble the behaviour of liquids. In this case, the gases will follow the equations of the fluid dynamics of incompressible fluids (Hughes and Brighton, 1991 Chapter 1).

2.2.1 Flow

Flow is usually divided into two types , laminar and turbulent flow. There is also a third type, namely ideal flow. Actually, no fluid flow is ever really ideal, but some flows do approach the ideal situation. (Hughes and Brighton, 1991 Chapter 1). In this case flow may be considered mathematically as frictionless and irrotational. In human airways the flow will be laminar, turbulent or a combination of both. Laminar flow, otherwise known as viscous flow, is characterised by fluid flowing in laminas or layers (figure 2.5a). A good example of laminar flow is honey being poured from a jar. Turbulent flow, as the name suggests, is a disorderly flow with a random fluctuation of the velocity components of all particles in the fluid (figure 2.5b). An example of turbulent flow is the process of mixing various raw materials in the mixing tank. However, the flow will, most often, be a combination of both turbulent and laminar components.

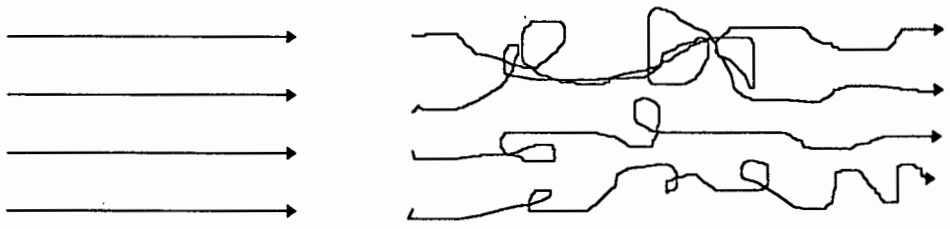

Figure 2.5. Laminar (a) and turbulent (b) flow. The lines indicate the paths of individual particles (Hughes and Brighton, 1991)

It is difficult to mathematically determine whether a flow is turbulent or laminar. Usually, the Reynolds Number (equation 2.1) can be used as an indicator of the likelihood of a particular flow profile.

$$N_R = \frac{\rho \cdot v \cdot D}{\mu} \qquad (2.1)$$

where: N_R - Reynolds number

ρ - fluid density

v - fluid speed

μ - fluid viscosity

D - diameter of the tube in which the fluid is flowing.

Generally, it is accepted that if the value of N_R in equation 2.1 exceeds 2000 then the flow usually becomes turbulent. However, there are cases where the flow is laminar despite very large Reynolds numbers. Practically, turbulent flow is more likely when the fluid density is high and laminar flow is more likely when the viscosity of the fluid is high (Hughes and Brighton, 1991 Chapter 1; Wood et al 1976).

Flow may be further divided into many other categories of which the most relevant to our study of flow limitation is a distinction between subsonic and supersonic flow. Subsonic flow involves velocities which are less than that of the sound in the fluid, while supersonic flow involves velocities exceeding that of the sound in the fluid. The Mach number, M, is the measure which distinguishes subsonic from supersonic flow.

$$M = \frac{V}{c} \tag{2.2}$$

where: M - Mach number

V - speed of flow

c - speed of sound in the fluid.

Thus M<1 represents subsonic flow; M=1 represents sonic and M>1represents supersonic flow (Hughes and Brighton 1991, Chapter 7).

2.2.2 Airway resistance

A pressure drop between a point A and a point B in a straight tube, causes a flow between these two points. The resistance in the tube can be calculated from the driving pressure (pressure drop between point A and B) divided by the flow. For steady fully developed laminar flow in a smooth, straight circular tube, the resistance to flow is given by (Peslin and Fredberg, 1986):

$$R = \frac{8 \cdot \mu \cdot l}{\pi \cdot r^4} \tag{2.3}$$

where: R - resistance to flow

l - length of the tube

r - radius of the tube

μ - viscosity of the fluid

Equation 2.3 is the Poiseuille formula for flow resistance (named after the French physician who derived this equation). Equation 2.3 shows that the pressure increases linearly with flow provided that viscosity of the fluid, length and the radius of the tube remain constant. Therefore, the resistance is constant.

Under conditions of turbulent flow, the driving pressure is proportional to the square of the flow and length of the tube (Scanlan et al, 1993).

$$Pd = Kt \cdot \dot{V}^2 \cdot l \qquad (2.4a)$$

where: Pd - driving pressure

Kt- turbulent flow constant

$\dot{V}$ - flow

l - length of tube

However, if the length of the larynx in infant's is small it can be regarded as being an orifice with the following pressure-flow characteristics (Peslin and Fredberg, 1986):

$$Pd = Kt \cdot \dot{V}^2 \qquad (2.4b)$$

Therefore, the resistance to turbulent flow is not constant (as in the case of laminar flow) but varies with flow (Peslin and Fredberg, 1986):

$$R = Kt \cdot \dot{V} \qquad (2.5)$$

In general, the driving pressure in human airways will be determined by both turbulent and laminar flow (West, 1991; Fry et al, 1954). Thus, the combined resistance will have the form

$$R = Kl \cdot l + Kt \cdot \dot{V} \qquad (2.6)$$

where: Kl - laminar flow constant

l - length of tube

Equation 2.6 is used very often by researchers to analyse the mechanics of airways (West, 1991; Fry et al, 1954).

2.2.3 Pressure during the breathing cycle

The intrathoracic or pleural pressure may be regarded as the algebraic sum of three pressure components (Fry et al, 1954) which may be divided into three categories. According to Fry et al, the first is the pressure used to accelerate the respiratory system. During normal tidal breathing, this pressure is negligible when compared to other pressure components. The second component of the intrathoracic pressure overcomes the retractive force, due to the elastic recoil of the lung. This is also known as the recoil pressure (recoil pressure may be further subdivided into elastic and surface tension effects). The third component overcomes the frictional resistance of the lung and its contents. This pressure is further subdivided into:

- the pressure required to overcome the frictional resistance caused by a movement of the lung parenchyma and other tissues of the intrathoracic cavity; and

- the pressure which overcomes the resistance to gas flow.

Both the recoil pressure and the pressure which overcomes the frictional resistance are significant components of the pleural pressure. Equation 2.7 shows the general representation of the pleural pressure, neglecting inertive pressure:

$$P_T = P_E + P_V + P_P \tag{2.7}$$

where: P_T - intrathoracic pressure (pleural pressure)

P_E - recoil pressure

P_V - pressure to overcome the frictional resistance caused by a movement of tissues

P_P - pressure to overcome the resistance to gas flow

Fry et al (1954) found that P_V is insignificant when compared with P_P. Equation 2.7 may be simplified even further, by neglecting P_V and by combining it with equation 2.6 (Fry et al, 1954):

$$P_T = P_E + (Kl \cdot \dot{V} \cdot l + Kt \cdot \dot{V}^2) \tag{2.8}$$

where: Kl - laminar flow constant

l - length of the airway

Kt - turbulent flow constant, which will not incorporate the length of the

airway if the orifice is considered in the analysis.

$\dot{V}$ - gas (air) flow

Equation 2.8 is the work-horse used to analyse the mechanics of flow in humans. It is an accepted convention that all the pressure terms in equation 2.8 are referenced to the atmospheric pressure and consequently the recoil pressure, P_E, is negative under normal circumstances. The pressure, P_P, will be negative on inspiration and positive on forced expiration, or when there is an obstruction to flow. The intrathoracic pressure is usually negative on expiration unless the value of P_P is large (for example, with an obstruction in the upper airways).

For normal children and adults the peak inspiratory flow does not correspond to the peak inspiratory intrapleural pressure because the recoil forces of the lung and airways are significant. Thus at end of inspiration the flow is zero but the absolute inspiratory intrapleural pressure is greatest because of the stretched elastic tissue of airways and lungs. Figure 2.6 shows the volume, the pressure and the flow during the breathing cycle (West, 1991).

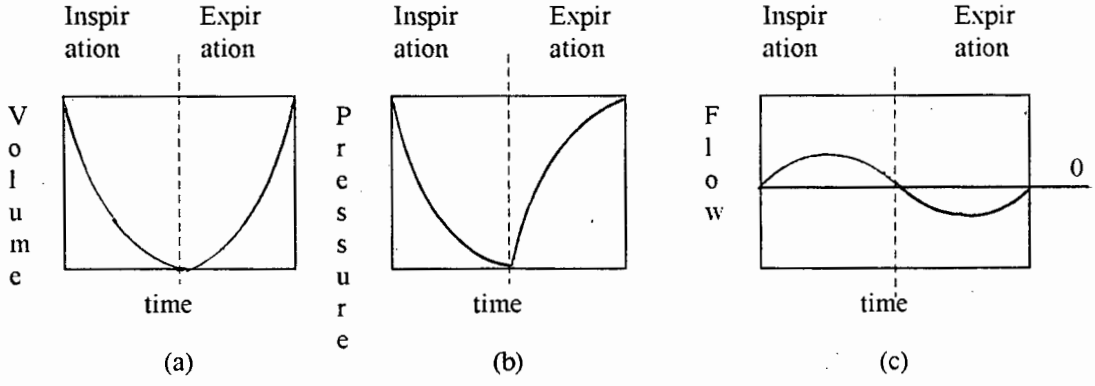

Figure 2.6 Relationship between the volume (a), the intrathoracic pressure (b) and the flow (c) during the breathing cycle. The hash-line marks the end of inspiration/beginning of expiration. The intrathoracic pressure curve is an idealised representation where both the resistive and the compliant forces exist during the breathing cycle. In this case, the lungs are assumed to be very compliant.

As the resistive forces become more significant than the lung's and the airways' compliance (as in croup) the intrapleural pressure changes will tend to follow the flow.

2.2.4 Constrictions

Generally, there are four constrictors used to measure flow or the pressure in various fluid dynamic applications. These are the orifice, nozzle, venturi meter and the Dall tube (Coulson and Richardson, 1988). They all work on the Bernoulli principle. The only difference between them is in the amount of pressure recovered at the exit of each of these meters.

Before one proceeds to further analyse the mechanics of a constriction, it is important to review some basic laws of fluid dynamics. In the previous section the components of the intrathoracic or pleural pressure (equation 2.7) were mentioned. In fact, each of these pressures is the total pressure which further consists of the static (lateral) pressure and the kinetic pressure (refer to Appendix A for basic definitions of fluid dynamics). This relationship, described by equation 2.9, is known as the Bernoulli equation (see Appendix B) which is a fundamental concept of fluid dynamics. Please note that for simplicity, the small deviations caused by gravity are ignored.

$$Po = P_L + P_K \tag{2.9a}$$

$$P_K = \frac{1}{2} \cdot \rho \cdot V^2 \tag{2.9b}$$

$$Po = P_L + \frac{1}{2} \cdot \rho \cdot V^2 \tag{2.9c}$$

where: Po - total pressure

P_L - static pressure

P_K - kinetic pressure

ρ - fluid density

V - speed of fluid flow = $\frac{\dot{V}}{A}$ (volume flow divided by the cross sectional area of the fluid). In this case the fluid is the air.

In Appendix B the derivation of equation 2.9 from the line integral of Euler's momentum equation (the derivation of the line integral has been explained by Owczarek (1964 section 3.4) is discussed.

Let us consider the simple situation shown in figure 2.7

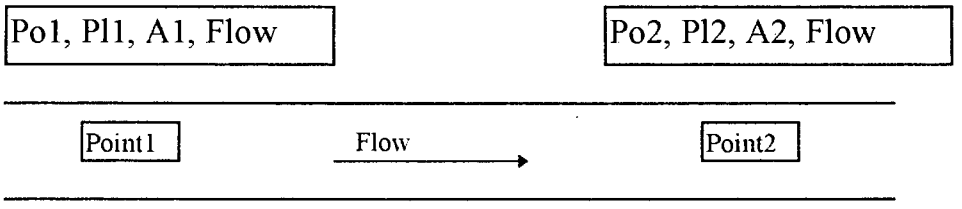

Figure 2.7 Fluid flowing in the tube. Let us assume that the fluid flows from point 1 to point 2. The flow at point 1 and point 2 is the same. Also, the areas 1 and 2 are the same. Po is the total pressure, while Pl refers to the lateral pressure at each point.

If the fluid in figure 2.7 flows from point 1 to point 2, then there is a pressure drop (i.e. Po1 - Po2). Since both the areas and the flows are the same, the kinetic components of Po1 and Po2 are the same (assuming that the fluid is incompressible). Therefore, the pressure drop between point 1 and 2 is purely determined by the drop in the static pressures (Pl1 - Pl2). This is a typical case for viscous losses. However, the situation changes when either the flow is large or the magnitude of area A1 is drastically different from that of A2. The flow now becomes turbulent and it will be the kinetic component of the total pressure which

will predominate (Appendix C1). This is particularly important in the use of electrical analogies to simulate the behaviour of airways (Solway et al, 1987).

Drastic changes in the area implies some sort of constriction. Therefore, the analysis of the mechanics of the constricted area primarily deals with a turbulent phenomenon.

Figure 2.8 shows the constricted area in the form of the flat-plate orifice (Hughes and Brighton, 1991, Appendix G)

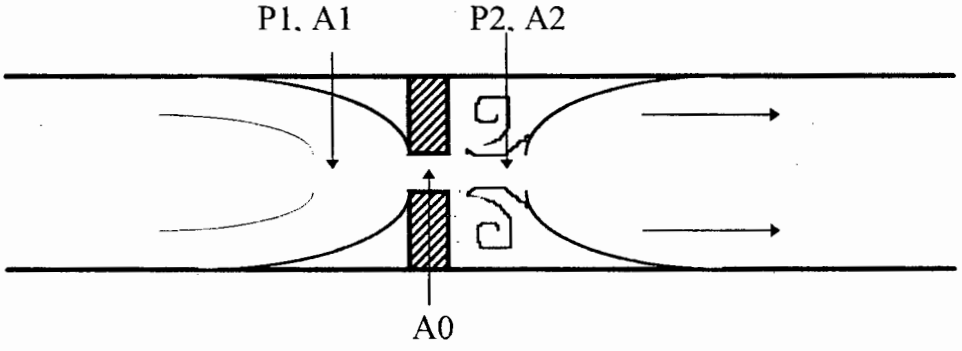

Figure 2.8 The flat plate orifice. P1 and P2 are the static pressures at indicated points. Similarly, A1 and A2 are the corresponding areas. It is important to note that areas are not determined by the tube walls but by the column of fluid. In this case A2 is limited by the fact that the flow is separated from the tube wall. This results in eddy currents which are characteristic of turbulent flow.

Equation 2.10 shows the solution to the flow (Appendix C2) for the arrangement shown in figure 2.7.

$$\dot{V} = C_d \cdot A0 \cdot \sqrt{\frac{2}{\rho} \cdot (P1 - P2)} \qquad (2.10)$$

where: $\dot{V}$ - flow through the orifice

C_d - overall discharge coefficient

A0 - orifice cross sectional area

ρ - fluid density

P1 and P2 - static pressures

Equation 2.10 is, in fact, universal to one type of the previously mentioned constriction devices. The only difference is in the value of the discharge coefficient, C_d, which is determined experimentally. The discharge coefficient is a dimensionless quantity which corrects for area differences and pressure losses. For a flat plate orifice, C_d is in the range of 0.6 to 0.8 (Hughes and Brighton, 1991, Appendix G). Note that a low value of Cd indicates large pressure losses with a small pressure recovery due to large eddy currents. The venturi meters have much higher discharge coefficients (0.98 to 0.99). These devices, which are similar to Dall tubes, are designed to reduce the effect of eddy currents. Figure 2.9 shows a typical venturi meter with sites of static pressure measurements.

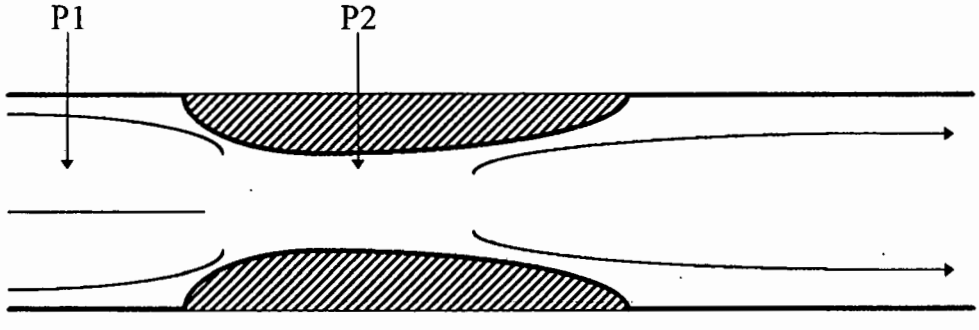

Figure 2.9 The venturi meter. The arcs serve the purpose of eliminating the eddy currents. The price the venturi pays for the arcs is the increase in viscous losses. However, because of the short length of the venturi the viscous losses will still be negligible. Therefore, the overall effect of the arcs is that the losses are smaller than in the case of the flat plate orifice. This results in a large pressure recovery at the outlet of the venturi meter (80%-90% (Coulson and Richardson, 1988)).

It is very difficult to estimate what kind of constriction occurs in respiratory systems. Generally, researchers regard the larynx as an orifice (even in the healthy state) (Wood et al, 1976; Peslin and Fredberg, 1986). This may be justified because the larynx may cause almost 60% of the total turbulence in air flow (Baier et al, 1977). However, a more detailed analysis of human adult laryngeal models (Van Den Berg et al, 1957) reveals that flow in the larynx may, for certain flows

and dimensions of the cross sectional area, be predominantly laminar. This would imply that the larynx behaves more like a venturi. However, there is no information on the structure of the larynx in infants with croup, except for X-rays but these are limited to the two dimensional images. This is not surprising because the technology to extensively investigate an infant's larynx in vivo is quite limited. In life-threatening croup, the affected larynx has a very small aperture which probably behaves like an orifice and produces no pressure recovery. The arrangement in which there is no pressure recovery has been investigated in the literature. Jones et al (1975) found that collapse, which is artificially produced in the excised human trachea, results in almost no pressure recovery. In this case, the static pressure inside the constriction is almost the same as the driving pressure.

Equation 2.11 is the solution of a flow under the condition of no pressure recovery at the outlet of the constriction (Jones et al, 1975).

$$\dot{V} = A0 \cdot \sqrt{\frac{2}{\rho} \cdot (\Delta P)} \qquad (2.11)$$

where: $\dot{V}$ - flow through the orifice

ρ - fluid density

A0 - cross sectional area of the constriction

ΔP - driving pressure.

Equation 2.11 resembles the orifice equation (equation 2.10) with a discharge coefficient of unity. However, if the discharge coefficient C_d=1, then one has an ideal zero loss situation and, therefore, full pressure recovery. What makes equation 2.11 different from the ideal case of equation 2.10 is that ΔP represents a driving pressure (difference in total pressures) and not the difference in static

pressures shown in equation 2.10 (also refer to fig. 2.8). In the case of no pressure recovery the static pressure inside the constriction is almost the same as the driving pressure (Jones et al, 1975).

The situation where there is no pressure recovery is probably not uncommon in physiological systems. Although, it is unlikely that a high loss constriction occurs in the respiratory systems of healthy individuals, it is possible that diseased airways may behave differently.

2.2.5 Flow limitation

So far the author has discussed situations in which the increases in pressure would result in increases of flow. The flow increases with the increasing pressure either linearly (laminar flow) or in a non-linear manner (turbulent flow). However, there is a limit to which the flow may increase. Once the flow reaches that maximum, further increase in the driving pressure will not increase the flow any more. This is known as flow limitation. Only the viscosity or the wave speed may determine the flow limitation in airways (Hyatt, 1983). Researchers treat these two causes of flow limitation separately (Hyatt, 1983; Lambert et al, 1982; Shapitro, 1977). Thus they regard the mechanics of the flow limitation as either the wave speed or the viscosity phenomenon, but not both.

2.2.5.(a) Flow limited by wave speed

In an incompressible fluid, the movement of a fluid particle at a point requires the simultaneous movement of all fluid particles in order for the density to remain

constant. This means that the velocities of wave propagation are infinite. However, in a compressible fluid, there is a greater distance between molecules than in the case of incompressible fluid (John 1969 Chapter 2). The small movement of the particles in a compressible fluid induces small disturbances in adjacent particles. These disturbances are elastic acoustic waves which propagate through the fluid at the speed of sound. Equation 2.12 shows the speed of sound in a fluid (see Appendix D for derivation of a more general form).

$$V_p = \sqrt{k \cdot \frac{P_0}{\rho}} \tag{2.12}$$

where: V_p - velocity of sound in the fluid $[\frac{m}{s}]$

P_0 - ambient pressure (for air at sea level this is $1.0132 \cdot 10^5$ [Pa])

ρ - density of the fluid (for air at normal pressure the value is $1.2047\ [kg \cdot m^{-3}]$

k - ratio of specific heats (for air at sea level k = 1.402).

Since the acoustic waves propagate at the speed of sound in the fluid, the sonic speed is often referred to by researchers as the wave speed. As long as the fluid particles travel at a speed less than that of wave speed, the pressure variation downstream will affect the flow upstream. The reason for this is that, under conditions of subsonic flow, the pressure wave (acoustic wave) - produced by a disturbance downstream - travels retrogradely with a velocity greater than zero relative to the fluid velocity. Once the magnitude of the fluid velocity reaches wave speed, the acoustic wave becomes stationary relative to the fluid particles. The pressure variation downstream no longer affects the flow upstream (Bertram and Raymond, 1991). In this case flow becomes limited and further lowering of

the downstream pressure will not increase flow (John, 1969, Chapter 3). This is often compared to the waterfall effect where the flow gradient increases to a point beyond which flow cannot increase.

The theory of flow limitation in rigid-walled pipes has been extensively investigated for decades (in fact no tube is ever totally rigid - even a brass tube has a finite compliance (Guelke and Bunn, 1982)). Almost every textbook on fluid dynamics has a chapter dedicated to this subject. The rigid walls of the tubes and pipes are unrealistic for the purpose of our study because the tissue surrounding the laryngeal portion of airways is not rigid (this may be seen during a laryngoscopy). However, the major problem is the fact that the derivation of the flow limitation in rigid walled tubes assumes a reversible (frictionless) and adiabatic (negligible energy transfer) flow of a perfect gas (John, 1969 Chapter 3). The author simply does not have the measuring capability to ensure that the flow conforms to the above assumptions.

The flow in compliant tubes is a more realistic approach to flow limitation in airways. This time, it is the combined effect of the compliance of both the gas and the tube wall which determines the flow limitation (Elliot and Dawson, 1977). If the compliance of the tube increases (i.e. the tube is easier to compress), then the value of the maximum flow decreases. In the airways the wall compliance and not the gas compression, primarily determines the value of the maximum flow.

Flow limitation in human airways has been known about for over forty years. The literature on this subject describes the maximum expiratory flow in the intrathoracic trachea of adults. However, our patients are not adults but infants and they exhibit flow limitation during inspiration (not expiration). In addition, these croup patients' inspiratory efforts depend on the severity of croup. The maximum

expiratory flow, on the other hand, requires maximum expiratory effort. Nevertheless, the theory of the maximum expiratory flow relates most closely to flow limitation in children with croup. If one selects the most severe cases of croup and assumes further that the maximum flow is predominantly determined by the airways' cross sectional area and the wall compliance, then the theory of the maximum expiratory flow should be sufficient to model the scenario of the croup mechanism. Fry et al (1954) were the first to provide a key observation to explain the mechanics of the maximum expiratory flow volume (MEFV) graphs. Although the MEFV graphs were used earlier to diagnose various respiratory problems, Fry et al established that each point on the MEFV curve may be represented by a family of isovolume pressure flow (IVPF) curves (Hyatt, 1983).

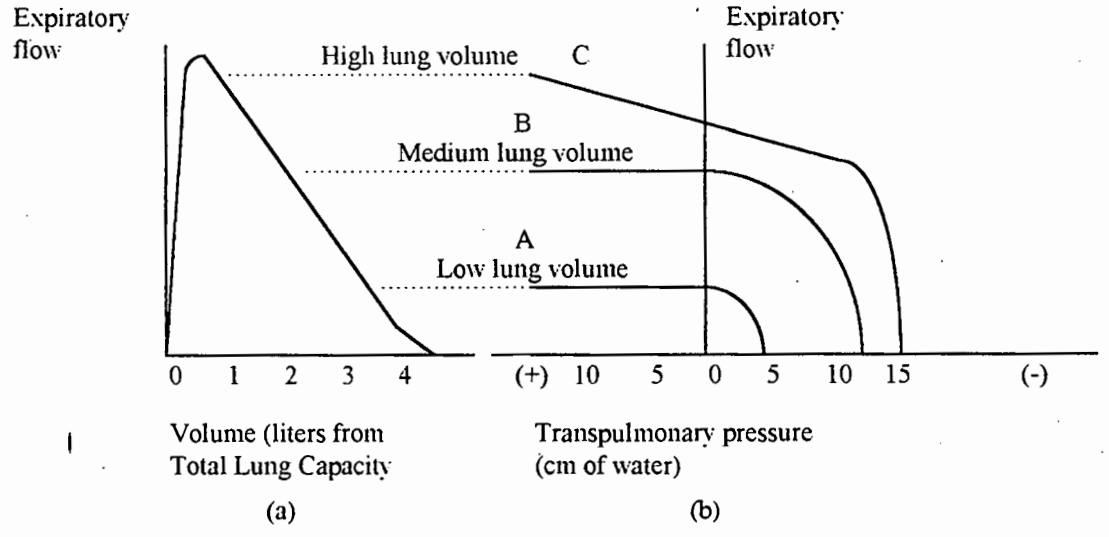

Figure 2.10 Three isovolume pressure flow (IVPF) curves (b) and the corresponding flows of the maximum expiratory flow volume (MEFV) curve (a) for a normal subject. Curves A and B of IVPF are flow limited while curve C is not.

Figure 2.10 shows that even a healthy individual may exhibit (under expiratory effort), expiratory flow limitation at low lung volumes. Although many scientists tried to explain the subject of flow limitation with varying success (Hyatt, 1983), it was Dawson and Elliot (1977) who eventually produced a mathematical model. They claimed that the flow becomes choked once the fluid velocity reaches the

speed of wave propagation in the medium. The maximum flow which can be attainable in an elastic tube is (Appendix E)

$$\dot{V}_{max} = \sqrt{\frac{A^3}{\rho} \cdot \frac{dP}{dA}} \qquad (2.13)$$

where: $\dot{V}_{max}$ - maximum flow

ρ - density of fluid

P - transmural pressure (static pressure inside minus static pressure outside the tube)

A - cross sectional area of the tube segment in which the flow cannot exceed $\dot{V}_{max}$

Equation 2.13 is a classic form in which the wave-speed, $\sqrt{\frac{A}{\rho} \cdot \frac{dP}{dA}}$, determines the magnitude of the maximum flow. In fact, the speed of wave propagation was first derived by physician Thomas Young in 1808 (Elliot and Dawson, 1977), who proposed his solution for incompressible fluids in elastic tubes. Therefore, to account for the fact that the project is dealing with gases and not liquids, the general solution to the maximum flow is (Elliot and Dawson, 1977)

$$\dot{V}_{max} = \frac{1}{\sqrt{\frac{\rho}{A^3} \cdot \frac{dA}{dP} + \frac{\rho}{P_0 \cdot k \cdot A^2}}} \qquad (2.14)$$

The term $\frac{\rho}{P_0 \cdot k}$ in equation 2.14 describes the gas compressibility (see equation 2.12) and is usually negligible compared to the wall compliance. Therefore, in

most applications in which tubes are elastic, equation 2.13 is sufficient to predict the maximum flow (Dawson and Elliot, 1977).

Figure 2.11 shows an idealised representation of the flow-driving pressure curve and the corresponding transmural pressure-cross sectional area curve (Elliot and Dawson 1977).

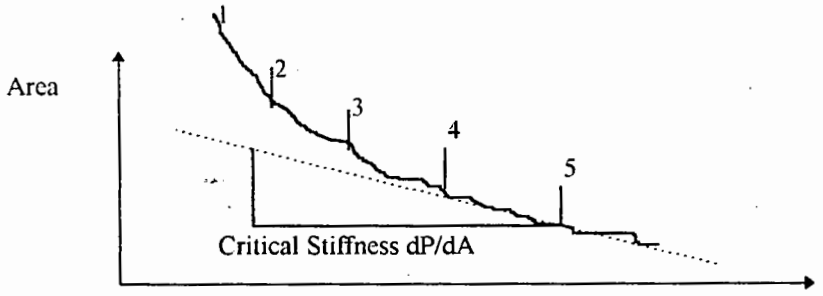

Transmural pressure, P, at the point where flow limitation will occur first. The transmural pressure is the difference between the static pressure inside the tube and the static pressure outside the tube or airway

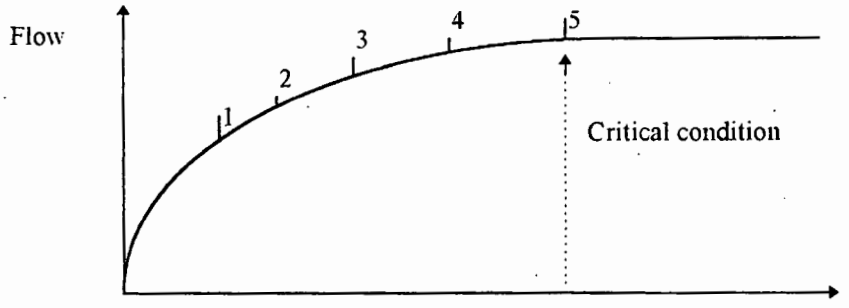

Driving pressure (pressure difference across the collapsible region)

Figure 2.11 Area-transmural pressure curve and the corresponding flow-driving pressure curve (Elliot and Dawson 1977). Point 5 indicates the critical condition where the flow becomes limited. The critical stiffness $\frac{dP}{dA}$ is the reciprocal of the tube compliance at onset of maximum flow. Please note that the driving pressure is the difference in total pressures while the transmural pressure, P, is calculated from the difference in static pressures.

The graphs of the pressure flow relationship do not always have the classical shape shown in figure 2.11. Knudson and Knudson (1973) showed that the isovolume pressure flow curves may indeed behave differently in different tracheae past the

point of maximum flow. For example, negative effort dependence shows a marked decline in flow after maximum flow is reached (Knudson and Knudson, 1973), while positive effort dependence , on the other hand, will produce an increase in flow in the flow limited domain (Allen et al, 1987). Both positive and negative effort dependence are the result of the mechanical properties of the airways (Dawson and Elliot, 1977; Allen et al, 1987).

Unfortunately, as will be seen later, the possibility of effort dependence prohibits one from deciding on the mechanism of flow limitation by a mere graphical inspection.

2.2.5.(b) Flow limited by viscosity

The wave speed phenomenon does not appear to be the only mechanism by which the flow can be limited. In the case of expiratory flow, the maximum flow at low lung volumes may also be determined by viscous flow limitation. Indeed, researchers are unable to predict the maximum flow at low volumes in excised lungs (Hyatt et al, 1980). This agrees with the mathematical model presented by Lambert (1982). Shapiro (1977) extensively investigated steady flow in a collapsible tube and he found the viscosity to limit the flow in his starling resistor model.

In the case of viscous flow limitation, viscous coupling with the tube compliance predominates and the coupling between tube compliance and convective losses is not the significant mechanism (Hyatt, 1983). Therefore, it is the laminar rather than the turbulent flow which is limited by viscosity.

2.3 Lumped component model

Researchers often use electrical analogies of acoustical or mechanical systems under investigation. In our study, it may also be advisable to model the entire system of airways in terms of electrical components which are mathematically manageable rather than to analyse a specific segment of airway in terms of flow limiting mechanisms. It is important to note that our measuring technique (see Chapter 4) is more suitable for investigating the general, rather than the specific characteristics of the respiratory tract. Although the electrical model does not directly apply to flow limitation in croup, this model may provide a suitable method to compare the predicted with the measured flow. The aim of this study is to find at what point the measured flow no longer follows predictions made from the linear, electrical representation of the respiratory system. It should be stressed that the electrical model cannot predict flow limitation because this model does not assume non-linear behaviour such as is the case in the flow limitation phenomenon. However, the point where the calculated flow significantly differs from the measured flow may indicate the region where flow does, indeed, become limited.

Electrical models of compliant tubes are often used as the research tool to explain the mechanics of respiration, phonation (Bickley, 1993; Solway et al 1987) and even hearing (Bunn and Guelke, 1983). Although the lumped theory is well established in the literature, the application may not always be realistic. In the case of this project, the limitation is with measurements (see Chapters 4 and 6) and the model proposed by Bickley (1993) cannot be realised. The author does not have the technology to precisely measure the laryngeal inertance, compliance and even resistance. The oscillation mechanics employed by leading researchers in this field (Jackson and Lutchen, 1987), although relevant to our study, cannot be

investigated because our equipment is not designed to perform this task. Therefore, the author decided to investigate the already established lumped component models of airway mechanics.

DuBois was a pioneer who represented the respiratory system in terms of three and six element models (DuBois et al, 1956). Since then, researchers have improved and developed lumped component airway models further (Peslin et al, 1985; Jackson and Lutchen, 1987), and five, eight and nine element models have been described (Lutchen and Costa, 1990). Figure 2.12 shows the three, five, six and nine element lumped component models of the respiratory system.

Unfortunately, each electrical component of figure 2.12 is unknown and it has to be estimated. Therefore, it is unrealistic to consider models of eight, nine or more components in our study. The five element model (or rather the interpretation of this model) is criticised by Jackson and Lutchen (1987) while, to the contrary, the six element model is regarded as quantitatively plausible (Jackson and Lutchen, 1987). Therefore, this study considers the three and the six element DuBois models. The three element model, although extremely simple, may in fact satisfactorily represent the six element model, if the compliance C1 in figure 2.12 (c) is small compared to C2.

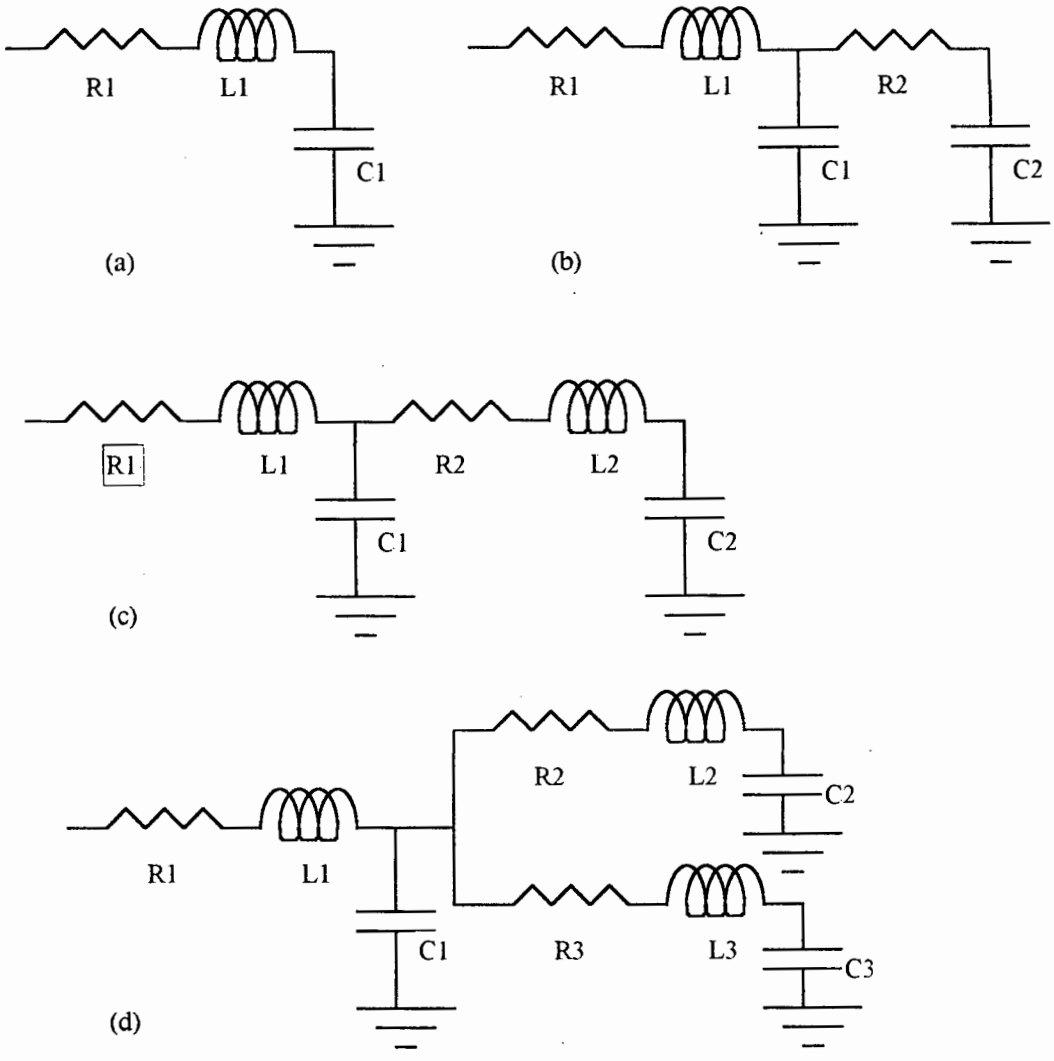

Figure 2.12. Lumped component models of the respiratory system: (a) the simple three element DuBois model; (b) the five element Pimmel model; (c) the six element DuBois model and (d) the nine element model (proposed by Peslin, 1985). Please note that this is not an exhaustive list of lumped component models used to model the respiratory system. Nevertheless, the models presented in this figure are often used by researchers (Jackson and Lutchen, 1987). R represents the resistance, L the inertance and C the compliance.

2.3.1 The three element DuBois model

Figure 2.12 (a) shows the three element model introduced by DuBois. The small number of components suggests that the model is the simplest representation of the mechanics of the airways. Therefore, the elements which describe the less significant structures and mechanisms are excluded. R1 is the total resistance of

the combined airways; L1 is the inertance of the chest wall and gas inertance; and C1 is the compliance of the chest wall and the gas compliance. In fact, R1 and L1 may, under the condition of negligible gas compressibility, represent the total respiratory resistance and inertance respectively (see section 2.3.2).

2.3.2 The six element model

Figure 2.12 (c) shows the six element model. This is a more realistic representation of the airways than the three element model. The resistance and the inertance of the gas flow in the airways (R1, L1) are separated from tissue resistance, inertance and compliance (R2, L2, C2) by the compliance C1 which researchers believe to be the gas compressibility (Jackson and Lutchen, 1987; DuBois et al, 1956).

If the gas compressibility, C1, has a negligible effect on the mechanics of the airways, then the six element model becomes a three element arrangement. This is because the series resistances (R1 and R2) and the series inertances (L1 and L2) can be added to form the total respiratory resistance and inertance respectively.

Although, the six element model is probably a more realistic representation of the airways, the model is difficult to implement. Firstly, the circuit introduces three additional components, thus the number of unknowns increases. Secondly, the introduction of the inertial resistor $Rb \cdot \dot{V}$ (see section 2.2.1) results in a quadratic equation with a large number of coefficients. This necessitates a long computational time for simulation.

3. Development of theory

This chapter is divided into two major subsections:

1) the development of a flow limitation model; and

2) the development of a lumped component model.

In the first subsection, the author mainly investigates the parameters of the flow limitation formula in relation to croup. A new formula for maximum flow is introduced and the application of this formula to croup is analysed.

The second subsection investigates the lumped component model. Here, the electrical analogy of fluid mechanics in croup is developed in which the assumption of a lack of pressure recovery provides a new concept towards conventional three and six element models. The aim of this subsection is to introduce an alternative, and possibly a more realistic, approach towards the analysis of flow limitation in croup.

3.1 Flow limitation model

The small size airways are always in danger of being occluded. This is particularly true in infants whose larynges are very small (Wolfsdorf and Swift, 1978). The small aperture of the glottis may not just attenuate, but also limit the flow. According to the literature, there may be two causes of flow limitation in airways, namely

1) viscous flow limitation and

2) wave-speed limitation.

Researchers regard these two causes of flow limitation separately (Hyatt, 1983; Lambert et al, 1982; Shapiro, 1977). Thus, the flow may be limited only by viscosity or wave speed, but not both. In the case of viscous limitation, the viscous coupling with the tube compliance predominates (Shapiro, 1977; Hyatt, 1983). Contrary to viscosity, wave speed is a convective loss phenomenon (Hyatt, 1983). It becomes problematic to identify which process (viscous or convective) may exist in the subglottis with croup.

3.1.1 A steady flow Model

The maximum flow equation for a straight, uniform tube under steady flow was derived (Appendix E) to be:

$$\dot{V}max = \sqrt{\left(\left(\frac{(K_1 \cdot l)^2}{\rho^2}\right) + \frac{A^3}{\rho} \cdot \frac{dP}{dA}\right)} - \frac{-K_1 \cdot l}{\rho} \qquad (3.1)$$

where: $\dot{V}max$ - maximum flow

ρ - density

K_1 - laminar flow constant

A - cross sectional area

$\frac{dP}{dA}$ - wall stiffness (changes of transmural pressure over changes of area)

l - tube length

In this equation the combination of the viscous term (laminar flow constant K_1), and wave speed term determines the limit for steady flow through a uniform, straight tube. Intuitively, it makes sense that, as K becomes very large (effectively the wave speed term becomes negligible) the maximum flow tends to zero. Thus the increase in viscosity always decreases the flow (including the maximum flow). Also, a decrease in stiffness (walls become more compliant) reduces the flow because the value of K_1 dominates in the above equation. If K_1 or l is small on the other hand, the equation becomes:

$$\dot{V}max = \sqrt{(\frac{A^3}{\rho} \cdot \frac{dP}{dA})} \qquad (3.2)$$

Equation 3.2 is the classic wave speed equation to calculate the maximum flow (see equation 2.13).

3.1.2. Transmural pressure

In this project one cannot produce a detailed model of the fluid mechanics in the subglottis of an infant. This is because neither the literature nor our measurements (see Chapter 4, 5 and 6) provide sufficient information regarding the pressure distribution through a child's larynx. Therefore, it would be unrealistic to consider every structure of an infant's larynx because the effect of each of these structures on airflow cannot be verified either through measurements or the literature. Thus, the movement of the vocal chords and the possibility of mucous in the larynx are not part of the model developed in this project. However, the author is aware that

mucus and the movement of the vocal chords may influence the mechanics of flow in the upper airways. Nevertheless, it was found, using videos made during laryngoscopies, that the aperture of the glottis formed by the vocal chords is usually larger than the aperture of the subglottis. It was also noticed, through a laryngoscope, that not all patients with croup are affected by significant mucus secretion. Therefore, our model of a larynx of a child with croup is a simple orifice. This is consistent with models of adult larynges introduced in the literature (Peslin and Fredberg, 1986).

The model of an infant' larynx used in the analysis of croup is shown in figure 3.1 in which all pressures are referenced to the atmospheric pressure.

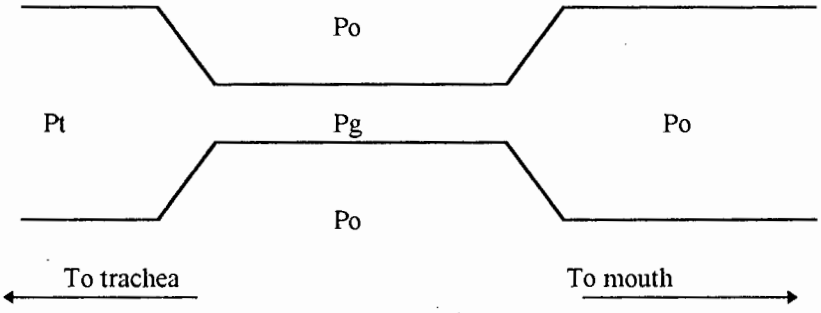

Fig 3.1. The simplified model of a human larynx (longitudinal view). Pt is the driving pressure, Pg is a lateral (static) subglottic pressure and Po is the total atmospheric pressure. For fluid dynamics terminology the reader is referred to Appendix A. All assumptions and approximations are explained in the text. Please note that the kinetic pressures are not shown.

The model shown in fig 3.1 is only a theoretical tool later employed in the computational analysis. The various pressures included in fig 3.1 are explained below. The author would recommend that the reader familiarises himself with the fluid dynamics terminology presented in Appendix A.

It is assumed that the pharyngeal and the atmospheric pressures (Po) are almost the same. This is not strictly true and indeed, in voice production, these pressures may

differ (Holmberg et al, 1988). During normal breathing, however, the pharyngeal impedance should be negligible as the cross sectional area of the pharynx is relatively large. An assumption is also made about the pressure which surrounds the larynx. In the laryngeal model of fig 3.1 this is the atmospheric pressure. In this case, the subglottic airway wall is the combination of all tissues starting from the airway subglottic epithelial lining to the outside of the neck's skin, with no pressure pockets in between.

The pressure Pt may cause controversy as this flow limitation model does not share some assumptions made by other investigators. These scientists (Chernick, 1990; Duncan, 1979) believe that the pressure drop across the larynx in a child with croup is so severe during inspiration that there is a prominent dynamic extrathoracic tracheal wall collapse (figure 2.4).

Although the dynamic collapse does exist in croup, the importance of this collapse may be exaggerated because the stenosis produced by croup in the subglottis is probably the cause of the largest pressure drop in the airways of a child with croup. This is particularly evident in patients with croup whose pressure and the flow measurements were made both before and after intubation. Figures 5.13 and 5.12 show an inspiratory cycle of the intrathoracic pressure and the flow before and after intubation respectively. If one assumes that the intubated patient's airways behave in the same manner as those of a healthy individual (see subsequent sections), then almost the entire pressure drop in the non-intubated patient is caused by the croup restriction. The pressure Pt in croup is therefore almost the same as the intrathoracic pressure. One must not, however, assume that the pressure drop caused by the remaining airways' resistance (see Literature Review) is always negligible. It is only in non-intubated patients with croup that the Pt almost equals the intrathoracic pressure.

The last variable of figure 3.1 is the lateral or static subglottic pressure Pg. The difference between Pg and the external pressure, in this case the atmospheric pressure, results in the transmural pressure P which is used in equation 3.1. Since Pg is not measured directly, it is necessary to relate this subglottic lateral (static) pressure Pg to the other variables of fig 3.1. Van Den Berg (1957) presented a model of an adult human larynx in which, over a major region of his measurements under the condition of a constant flow, the following holds:

$$Pt = Constant1 \cdot Pca \tag{3.3}$$

$$Pg = Constant2 \cdot Pca \tag{3.4}$$

where: Pca - convective acceleration (see Appendix C1).

Although, equations 3.3 and 3.4 were analysed in the case of adults, there is no reason why a similar relationship, but with different values for the constants, would not apply to infants.

By combining equations 3.3 and 3.4, it may be shown that $Pg = Constant3 \cdot Pt$ in which $Constant3 = \frac{Constant2}{Constant1}$. The transmural pressure P of equation 3.1 is therefore:

$$P = Pt \cdot Constant3 \tag{3.5}$$

3.1.3 Cross sectional area

Ideally the cross sectional area in the flow limitation equation should be a measured variable but that was not possible in this project. Therefore, the cross sectional area of the subglottis is calculated from the flow-intrathoracic pressure data.

The relationship between the flow and the pressure in any non-compliant airway structure may be approximated by equation 3.6 (see equation 2.8):

$$Pd = Kl \cdot l \cdot \dot{V} + Kt \cdot \dot{V}^2 \qquad (3.6)$$

where: Pd -pressure drop in airway

Kl and Kt constants (Kl is the laminar and Kt is the turbulent term)

l - length of airway

$\dot{V}$ - flow through airway

The laminar flow in the larynx will contribute very little because the length l of the subglottis in infants is very short and this short length creates an orifice with very large turbulent forces just outside the outlet of this orifice. This leaves us with the turbulent flow which, many researchers believe (Peslin and Fredberg, 1986; Woods et al, 1976), primarily determines the laryngeal pressure drop Pd.

Peslin and Fredberg (1986) show that the laryngeal resistance is given by the orifice equation which is derived purely from the turbulent flow contribution (see Appendix C2 for derivation):

$$R = \frac{\rho}{(2 \cdot Cd^2 \cdot A^2)} \cdot |\dot{V}| \qquad (3.7)$$

where: R - translaryngeal resistance

ρ - air density

Cd - discharge coefficient

A - cross sectional area

$\dot{V}$ - volume flow

The discharge coefficient Cd is a dimensionless quantity and depends on the orifice dimensions (see Appendix C2). For the adult larynx, Cd is about 0.6 (see section 2.2.4). The R term represents a pressure drop across the larynx divided by the flow (Ohms Law). Therefore, the cross sectional area, A, from equation 3.7 is:

$$A = \frac{\dot{V}}{Cd\sqrt{\frac{\rho}{(2 \cdot P)}}} \qquad (3.8)$$

It is usually difficult to estimate the Cd term precisely. In our study, it is impossible. If one assumes, however, that the diseased suglottis produces an abrupt change of the area in the transition between the glottis and the subglottis (infraglottic cavity) and the same change between the glottis and the vestibule (region where total pressure almost equals the atmospheric pressure i.e. zero), then Cd=1, P=static pressure inside the constriction (see section 2.2.4) and there is no pressure recovery (Jones et al, 1975) (in this case the model introduced by Van Den Berg (1957) uses Constant3=1 in equation 3.5). However, as pointed out in section 3.2.4, one must not assume that when Cd=1 there is a maximum pressure loss. On the contrary, Cd=1 is a zero-loss situation (in practice, impossible). In the case of the lack of pressure recovery, Cd simply does not apply anymore because

the losses are so high that the pressure drop across the constriction equals the driving pressure.

As was mentioned above, it is very difficult to measure the discharge coefficient Cd in a living individual whose airways are very small. The same applies to the measurement of pressure recovery in the subglottis of a child with croup. Since the lack of pressure recovery under the condition of turbulent flow is a necessary requirement to estimate the cross sectional area, the hypothesis that the static pressure does not recover downstream from the narrowed subglottis (see section 5.1) is examined.

The major cause of lack of pressure recovery is an abrupt change of area, high volume flow or a combination of both. Unfortunately, there is no mathematical relationship between lack of pressure recovery and other parameters such as flow, pressure or change of area versus airway length. Jones et al (1975) (see figure 3.2) performed experiments which showed a lack of pressure recovery downstream a region of rapidly changing airway area. It can be deduced that if the rate of change of area with distance along an airway exceeds that which was the case in Jones et al's experiments, then it is likely that there is also no pressure recovery in that airway.

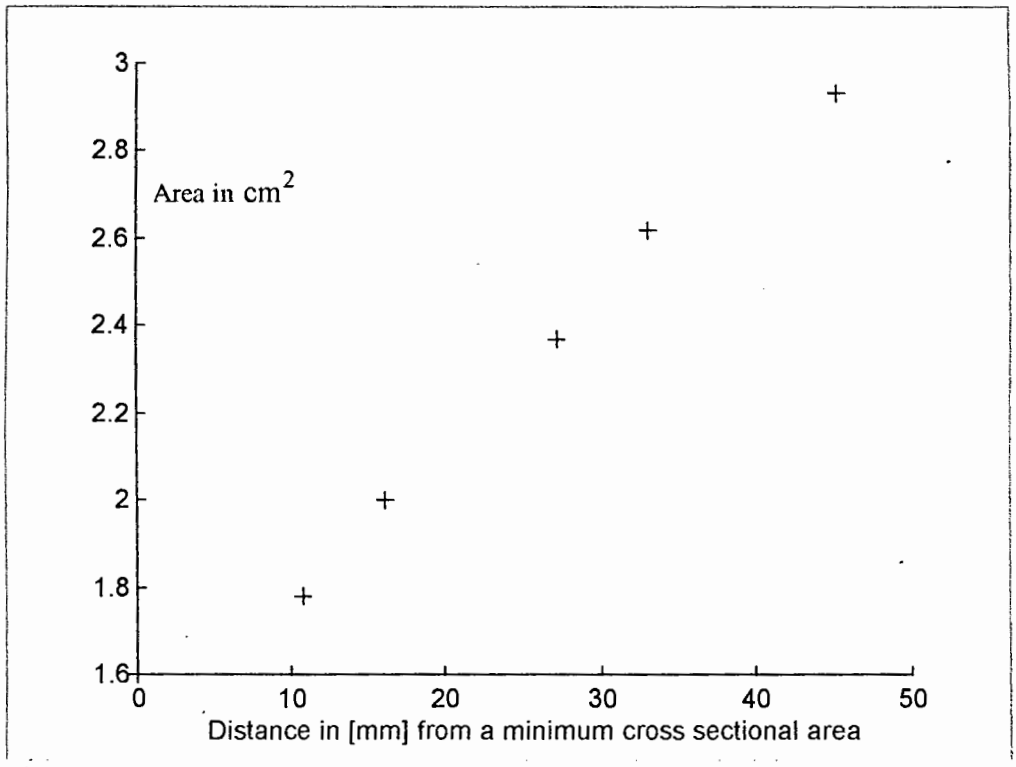

Figure 3.2 Cross sectional area versus distance in a trachea which showed lack of pressure recovery according to Jones et al (1975).

Fortunately, it is not necessary to measure the cross sectional areas precisely in order to compare the area profile of a child with croup with the profile presented by Jones et al (1975). In Chapter 6 there is a discussion to why the assumption that there is a lack of pressure recovery in patients with croup is valid.

3.1.4 Density

Fluids are generally divided into gases and liquids. Gases, as compared to liquids, are very compressible fluids. The large compressibility of gases complicates the solution to many problems in fluid dynamics. The relationship between the changes of the pressure p and the density ρ in fluids is

$$dp = \beta \cdot \frac{d\rho}{\rho} \qquad (3.9)$$

where β is the bulk compression modulus. For adiabatic compression of atmospheric air β is about $1.4 \cdot 10^5 Pa$. If one assumes that the maximum driving pressure in a child with croup is about 60 cmH_2O, then the density change (under adiabatic conditions) is only $0.04 \frac{kg}{m^3}$ (this is only 3% of the density of air at the sea level). If one assumes that there is no pressure recovery in the larynx of a patient with croup (see Chapter 5), then the driving pressure (relative to atmospheric) is almost the same as the lateral subglottic pressure and so, under these conditions, the density changes may be ignored.

3.1.5 Wall compliance

Equation 3.2 shows that when limited by wave speed, the maximum flow is directly proportional to the square root of a wall stiffness dP/dA. The reciprocal of the wall stiffness is the compliance dA/dP or more precisely, the compliance per unit length of the airway. In order to calculate the compliance per unit length, one needs to know the change of area A resulting from a change in the transmural pressure P. However, both P and A may only be obtained under certain assumptions, such as a lack of pressure recovery. This means that any error made in estimating the transmural pressure P and the cross sectional area A will be carried over to the estimation of dA/dP.

In order to estimate the compliance, dA/dP, two methods are employed:

1) calculation of dA/dP from the graph of the calculated cross sectional area versus the transmural pressure; and

2) calculation of dA/dP from an assumed value for the Young's Modulus of the tissue surrounding the airway with croup.

3.1.5.a Cross sectional area versus transmural pressure

By plotting the calculated area versus transmural pressure and taking a gradient, one is able to determine the compliance dA/dP. For most applications it is better to use an average value of the gradient just preceding the point of flow limitation. It is important to use the average as small undulations in gradient resulting from the secretion of mucous or from muscle activity, may lead to nonsensical results. Figure 3.3 demonstrates the method used to calculate the compliance dA/dP which is used in equation 3.2. Figure 3.3 shows that to calculate the slope dA/dP it is better to consider a general trend of data, rather than two consecutive samples, at the suspected point of flow limitation.

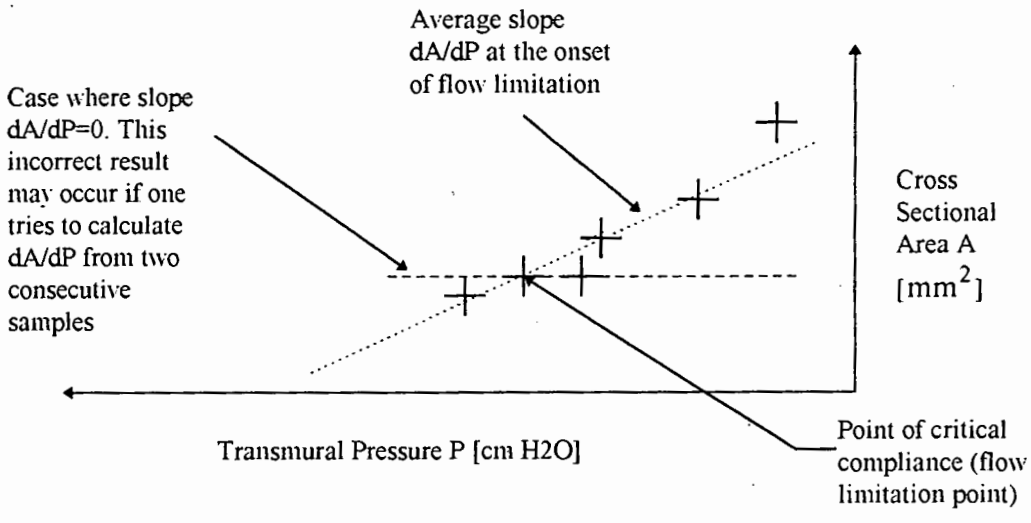

Figure 3.3 The dotted line represents an average dA/dP just preceding the point of flow limitation. The dashed line shows the incorrect value obtained when one tries to calculate dA/dP from two consecutive samples.

3.1.5.b Assumed Young's Modulus

In this subsection an alternative method was examined in order to calculate the compliance dA/dP. In this method it is assumed that the subglottal Young's Modulus is approximately the same among all infants with severe croup.

It is rather unlikely that the value of Young's Modulus for a subglottal wall should differ significantly among infants because the properties of the airway walls are very similar for young children. A study by Lanteri and Sly (1993) provided evidence that there are little differences in airway wall compliance and resistance among infants.

For this alternative estimate for the subglottal compliance the author has assumed that the subglottis has a circular profile in an anterior-posterior view, and that the Poisson's ratio for the wall is 0.5 (Thompson and Stevens, 1989):

$$Cw = \frac{3 \cdot \pi \cdot r^3}{2 \cdot E \cdot t} \tag{3.10}$$

where Cw - wall compliance

r - radius of the circular cross sectional area

t - wall thickness

E - Young's Modulus (stress/strain). Young's Modulus is assumed to be constant amongst different patients with croup

Taking $t/r \sim 0.1$ as a general approximation

$$E = \frac{15 \cdot A}{2 \cdot Cw} \tag{3.11}$$

where A - cross sectional area.

In order to estimate the Young's modulus E, it is necessary to choose a patient whose calculated area and compliance (as a first approximation the compliance is calculated using the method described in subsection 3.1.5.a) is consistent during various pressure-flow measurements. The parameter E is then calculated from equation 3.11 and used as a constant for all other patients with croup. This reduces equation 3.11 to a linear relationship between the calculated cross sectional area A and the wall compliance Cw.

3.1.6 Maximum flow

The model of the flow limitation in croup presented in this thesis is based on equation 3.1. Only the subglottic transmural pressure P, the subglottic cross sectional area A and the air density ρ are necessary to calculate the maximum flow $\dot{V}max$ in the patient with croup. In the patient with croup the I term in equation 3.1 is, due to the very small length of the subglottis, a negligible quantity. This means that the product of the viscosity and the length in equation 3.1 will also be negligible (see Table 5.2). This reduces equation 3.1 to the familiar form for calculating the wave speed known as the Young equation (equation 3.2 - see also section 2.2.5 and Appendix E).

$$\dot{V}max = \sqrt{\frac{A^3}{\rho} \cdot \frac{dP}{dA}} \tag{3.2}$$

The transmural pressure P in equation 3.2 is the difference between the static subglottic pressure Pg and the total atmospheric pressure Po. One cannot measure Pg directly, but equation 3.5 may be used to relate Pg to pressure Pt, where Pt is a driving pressure. Since all pressures are relative to the atmosphere, equation 3.5 may be restated as:

$$P = Pt \cdot Constant3 = (P_T - Pe) \cdot Constant3 \qquad (3.12)$$

where P_T - pleural pressure

Pe - elastic recoil pressure

The substitution of equations 3.8 and 3.12 into equation 3.2, results in the equation which is used to calculate the maximum flow $\dot{V}max$ without measuring the cross sectional area A.

Both Constant3 in equation 3.12 and Cd in equation 3.8 are unknown constants. However, if one assumes that Constant3 in equation 3.5 is constant for most of the pressure and the flow measurements (as is the case in Van den Berg's model), then it may be shown that equation 3.2 will be insensitive to the value of Constant3. The Cd term is unity under the assumption of lack of pressure recovery (Jones et al, 1975).

A computer algorithm to perform these calculations is described in Chapter 5.

3.1.7 Computer simulation

The aim of the MATLAB programme (Appendix F) is to compare the maximum flow, calculated from equation 3.2, with the measured maximum flow. One must bear in mind that the maximum flow does not necessarily have a constant maximum value. Indeed, in the case of positive and negative effort dependence maximum flow varies with effort (see section 2.2.5). Also, the flow not necessarily has to show a characteristic plateau. Since the first appearance of the maximum flow on the flow pressure graphs is crucial for equation 3.2, the possibility of effort dependence and the lack of a plateau will further complicate our analysis.

3.2 Lumped component model

In the previous section it was pointed out that the flow may become limited under certain conditions as predicted by equation 3.1. However, it is not known if these conditions exist in patients with croup. For instance, it is possible that in these patients flow is not limited, but simply attenuated. If this is the case, then a lumped component model should describe the pressure/flow plots (note that in this case an increase in driving pressure will always produce an increase in flow, even if non-linear or turbulent conditions predominate). The major goal of this section is to use a more general approach to investigate whether the flow in croup really becomes limited or whether it is just attenuated.

3.2.1 Three element DuBois model

The three element DuBois model of the airway mechanics is shown in figure 2.12(a). R1 is the total airways resistance; L1, the combined inertance of the chest wall and the gas in the airways; and Cw, the combined compliance of the chest and the air in the airways.

The representation of airway mechanics in terms of electrical analogies must be approached with caution since, for example, there is no representation of the Bernoulli effect in electrical systems. However electrical circuits have been used effectively, albeit with limiting assumptions, to analyse lung and airway function. In healthy individuals the representation of flow as being laminar may be sufficient, though better estimates of transpulmonary resistance do include quadratic terms characteristic of a turbulent behaviour (see section 2.2.2).

The larynx is one of the most significant sources of turbulence (inertial pressure loss) in airways (Wood et al, 1976; Peslin and Fredberg, 1986). In a healthy adult the larynx will not produce large pressure losses under normal breathing conditions. However, in croup the pressure drop across the larynx dominates. Therefore, the DuBois three element model will have to be modified to account for that extra turbulent effect. Figure 3.4 shows the modified three element DuBois model.

Appendix C shows that the inertial pressure losses which occur (if assuming the model of figure 3.1) as a result of the momentum transfer between the gas in the glottis and the gas in the vestibule (expiration) or the momentum transfer between the gas in the glottis and the subglottis (inspiration) can be calculated using Bernoulli's equation, that is

$$Pca = 0.5 \cdot \rho \cdot \frac{\dot{V}^2}{Ag^2} \cdot \qquad (3.13)$$

where: Pca - convective acceleration (kinetic pressure) of subglottis

ρ - density of air

$\dot{V}$ - volume flow

Ag - cross sectional area of the subglottis.

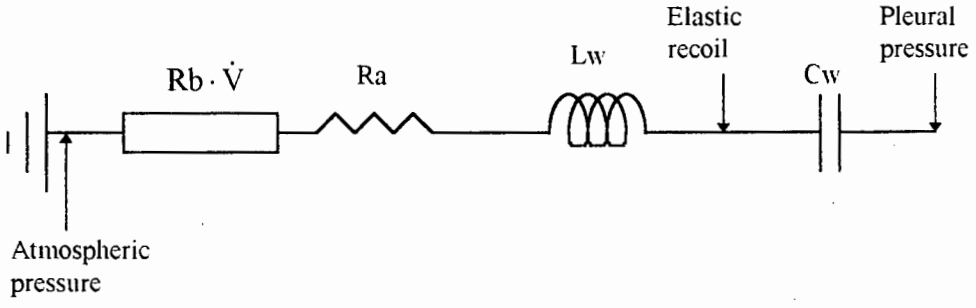

Fig 3.4 The modified three element DuBois model. The resistance Ra, the inductance Lw and compliance Cw are all explained in section 2.3.1. The $Rb \cdot \dot{V}$ term is the resistance representing the inertial pressure loss under conditions of turbulence. Note that the pleural pressure changes are approximately equal to changes in the intrathoracic pressure, which can be measured using an oesophageal balloon. Also, it is important to note that the ground potential is a relative indication of the reference point. In fact the atmospheric pressure (ground potential) may be exchanged with the pleural pressure as long as the sign of the pressure and the flow values is also changed accordingly. In Appendix G the author uses the literature convention in which the ground potential and the pleural pressure are exchanged.

As the area Ag in equation 3.13 becomes smaller, assuming constant volume flow, the contribution of Pca to the total subglottal pressure increases. Since the human body needs a certain amount of oxygenation over a specific time, children will obviously try to maintain the level of flow necessary to sustain minimum metabolic requirements. This means that the child will attempt to sustain the same volume flow as a normally breathing, healthy child. However, the effort (driving pressure) necessary to maintain such a flow will be significantly greater in children with croup then in our non-croup or intubated patients. Indeed, the maximum flow

of the child with croup, prior to intubation, is not much lower than the maximum flow of the same child after intubation. However, the driving pressure produced by the patient with croup before intubation is much larger then the driving pressure produced by this patient after the insertion of the endotracheal tube (see Chapter 5). This means that, in croup, the subglottal kinetic pressure (Pca) may be almost equal to the total subglottal pressure relative to atmospheric pressure. Since flow in the larynx is predominantly turbulent, Pca may further be approximated by equation 3.14:

$$Pca \sim Rb \cdot \dot{V}^2 \qquad (3.14)$$

where: $Rb \cdot \dot{V}$ - is the inertial term shown in figure 3.4

$\sim$ - approximately equal to.

Equation 3.15 shows a mathematical representation of figure 3.4

$$P_{pleural} = 0.5 \cdot \rho \cdot \frac{\dot{V}^2}{Ag^2} + Ra \cdot \dot{V} + Lw \cdot \frac{d\dot{V}}{dt} + Pc \qquad (3.15)$$

where: $P_{pleural}$ - pleural pressure (driving pressure) relative to the atmospheric pressure

$\dot{V}$ - flow

Ag - subglottal cross sectional area

Ra - total respiratory laminar flow resistance

Lw- inertance of the chest wall and gas inertance.

Pc - pressure drop due to the lung wall and chest compliance as well as the compliance of the air in the lungs

3.2.2 Computer model

Equation 3.15 describes the dynamics of the respiratory system in terms of the modified three element DuBois model. This equation is the basis of the MATLAB computer programme presented in Appendix F, which allows us to compare the theoretical flow, calculated from the measured pleural pressure, with a true (measured) flow. However, it should be obvious that the prior knowledge of all components of figure 3.4 is a necessary requirement to solve for the flow in equation 3.15. Otherwise, there would be a situation of one equation with four unknowns (Ra, Lw, Ag and Pc in equation 3.15) which cannot be solved. Therefore, some kind of a best-fit approach towards the measured data is necessary. In this approach, the values of the components of figure 3.4 are adjusted until the best-fit is achieved between the calculated flow and the measured flow. Ideally, one would like to have a model in which the number of variables, to which different values have to be assigned, is as small as possible. Also, the values of the variables of such a model must be restricted to lie within a physiological range (that is the values of the components of figure 3.4) and must be reasonable in comparison with the results produced by researchers in the field of lumped component airway modelling (DuBois et al, 1956; Jackson and Lutchen 1987).

The modified three parameter DuBois model described above can be used to calculate the flow both in inspiration and expiration (Appendix F). It is likely that the average compliance, Cw of figure 3.4, during expiration will be equal to the average compliance during inspiration (Lanteri and Sly, 1993). It is also probable that the average inertance Lw will be identical during both inspiration and expiration (Lanteri and Sly, 1993). However, the average airway resistance Ra of figure 3.4 is known to be different in expiration to its value during inspiration (Fry

et al 1954). In healthy individuals the resistance caused by turbulence is mainly in the large airways when flows are the largest and the dimensions are the greatest. Since the original DuBois model (model without turbulence) worked reasonably well for healthy adults, the inertial losses are probably insignificant when compared with Ra. However, in children with croup, laryngeal inertive losses dominate, and the inertive losses in other airways as well as losses due to Ra become negligible. Therefore, the subglottal cross sectional area Ag, in equation 3.15 will determine the flow during tidal breathing in patients with croup (assuming that there is no maximum effort), while the Ra will largely determine the value of tidal flow in healthy or intubated children. All the lumped parameter models assume a constant airway area over respiratory cycle. In order to apply this theory, it was therefore necessary to use an average area for the subglottis. Our videos showed that the subglottal area does change slightly during the respiratory cycle but this was negligible in most of our patients. It has thus been assumed that the subglottal area is constant, and therefore the same value has been used to represent the subglottal area during inspiration as has been used during expiration.

3.2.3 Patients

The laryngeal inertial resistance will, according to the theory presented, dominate the mechanics of patients with croup. However, it is unlikely that the total compliance and the total inertance will be significantly different in the same child before and during infection. The author also hypothesises that if the larynx is the major source of turbulent flow in croup (Chernick, 1990), then the linear resistance (Ra in figure 3.4) will also be relatively unaffected by croup. Therefore, if one fits the average compliance Cw, inertance Lw and resistance Ra to the three element model of a healthy child, then one should obtain similar results if the same

child becomes a patient with croup. The major difference is in the value of the Rb term of figure 3.4. The value of the Rb term is inversely proportional to the smallest airway's cross sectional area - in our case the subglottal area Ag. For healthy patients one can use a value for Ag of 7 mm^2 which is approximately the cross sectional area of the endotracheal tube used to intubate children with severe croup. The reader should be cautioned, however, that the value of 7 mm^2 is most likely to be an underestimate. Indeed, if one assumes that the subglottal cross sectional area has an elliptical shape then the dimensions of the aperture of the healthy infant's larynx presented by Wolfsdorf and Swift (1978) should give the subglottal cross sectional area a value of 12 mm^2. However, a value of 7 mm^2 for Ag is sufficient to allow children to breathe normally (this may be confirmed from flow pressure data of intubated children).

The compliance, inertance and linear resistance, as was mentioned earlier, should not change significantly in a child before and during croup infection. On average, these parameters will probably be very similar in different children within the age group involved in this investigation (Lanteri and Sly, 1993). Thus, it should be possible to use the average values of compliance, inertance and linear resistance obtained from the best-fit data of healthy children and apply these three parameters to children with croup. To analyse these patients with our model, one needs to know in advance the approximate values of the subglottal cross sectional area, linear resistance and the total compliance. It is possible to roughly estimate the subglottal cross sectional area with the assumption that turbulent flow predominates in the larynx with croup (Chernick, 1990) and that there is very little pressure recovery in the subglottis. In this case one can use equation 2.11. Finally, the value of the inertial resistor coefficient Rb in children with croup could then be obtained from the estimated cross sectional area.

4. Materials and methods of measurement

It was not possible to obtain both pressure and flow as well as laryngoscopic measurements on the same patient with croup. However, a database of pressure and flow measurements performed on a group of twenty patients with croup, as well as cross sectional X-rays of the larynx from a second group of another twenty patients with croup were available. In addition to this data laryngoscopic video recordings of the glottis and the subglottis in another five cases with croup were made for this project. The information was analysed as follows:

1) The pressure and flow database was used to calculate the minimum cross sectional area and the maximum flow according to the theories of flow limitation. This database was also used to estimate the parameters of the lumped component model which in turn was used to calculate the flow from the pressure during both inspiration and expiration (see section 4.1).

2) The videos made during laryngoscopy allowed to estimate the degree of collapse in the airways of typical patients with croup, as well as an estimate of the minimum cross sectional area in these patients (see section 4.2).

3) The dimensions measured from X-rays were used to calculate the cross sectional area along the length of the airways of typical children with croup, from the larynx to the trachea. In this way the rate of change of area with distance along the airway could be calculated (through the area of subglottic swelling). An estimate of the minimum subglottal area in these children with croup could also be obtained from the X-rays (see section 4.3).

All measurements were performed by an experienced paediatrician, who is also the project initiator and supervisor, and his medical staff, according to the ethical requirements of the Red Cross War Memorial Children's Hospital.

4.1 Pressure flow data

The pressure and flow database consists of the intrathoracic pressure change and volume flow during tidal breathing in groups of croup, intubated and non croup children.

4.1.1 Pressure

The intrathoracic pressure was measured with a saline filled catheter which was inserted via the nasal passages into the intrathoracic oesophagus. The oesophageal pressure change was then assumed to equal the intrathoracic pressure change (Stocks et al, 1996). The pressure was converted into an electrical signal using a pressure transducer (HP 1290A OPT006), which was amplified and recorded on paper tape. Finally, the recording was digitised at intervals of 20 milliseconds.

The under- or overdamped response of a catheter is always a potential source of error (Stocks et al, 1996). This means, that the measured signal may be erroneously modified by the catheter. In order to eliminate the catheter's effect on the pressure measurements, the Autoregressive Digital Technique for Pressure Restoration developed by Boonzaier (1978) was employed. Equation 4.1 (see Boonzaier, 1978) describes the above technique's recurrence relationship which extracts the true signal y from the measured signal x. The resonant angular

frequency ω and the damping constant β in equation 4.1 are calculated from figure H.1 of Appendix H which shows the response of our catheter to a step signal at the input.

$$y(n) = (x(n) - 2 \cdot e^{(-\beta \cdot T)} \cdot \cos(\omega \cdot T) \cdot x(n-1) + e^{(-2 \cdot \beta \cdot T)} \cdot x(n-2)) / K \qquad (4.1)$$

where y - true signal

x - measured signal

n, n-1, n-2 - current and previous sample numbers

T - one sampling interval (0.02 [s])

ω - resonant angular frequency (90.3 [rad/s])

β - dumping constant (23.11 [rad/s])

K - DC value = $1 - 2 \cdot e^{(-\beta \cdot T)} \cdot \cos(\omega \cdot T) + e^{(-2 \cdot \beta \cdot T)}$

The values presented above were obtained from the step response of the catheter used in this project (see figure H.1). In addition Fast Fourier Transform (FFT) analysis was performed on the patients' pressure data and was found that the highest significant frequency does not exceed 2Hz or 12.5 rad/s. This means that the Nyquist sampling criteria (our sampling rate is 50Hz) is preserved. The Nyquist sampling criteria is important because if the signal had to be sampled below this rate aliasing would result. It is equally important to avoid the region around the natural resonant frequency because the amplitude and the phase of the signal in this frequency region is primarily determined by the system response and not by the input signal. Nevertheless, equation 4.1 is designed to correct the amplitude and the phase of the signal from any unwanted artefacts which may result from the catheter response characteristics. For this reason equation 4.1 is used to correct the pressure data in the computer algorithms (see Appendix F).

4.1.2 Flow

Each patient wore a face mask which was attached to a plastic tube leading to a Fleish pneumotachograph. The flow was measured by measuring the pressure difference across the pneumotachograph using a single differential pressure transducer (Sanborn 270). The differential pressure transducer produced an electrical signal which was proportional to the airflow. This was amplified and recorded on paper with an HP 7754D module. The paper recorded flow signal was then digitised at intervals of 20 milliseconds.

The Sanborn 270 has a flat frequency response between 0 and 10Hz.

4.1.3 Phase difference between flow and pressure

Figure 4.1 shows the setup used to investigate the phase difference between the flow transducer and the pressure transducer. This setup consists of a perspex box which has three openings: one for an air balloon and a respirator, and the other two for pressure and flow transducers. To avoid adding extra phase, transducers were placed at the same distance from the axis of the air balloon. The respirator (not shown in figure 4.1) inflates and deflates the air balloon. This produces changes in the volume of the box, which in turn results in changes in the box pressure. Both pressure and flow were then measured with the transducers and finally amplified and plotted against time (using an HP 7754D module not shown in figure 4.1).

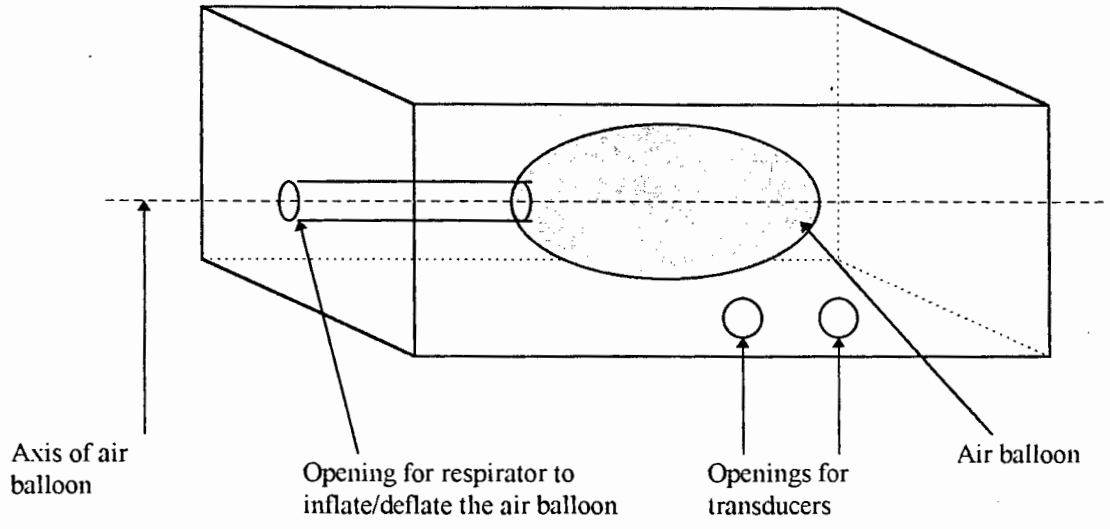

Fig 4.1 The setup used to investigate the phase difference between the pressure transducer and the flow transducer (see text).

Figures H2, H3, H4, H5 in Appendix H show plots of the flow (bottom trace) and the pressure (upper trace) which were produced by a respirator which inflated and deflated the air balloon at 30, 40, 60, 80, 100 and 120 cycles per second.

The graphs shown in Appendix H indicate that there is no significant phase difference between the pressure and the measured flow.

4.2 Laryngoscopy

The bronchoscopic telescope used is a HOPKINS telescope of 4mm external diameter. It is connected to a fibre-optic cable attached to the light source and a camera (Sony). The signal from the camera is displayed on a television set (Sony) and recorded on video cassette using a video recorder (Sony).
In order to perform the laryngoscopies, the bronchoscopic telescope was inserted into the pharynges of patients while they were inhaling anaesthetic gases

administered through a tube into the nasopharynx. Typically these anaesthetic gases would be 50% nitrous oxide, 45% oxygen and 5% halothane.

4.3 X-ray

X-ray pictures were taken of the larynx of a group of twenty patients with croup. Only eight of the twenty patients had X-rays with well-defined, both anterior-posterior (coronal) and lateral, views of the larynx. The remaining twelve patients were analysed with anterior-posterior views only. Only one of these twenty patients also had pressure and flow measurements. It was simply too difficult for medical staff to perform all measurements on children who required immediate drug treatment or intubation. Therefore, not all tests could be performed without the possibility of endangering the life of these patients. This is also the primary reason why the bronchoscopic telescope was used merely as a display method rather than as the measuring device of the subglottic cross sectional area.

4.3.1 X-ray digitisation

All X-rays were digitised using a reflex microscope (Prior S2000), a computer and an interface which translates microscope readings into a digital signal. The X-rays were placed on the microscope table and illuminated. Then an optical dot was placed on the boundaries of the airway and the position of the dot was digitised using a TRUE BASIC programme. In this way the outline of the airway, along its course, was obtained in each of the patients. These measurements were used to calculate the cross sectional area along the course of the airway.

4.3.2 Cross sectional area calculations

X-rays offer only a two dimensional view of the investigated structure. Even with both the anterior-posterior and the lateral views of the larynx it is very difficult to precisely determine the cross sectional area of the airway. Therefore, it is assumed that airways are elliptical and that the width of the larynx in the lateral view is constant (see Chapter 5 and 6). The elliptical shape of the cross sectional area was chosen based on evidence from the videos made during laryngoscopies of children with croup, which showed that the subglottic structure is more slit-like than circular. The assumption that the width of the larynx in lateral view may be assumed constant is investigated in Chapter 5.

Figure 4.2 graphically explains the method employed to obtain data for the cross sectional area calculations, and it also shows how this area was calculated along the length of the larynx.

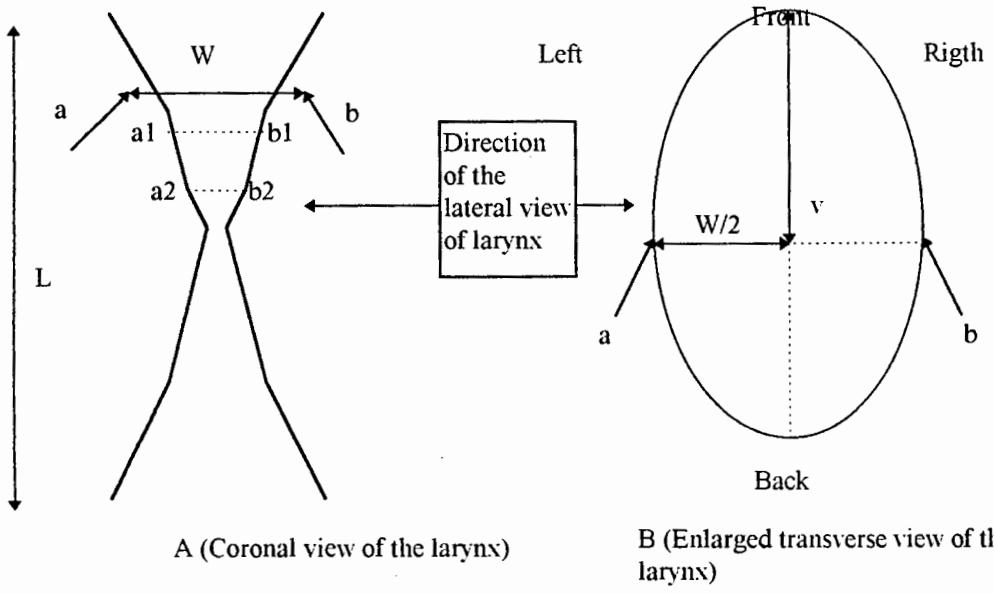

A (Coronal view of the larynx)

B (Enlarged transverse view of the larynx)

Figure 4.2 An idealised view of a coronal section through the larynx taken from an X-ray (drawing A). W is the width calculated from points a to b. L is the length over which a series of measurements a1, b1, a2, b2 were performed with the reflex microscope. The length v of the transverse section of the larynx (drawing B) is assumed to be constant over length L and the geometry of the airway is assumed to be elliptical (see discussions). The cross sectional area in transverse view (B) at any point a and b of a coronal view (A) equals $0.5 \cdot W \cdot v \cdot \pi$ (Swokowski, 1988).

5. Results

The following results are presented in this chapter:

- The area calculated from X-rays of the larynx of children with croup (aimed at investigating the lack of pressure recovery);

- The flow calculated from the wave-speed formula; and

- The flow estimated from the lumped component model.

5.1 The cross sectional area from X-rays

X-rays of twenty patients with croup were used in this analysis, eight of whom had well-defined coronal and lateral views of the larynx and twelve had coronal views only. Only one of these patients had pressure and flow measurements as well. Table 5.1 shows the results of this patient's cross sectional area calculated from the digitised X-ray (see section 4.3). Twenty two samples were measured on the coronal view (using a reflex microscope) over a distance of 1.5 cm from the glottis towards the trachea. The lateral view was not available, and so, as a worst case approximation, the anterior-posterior axis of the airway was assumed to be, on average, 6.23 mm in length (see discussion).

Distance from the glottis towards the trachea [mm]	Cross sectional area calculated according to figure 4.2 [mm^2]
0	4.6 (glottis)
1.2	5.5
2.4	5.7
4	6.4
5.4	8.4
6.8	11
8.4	12.4
9.1	15.2
12.1	17.9
13.4	19.5
15	21.6 (trachea)

Table 5.1 Cross sectional areas calculated from points digitised from an X-ray picture of the larynx of a single patient with croup. Samples were taken over a distance of approximately 1.5 cm from the glottis towards the trachea.

Figure 5.1 shows a graphical representation of Table 5.1 together with the results produced by Jones et al (1975).

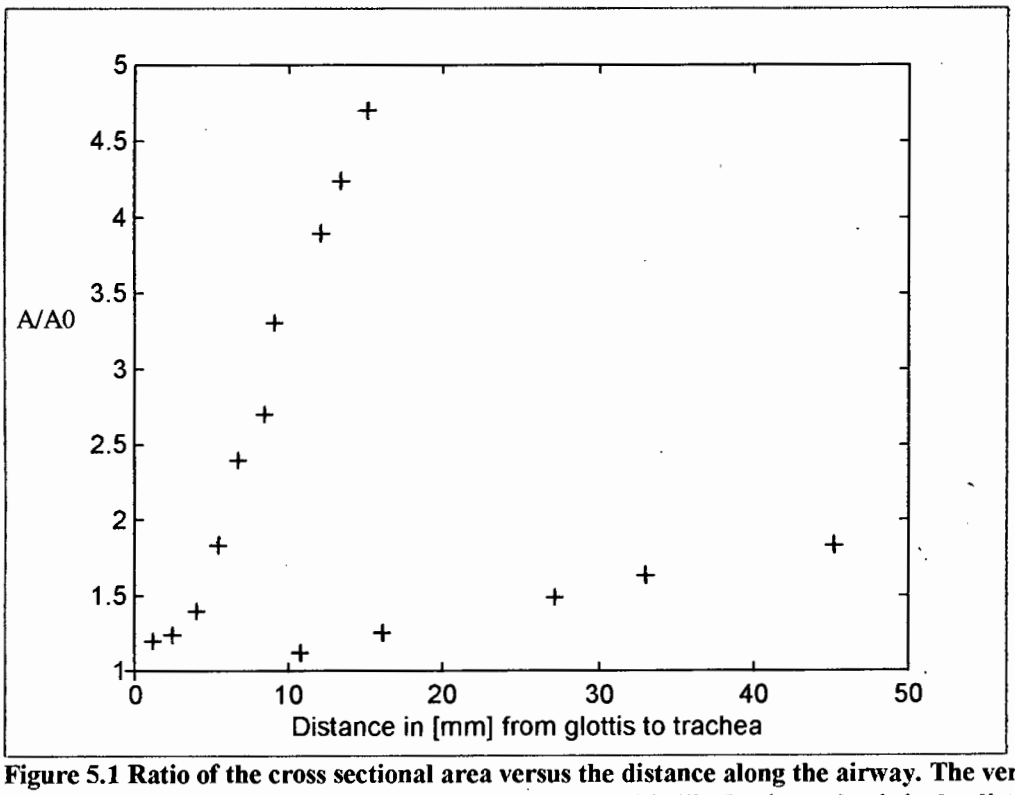

Figure 5.1 Ratio of the cross sectional area versus the distance along the airway. The vertical axis shows the actual area A divided by the minimum area A0. The horizontal axis is the distance in [mm] from the minimum measured area. The blue samples are collected and calculated from an X-ray and the green samples are taken from the Jones study (Jones et al, 1975).

Table 5.2 contains a summary of all the X-ray measurements for our twenty croup patients with X-rays. Also included in this table are the resistances of the airways calculated under the assumption of laminar flow. For this purpose the formula introduced by Boussinesq (Rayleigh, 1929) was used which calculates the resistance caused by laminar flow in elliptical ducts.

$$R = \frac{4 \cdot \mu \cdot ((W/2)^2 + v^2) \cdot 1}{\pi \cdot (W/2)^3 \cdot v^3} \qquad (5.1)$$

where : R - resistance to laminar flow

W/2 and v - minor and major axis of an ellipse (see figure 4.2)

1 - length of airway section over which a and b are constant

μ - viscosity of air

Please note that the resistance of each small length between successive measuring sites is calculated using equation 5.1, and these resistances are summed to produce the total resistance which is included in table 5.2.

Patient (20)	Smallest cross sectional area $[mm^2]$	Average lateral width [mm] (anterior-posterior distance)	Resistance to laminar flow $10^5[\frac{Pa}{m^3 \cdot s^{-1}}]$
W	4.58	5.79 ±0.729	2.35
Fi	5.6	8.36 ±0.96	2.28
Ch	2.2	6.23 ±0.55	11.04
Jj	6.39	6.61 ±1.23	1.07
K	13.21	7.02 ±0.73	0.19
Mbe	4.81	6.14 ±0.27	0.62
U	6.03	5.65 ±0.72	0.88
Ab	4.25	6.27 ±0.11	1.16
Fe	4.6	6.23	2.22
Pi	4.5	6.23	1.41
L	2.77	6.23	4.33
C	4.23	6.23	1.63
Le	2.34	6.23	1.57
Mb	5.17	6.23	1.77
Mi	7.48	6.23	0.60
Ph	1.39	6.23	28
Tsh	4.45	6.23	0.86
Tu	2.77	6.23	1.80
V	5.35	6.23	1.18
Z	6.88	6.23	0.76

Table 5.2 The smallest area is calculated from the smallest visible dimensions of the X-ray. Therefore, this may not be the smallest true area of the patient. Average lateral length is the average width of the airway with its standard deviation, which is viewed from the side (v distance in figure 4.2 B). The blue colour indicates all those patients whose lateral view could not be measured (6.23 is the average calculated from average lateral lengths of patients whose lateral view could be measured). All areas are assumed to have an elliptical geometry. The last column represents the laryngeal resistance which is calculated for the case of laminar flow only (see equation 5.1).

5.2 Wave speed limitation

Although flow and pressure data from twenty patients was available only those twelve patients who showed a clear pattern of flow limitation were included in the analysis which follows.

Section 5.2.1 analyses the pressure flow data of these patients with croup using software which was written for this purpose in MATLAB (Appendix F). The aim of the computer programme is to compare the maximum flow, calculated from equation 3.2, with the maximum flow taken directly from measurements. Figure 5.2 graphically represents the algorithm employed in the programme.

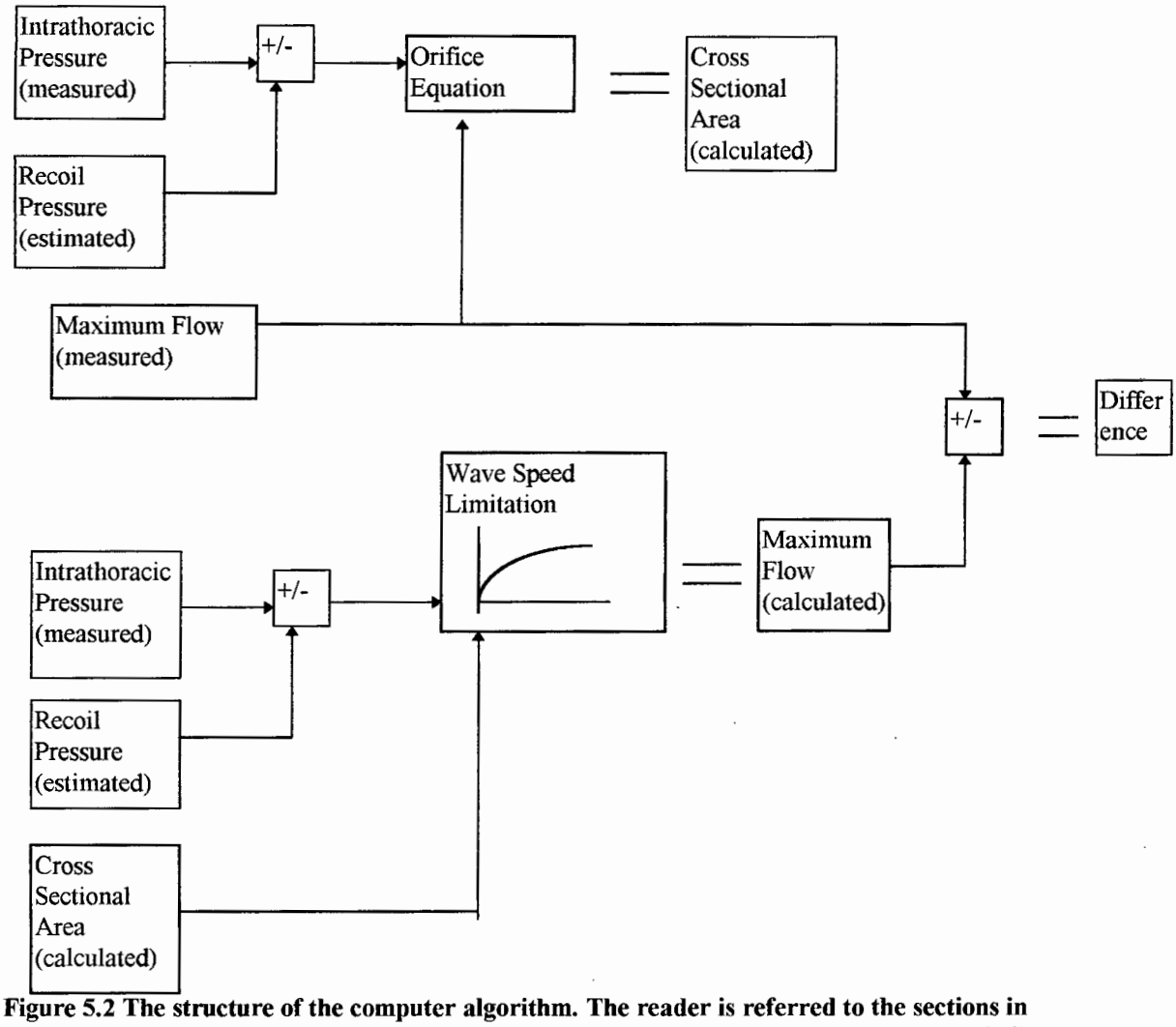

Figure 5.2 The structure of the computer algorithm. The reader is referred to the sections in literature review and theory development in order to understand the various stages in this figure. It is important to note that the maximum flow does not have to have the highest value (see Literature review).

Section 5.2.2 contains a graphical comparison between croup and non-croup patients, as well as between croup, non-intubated patients and croup, intubated patients.

5.2.1 Patients with croup

Two methods are employed to calculate the maximum flow:

1) The compliance of the airway is estimated graphically as described in figure 3.3, and used to calculate the maximum flow.

2) A typical Young's Modulus is assumed for the wall, from which the compliance of the airway, and hence the maximum flow, can be calculated for each patient.

5.2.1.a Calculated compliance

Figure 5.3 shows the pressure-flow and pressure-area relationship for the patient with croup whose X-ray was investigated in section 5.1. Pressure and flow were measured while the area was calculated from equation 3.8 (see discussion). The straight line is the slope estimated from linear regression. Since the start of the flow limitation cannot be chosen objectively (see Literature Review), the slope (dP/dA) is also based on a subjective estimate. The arrow indicates a point which is assumed to represent the start of flow limitation.

The maximum flow is calculated from equation 3.2 where $\frac{dP}{dA}$ is represented by the slope of the line in figure 5.3 and the area is directly taken from the point indicated by the arrow (flow limiting point).

The calculated and measured maximum flows are 133 ml/s and 139.6 ml/s respectively, which represents a difference of -4.7% of the maximum inspired flow. Figure 5.4 shows another inspiratory cycle for the same patient. In this case the calculated and measured maximum flows are 135.9 ml/s and 127.3 ml/s respectively, which represents a difference of 6.7% of the maximum inspired flow. Figure 5.5 and 5.6 show examples of the inspiratory cycles of two further patients with croup. The difference between the calculated and measured inspiratory flow was less than 10% of the maximum inspiratory flow in both cases. The average absolute difference between the calculated and measured maximum flows for all patients in this study was 12%, which is between the median (11.3%) and the 90th percentile (18.3%).

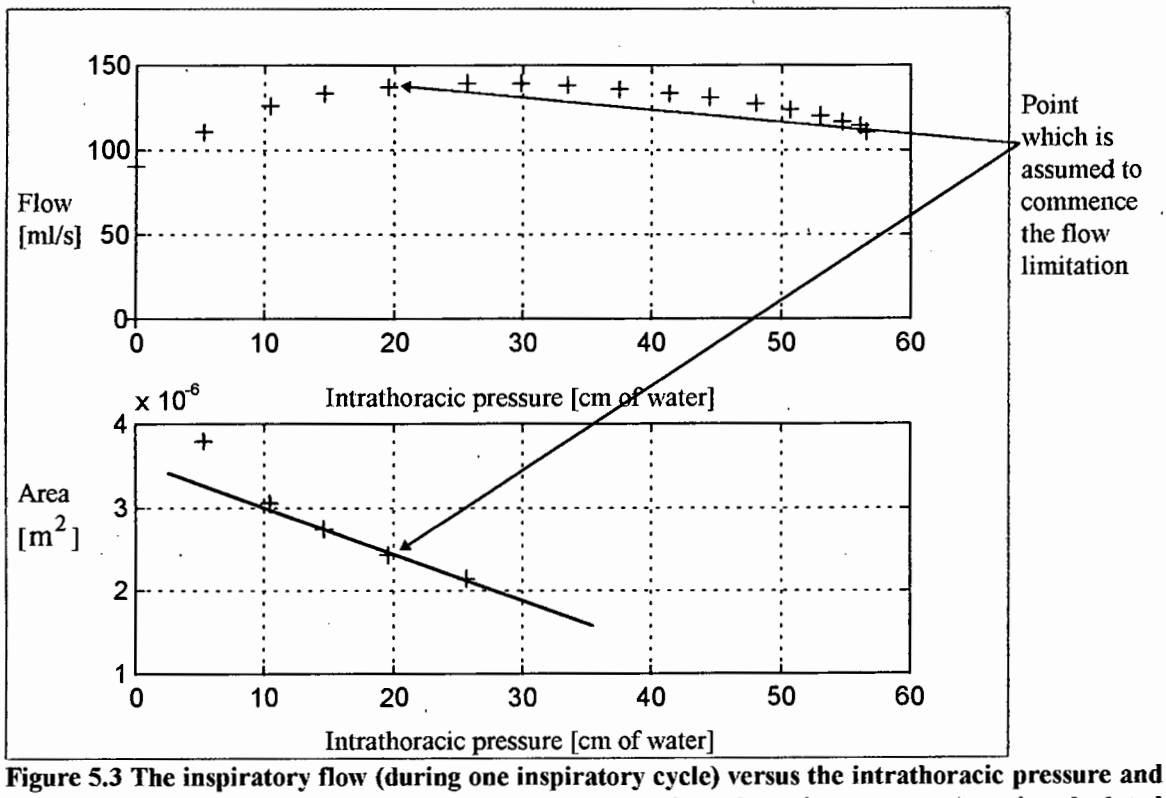

Figure 5.3 The inspiratory flow (during one inspiratory cycle) versus the intrathoracic pressure and corresponding subglottal cross sectional area versus the intrathoracic pressure. Area is calculated from equation 3.8. The line indicates an average stiffness at the point which is assumed to commence flow limitation (arrow). The first two points and the points beyond flow limitation site in the flow pressure graph are disregarded from the area calculation (see discussions).

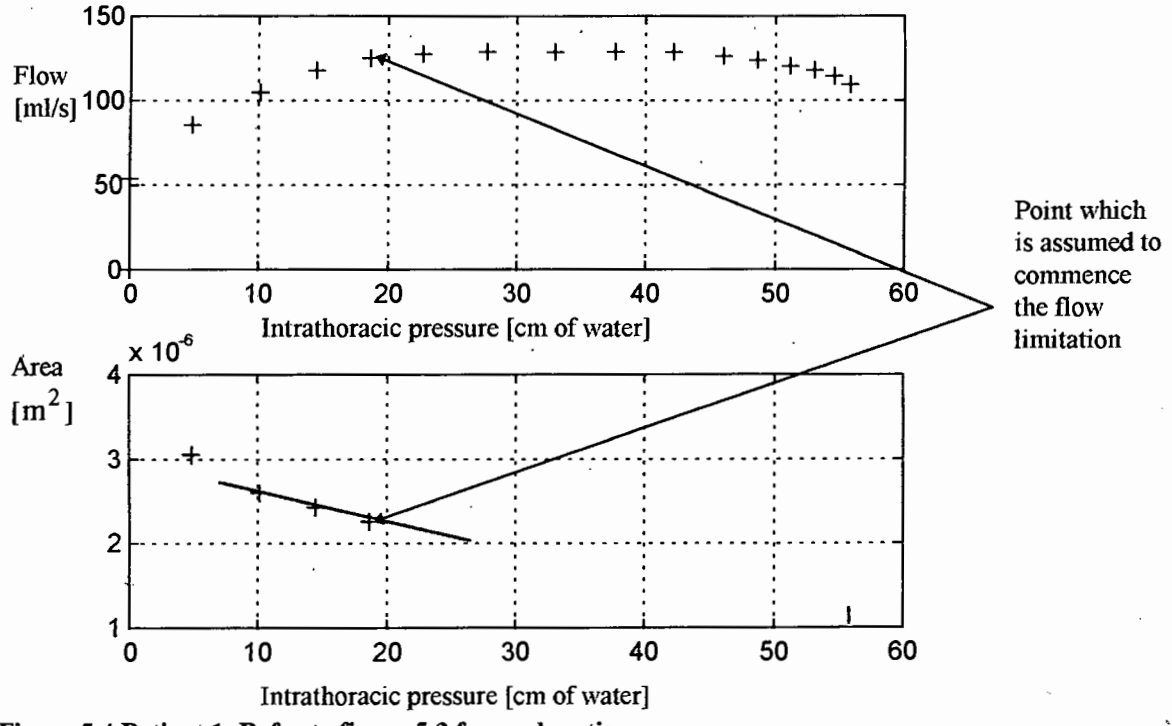

Figure 5.4 Patient 1. Refer to figure 5.3 for explanation.

Figure 5.5 and 5.6 show data of two different patients who were diagnosed with severe croup.

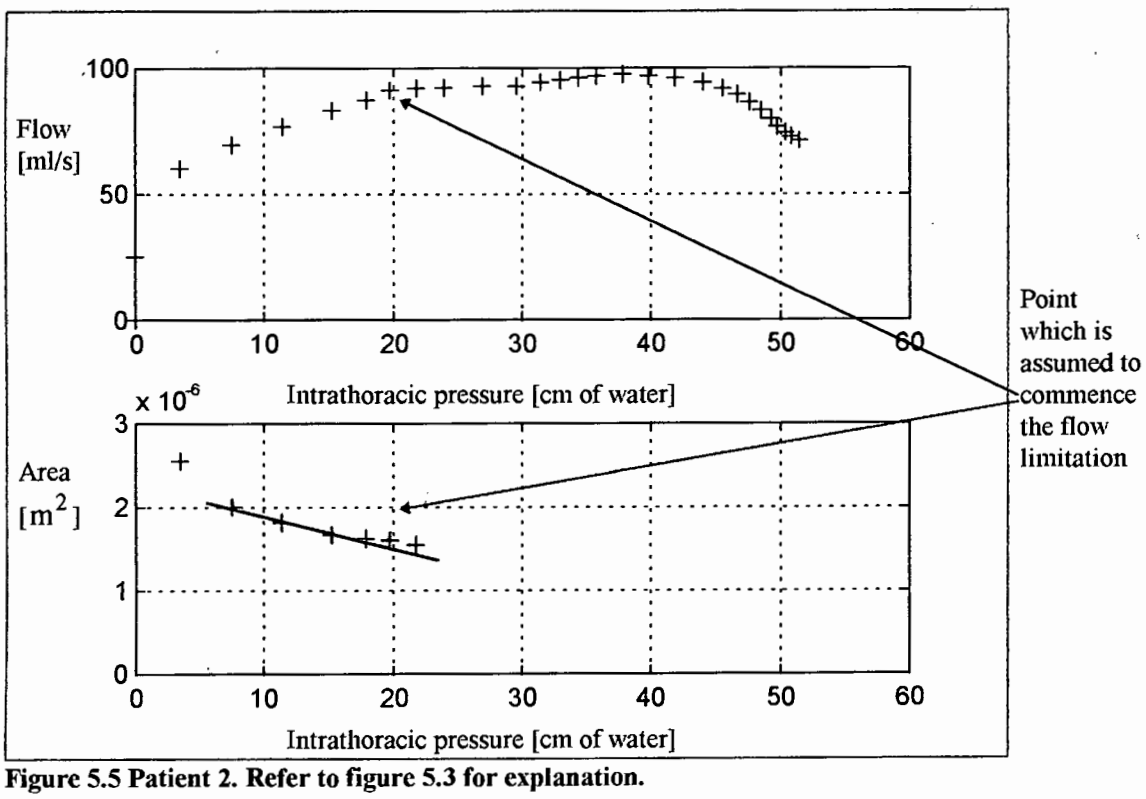

Figure 5.5 Patient 2. Refer to figure 5.3 for explanation.

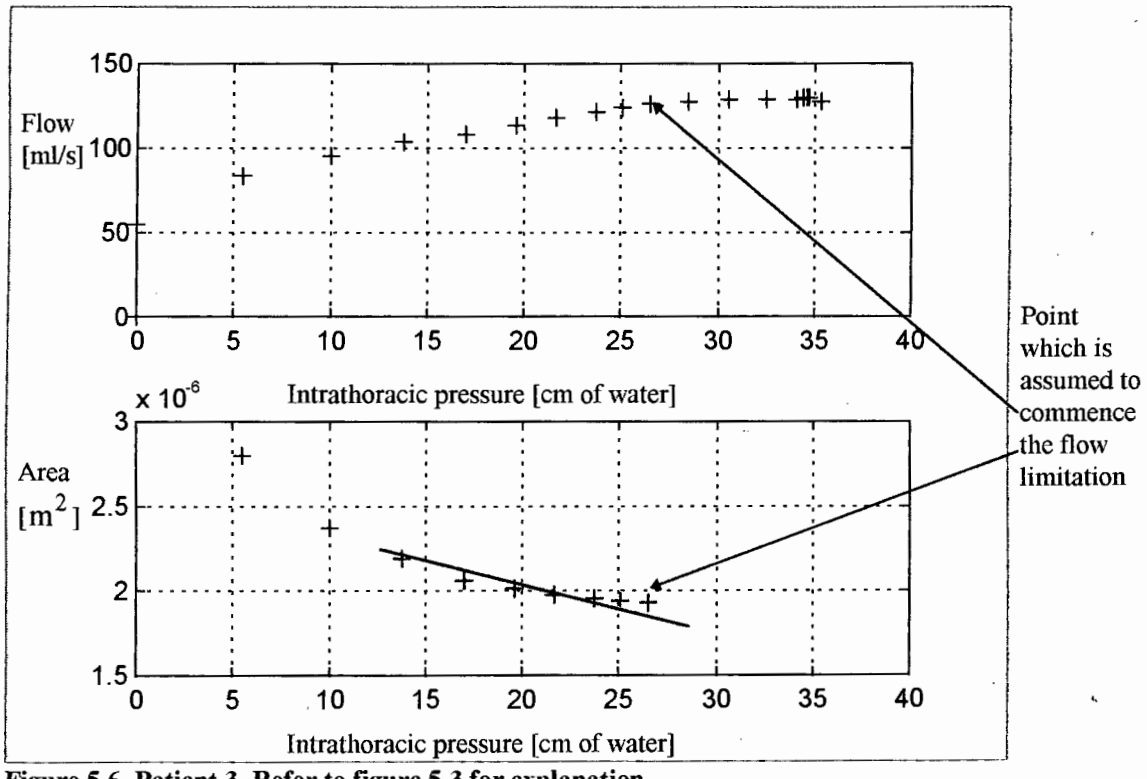

Figure 5.6. Patient 3. Refer to figure 5.3 for explanation.

Figure 5.7 shows the measured maximum flow plotted against the calculated maximum flow (red samples). The green line represents the best linear fit through the data points. The correlation coefficient between the calculated and measured maximum flows is 0.88 and the slope of the linear fit is 0.98 which are significant at the $p<0.05$ level (nonparametric test by Conover) (Daniel and Terrell, 1989) - see discussion.

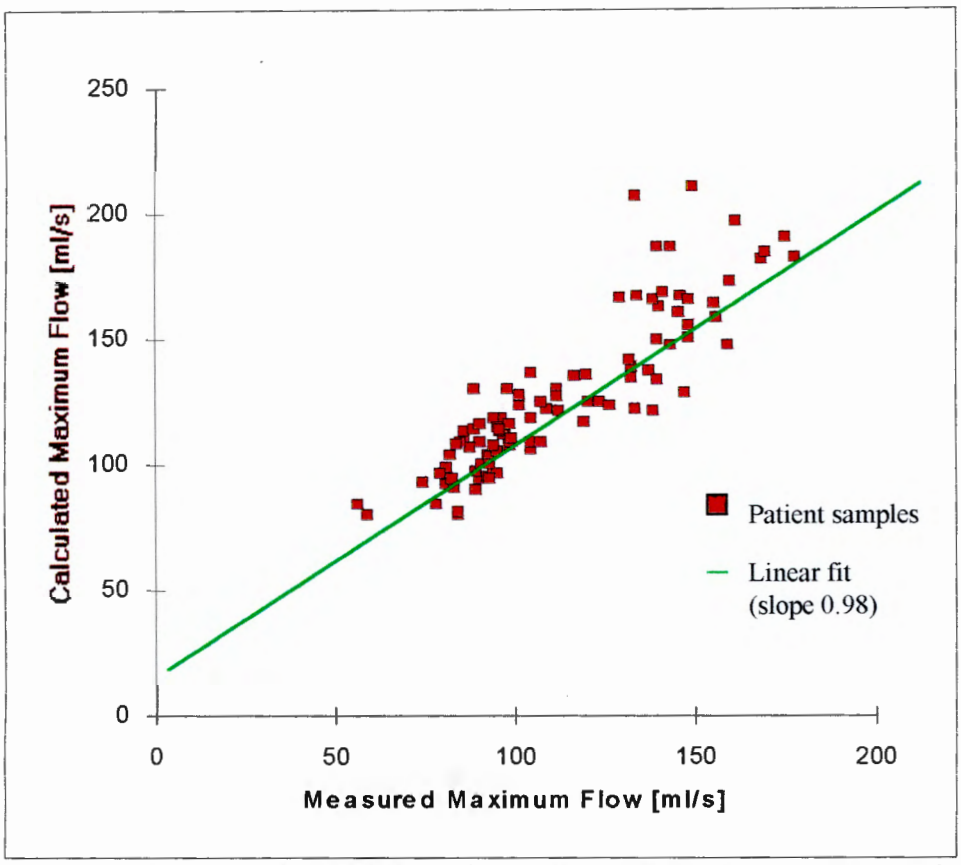

Figure 5.7 The measured maximum inspiratory flow versus calculated maximum inspiratory flow (red squares). Each point represents one inspiratory cycle of one of the twelve patients. At most three inspiratory cycles were analysed for each of the patients. The green line represent the best-fit line. The correlation coefficient is 0.88 with a $p<0.05$

5.2.1.b Assumed Young's Modulus

In order to determine the Young's Modulus E, it is necessary to choose a patient whose calculated area and compliance are not affected by muscular action or mucous flow. For such patients we estimated the Young's Modulus to be 10^5[Pa] which, incidentally is similar to that for arterial wall. The wall compliance Cw, calculated from the above Young's Modulus (see equation 3.11) for all twelve patients produces, on average, the smallest difference between the calculated and the measured maximum flow (this may be shown empirically). Figure 5.8 shows a graph of calculated versus measured maximum flows for a constant Young's

Modulus E=10^5[Pa]. The correlation coefficient between the calculated and measured maximum flow is 0.82, with a $p<0.05$.

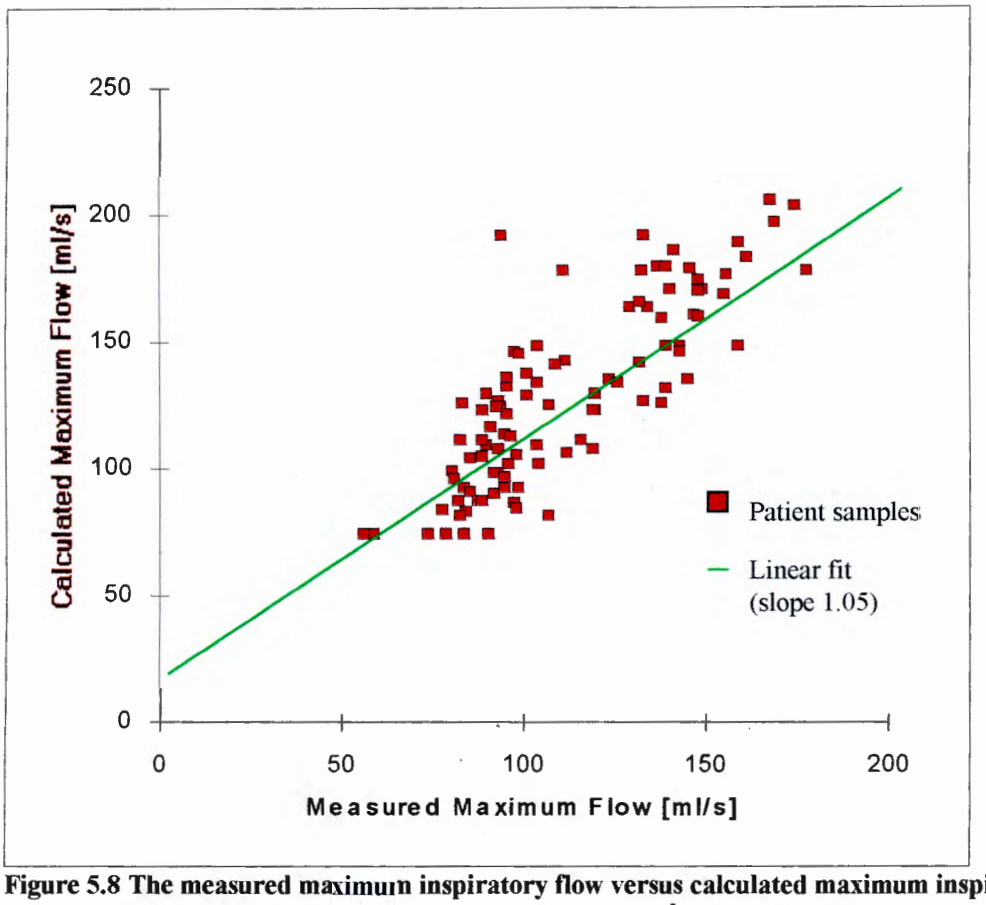

Figure 5.8 The measured maximum inspiratory flow versus calculated maximum inspiratory flow (red squares) using a constant Young's Modulus of E = 10^5 [Pa]. Each point represents one inspiratory cycle of one of the twelve patients. At most three inspiratory cycles were analysed for each of the patients. The correlation coefficient is 0.82 with a $p<0.05$.

5.2.2 Croup, non-croup and intubated croup patients

This section graphically compares the inspiratory pressure-flow data of patients with croup with pressure-flow data of non-croup and intubated croup patients. Figure 5.9 shows three graphs of patients with croup (green samples), three graphs of non-croup children (blue samples) and three graphs of intubated, croup patients (black samples). Please note that intubated and non-croup children cannot be

analysed according to the method presented in section 5.2.1 because the theory presented in Chapter 3 is applicable only to children with croup.

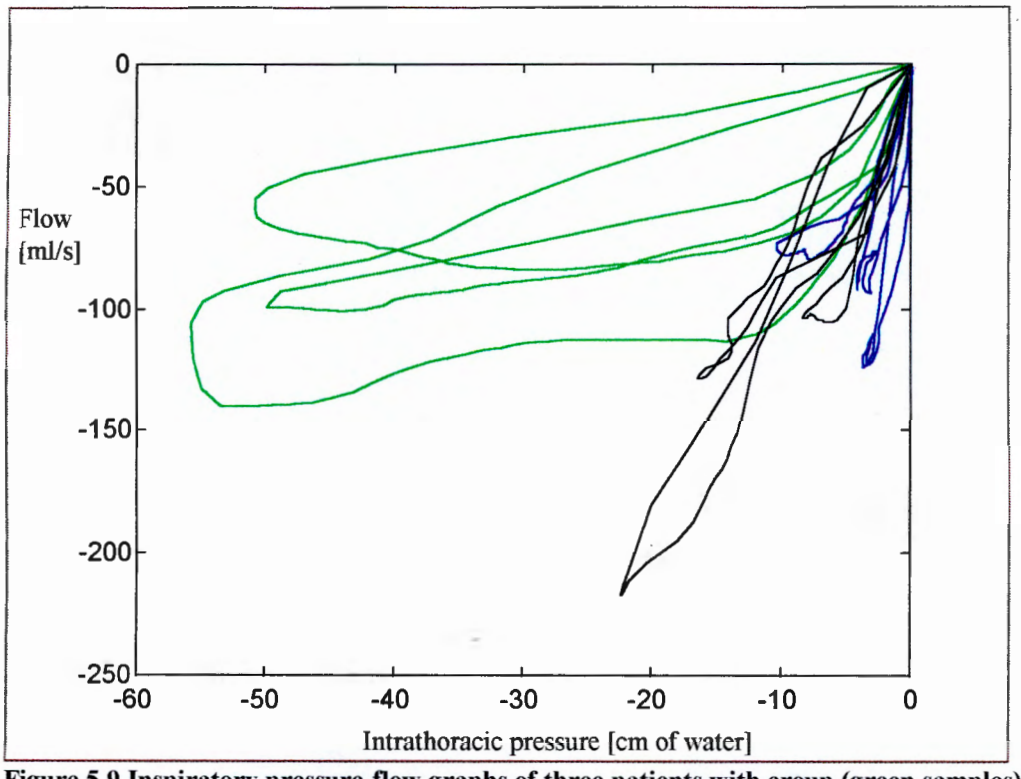

Figure 5.9 Inspiratory pressure-flow graphs of three patients with croup (green samples), three non-croup patients (blue samples) and three intubated croup patients (black samples).

5.3 Lumped component model

The results presented in this section are obtained using a MATLAB computer programme 'lumped' (see source code in Appendix F). This programme is based on equation 3.13. The aim of the programme is to compare the theoretical flow, calculated from the measured pleural pressure (using equation 3.13), with the true (measured) flow. Non-croup, intubated croup and croup patients are analysed separately using a modified three element DuBois model.

5.3.1 Non-croup patients

Figure 5.10 represents a single patient's data and shows the flow (blue) which is calculated from the measured pressure and the measured flow (green). The following parameters were estimated, using a method described in section 3.2, to calculate both the flow and the recoil pressure using equation 3.13:

inspiratory linear resistance - $0.022 \cdot 10^{8} [\mathrm{Pa} \cdot \mathrm{s} / \mathrm{m}^{3}]$

expiratory linear resistance - $0.024 \cdot 10^{8} [\mathrm{Pa} \cdot \mathrm{s} / \mathrm{m}^{3}]$

glottal cross sectional area - $10[\mathrm{mm}^{2}]$

total compliance - $1.0 \cdot 10^{-7} [\mathrm{m}^{3} / \mathrm{Pa}]$

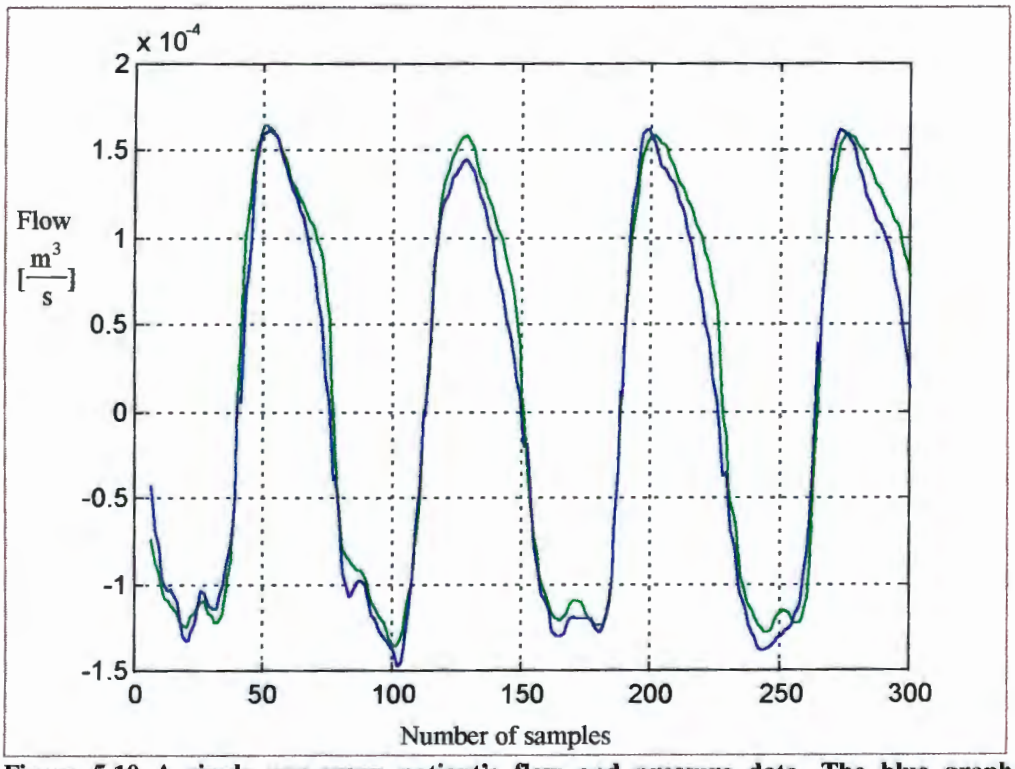

Figure 5.10 A single non-croup patient's flow and pressure data. The blue graph is the flow calculated from the model described in section 3.2 while the green graph is the measured flow. The horizontal axis shows the sample number which represents a sampling period at 20ms; the vertical axis shows the flow. Negative flow values indicate inspiration.

Figure 5.11 represents the relationship between the measured and the calculated (fitted) flow for three different non-croup patients. Again, the green graph represents the measured flow and the blue graph is the calculated flow.

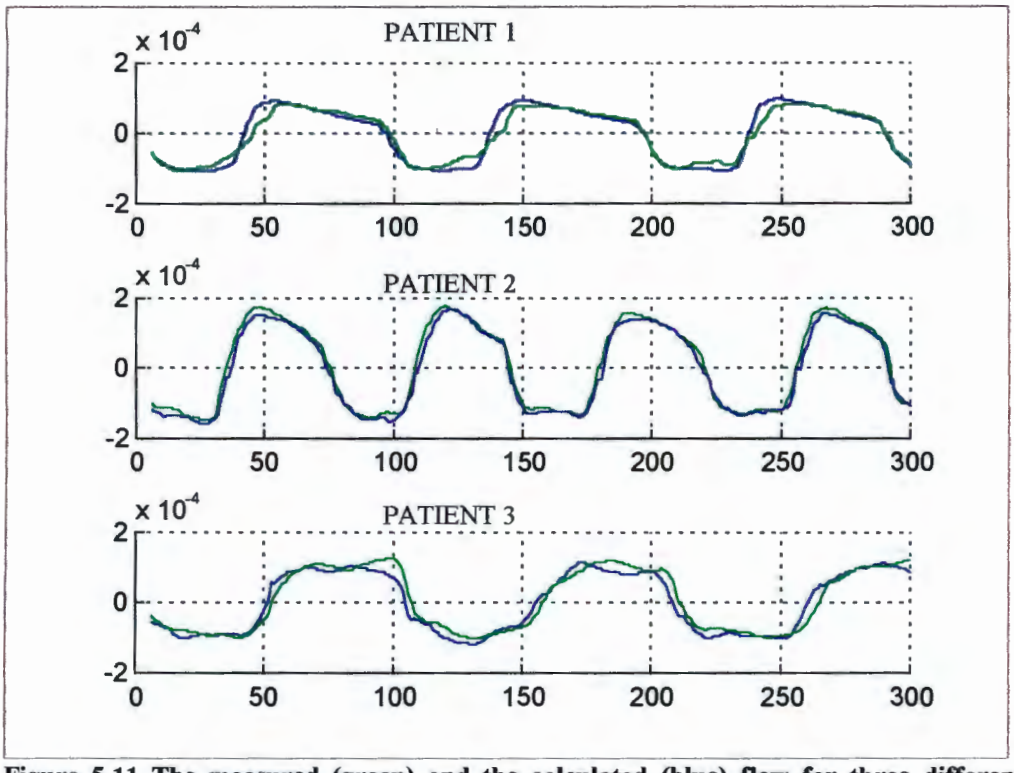

Figure 5.11 The measured (green) and the calculated (blue) flow for three different, non-croup patients. The horizontal axis shows the sample number with a sampling period of 20ms; the vertical axis shows the magnitude of the flow in $[m^3/s]$.

Table 5.3 shows various parameters used to calculate the flows in figure 5.11 (blue graph).

Patient number (refer to figure 5.11)	**Inspiratory linear resistance** $10^8 \cdot [Pa \cdot s/m^3]$	**Expiratory linear resistance** $10^8 \cdot [Pa \cdot s/m^3]$	**Total compliance Cw** $10^{(-7)} \cdot [m^3/Pa]$	**Subglottal cross sectional area Ag** $[mm^2]$
1	0.065	0.075	1.0	16
2	0.024	0.026	1.0	12
3	0.02	0.022	1.3	10

Table 5.3 The inspiratory linear resistance, the expiratory linear resistance, the total compliance and the subglottal cross sectional area used to calculate the flows for the three patients in figure 5.11.

We found that the wall inertance has a negligible effect on results and therefore, Lw was omitted from the analysis. Using Jackson and Lutchen's data (1987) it may be shown that the value of inertance may be increased 1000 times without affecting the calculated flows.

5.3.2 Intubated patients

Figure 5.12 illustrates the data for the measured and the calculated flows for three intubated patients.

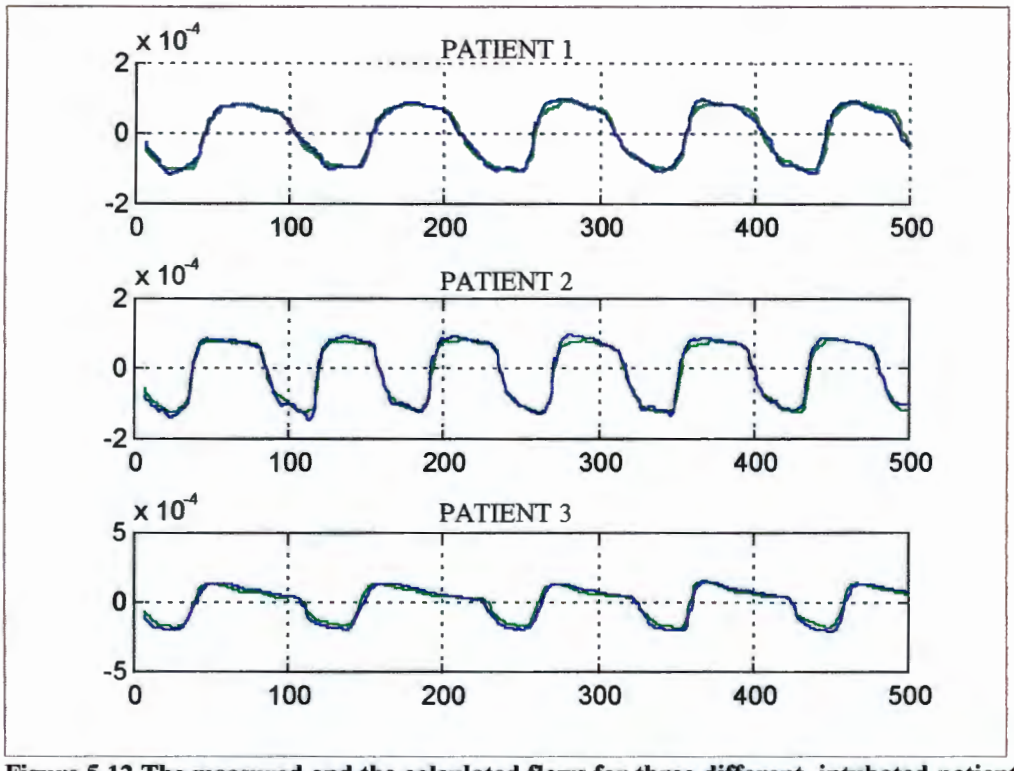

Figure 5.12 The measured and the calculated flows for three different, intubated patients. The green graph represents the measured flow. The blue graphs are the models' predictions (see section 3.2). The horizontal axis shows the sample number for a sampling period of 20ms; the vertical axis shows the magnitude of the flow in $[m^3/s]$.

Table 5.4 shows estimated parameters used to calculate the flows of figure 5.12. The value of 7 mm^2 for the subglottal cross sectional area is the true value for the cross section of the endotracheal tube.

Patient number (refer to figure 5.12)	**Inspiratory linear resistance** $10^8 \cdot [Pa \cdot s/m^3]$	**Expiratory linear resistance** $10^8 \cdot [Pa \cdot s/m^3]$	**Total compliance Cw** $10^{(-7)} \cdot [m^3/Pa]]$	**Subglottal cross sectional area Ag** $[mm^2]$
1	0.06	0.06	1.0	7.0
2	0.1	0.15	1.0	7.0
3	0.06	0.06	1.0	7.0

Table 5.4 The inspiratory linear resistance, the expiratory linear resistance, the compliance and the subglottal cross sectional area used to calculate the flows for the three patients of figure 5.12. Please note that the length of the endotracheal tube is not necessarily the same for all patients and thus the linear resistance for patient 2 is different from the other two patients.

The wall inertance Lw was omitted from the analysis because, as presented in section 5.3.1, Lw has a negligible effect on the calculated flow of figure 5.12.

5.3.3 Patients with croup

Figure 5.13 shows the calculated (blue graph) and the measured (green graph) flows for three patients with croup.

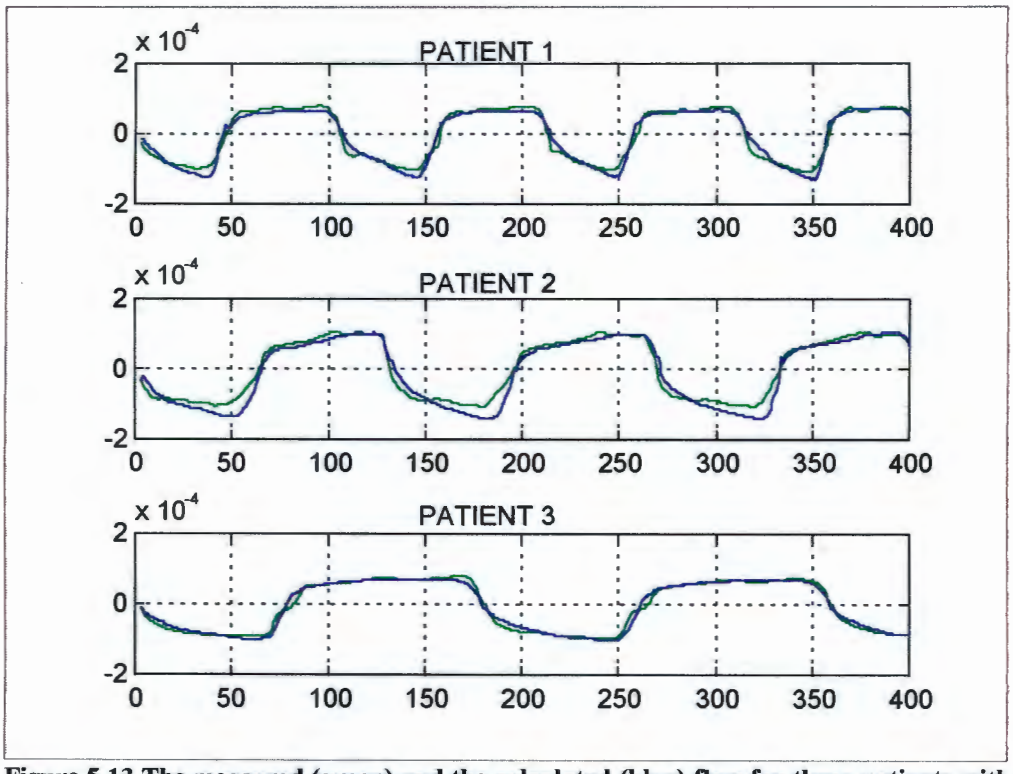

Figure 5.13 The measured (green) and the calculated (blue) flow for three patients with croup. In all cases the compliance is $1.0 \cdot 10^{(-7)} \cdot [\mathrm{m}^3 / \mathrm{Pa}]$ and the linear resistance (in both directions of flow) is $0.06 \cdot 10^8 \cdot [\mathrm{Pa} \cdot \mathrm{s} / \mathrm{m}^3]$ (see discussions). The horizontal axis shows the sample number with sampling period of 20ms; the vertical axis shows the magnitude of the flow in $[\mathrm{m}^3 / \mathrm{s}]$. Cross sectional areas were estimated using equation 3.8.

As in section 5.3.1 and 5.3.2, the wall inertance Lw was excluded from the analysis. Table 5.5 shows estimated parameters used to calculate the flows of figure 5.13. The application of the modified six element model also reveals that the value of C1 (shunt compliance in figure 3.3) proposed by Jackson and Lutchen in their experiments on dogs, is a negligible quantity and produces identical results to the modified three element model.

Patient number (refer to figure 5.13)	Inspiratory linear resistance $10^8 \cdot [Pa \cdot s/m^3]$	Expiratory linear resistance $10^8 \cdot [Pa \cdot s/m^3]$	Total compliance Cw $10^{(-7)} \cdot [m^3/Pa]]$	Subglottal cross sectional area Ag $[mm^2]$
1	0.06	0.06	1.0	2.2
2	0.06	0.06	1.0	1.8
3	0.06	0.06	1.0	2.1

Table 5.5 The inspiratory linear resistance, the expiratory linear resistance, the compliance and the subglottal cross sectional area - all estimated to calculate the flows for the three patients of figure 5.13. See Chapter 6 for a discussion of the parameters presented in the table.

5.3.4 Analysis of the cumulative error between the measured and calculated flows

It is not always possible, from a pressure-flow graph, to determine if the patient exhibits flow limitation or if his/her flow merely becomes attenuated (see Chapter 3).

The graphs shown in figure 5.13 may also be inconclusive as to the mechanism of the flow limitation. This is especially true if one compares the amplitude of the calculated flows with the amplitude of the measured flows. Even for cases of flow limitation, both amplitudes may be similar because the critical flow (flow at which flow limitation commences) may be just enough to sustain the minimum respiratory requirements. In this case, the patient's flow will not be significantly different from the value of healthy individuals. However, the lumped component model presented in this project does not include any non-linearities which may result from flow being limited. Therefore, the error between the calculated and the measured inspiratory flows should be less for non-croup and intubated children than it would be for patients with croup. This hypothesis should hold despite a possibility that the calculated and measured flows may not necessarily be different for patients with croup. We summed squares of differences between the calculated and the measured inspiratory flows for all patient groups (non-croup, intubated

and croup). The mean and standard deviation of the mean were also calculated. The results of this analysis are shown in figure 5.14 below

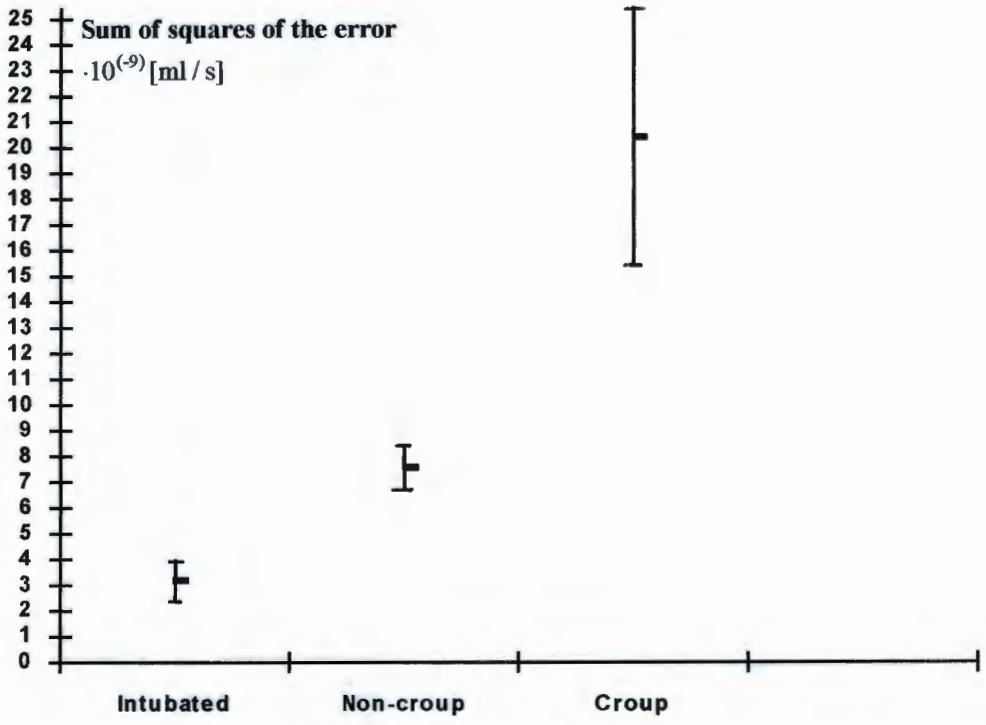

Fig 5.14 The mean and the standard deviation for the sum of squares of the differences between the measured inspiratory flows and the calculated inspiratory flows using the lumped component model.

5.4 Laryngoscopy

Figures 5.15 and 5.16 represent results of laryngoscopy. These pictures show that the aperture of the trachea during dynamic collapse is much larger than the cross sectional area of the subglottic swelling.

Figure 5.15 A photograph of the subglottis affected by croup. This photograph was made during laryngoscopy which was performed on a child with croup.

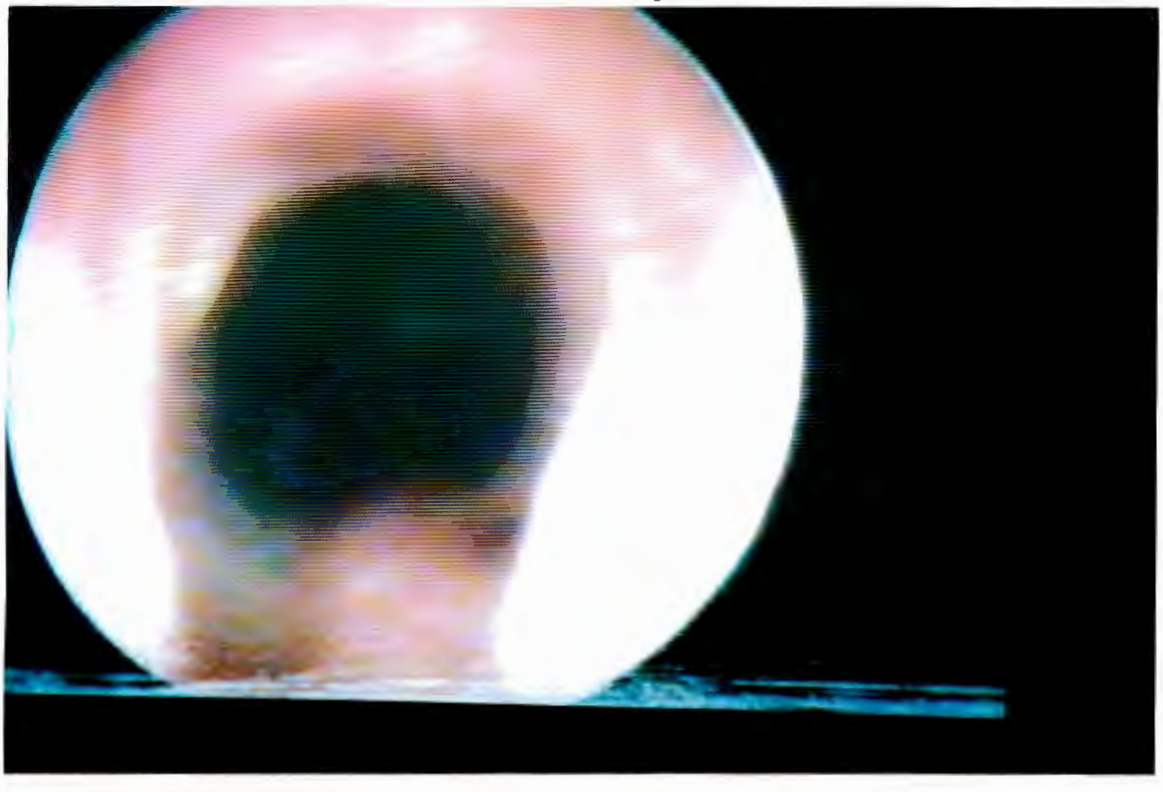

Figure 5.16 A photograph of the extrathoracic trachea (just below the subglottis) which shows a dynamic collapse (at the bottom). This photograph was made during laryngoscopy performed on the same child with croup as in figure 5.15. Please note the size of the opening of the trachea when compared with the size of the opening formed by the subglottis of figure 5.15.

6. Discussion

Croup in infants may be life threatening, especially in cases where the subglottic area is small. Despite this, there have been relatively few attempts to study airflow changes that occur in croup. In particular the flow limitation mechanism, and indeed whether flow is in fact limited at all or just attenuated, is poorly understood. In this thesis it was attempted to shed some light on the mechanism of flow limitation by:

1) studying the anatomy of the subglottic region using both laryngoscopy and X-rays

2) estimating the speed of gas particles flowing through the subglottis and comparing this speed with the calculated speed of sound within the airway

3) attempting to use the pressure-flow data from our patients to determine the parameters of a lumped component model

The second approach calculates the maximum inspiratory flow in airways, using equation 3.2, which would be possible if the gas particles travelled at the speed of sound in these airways. This maximum inspiratory flow is compared with the measured maximum flow which occurs in a group of children with croup. The smaller the absolute value of the difference between the measured and the calculated maximum flow, the closer the velocity of the gas molecules is to the speed of sound, and hence the more realistic the hypothesis of flow limitation.

The third approach investigates how well the flow which is calculated using a model of the airways correlates with the flow measured using a

pneumotachograph. Note that the inspiratory measured pressure is used to drive the model (input) and the output from the model is the calculated flow. Thus, the lumped component model introduced in this study does not test the mechanics of flow limitation. However, if it cannot fit the measured flow curves, then it is possible that flow limitation rather than attenuation, is the predominating factor.

6.1 Assumptions

This section discusses two very important parameters of equation 3.2 which were too difficult to measure directly:

1) the subglottal static pressure

2) the subglottal cross sectional area

Finally, the assumptions made towards the lumped component model are discussed.

6.1.1 The subglottal static pressure

The pressure data is obtained by inserting a fluid filled catheter into the intratoracic region of the patient's oesophagus. The catheter is well suited for our measurements because its resonant frequency is much higher (seven times higher) than the highest significant frequency measured with our patients. In addition the sampling is twenty five times the highest significant frequency component of our data and thus the Nyquist criteria is not violated. In section 3.1.2 it was shown that

in adults the intrathoracic pressure equals the subglottal static and kinetic pressure when multiplied by a constant. It was then assumed that the same is true in the case of infant's subglottis. Further evidence to this effect is presented in section 3.1.3 and 5.1. If one assumes that there is a lack of pressure recovery in the subglottis and that there is a very large pressure drop across the subglotal region, then the intrathoracic pressure will closely correspond to static subglottal pressure. Figure 5.1 shows that the profile of the cross sectional area versus distance is much steeper than is the case in Jones et al (1975) studies. This indicates that lack of pressure recovery is also likely to occur in children with croup. Furthermore, figure 5.9 shows that pressure-flow graphs of intubated patients have far smaller negative intrathoracic pressures when compared to croup cases. This means that in croup the subglottis causes the largest pressure drop in an infant's airway. Thus, any pressure drop across a small section of the airway between the intrathoracic region and the subglottis as well as any errors in estimating the elastic recoil will be insignificant when compared to the total pressure drop across the subglottis. Therefore, it is assumed that the intrathoracic pressure closely corresponds to the static subglottal pressure in children with croup.

In normal children there is probably also a lack of pressure recovery but the pressure drop across subglottis is too small to assume that the elastic recoil and the pressure drop between the subglottis and intrathoracic region is negligible.

6.1.2 The subglottal cross sectional area

The cross sectional areas were calculated using either:

1) the orifice equation (equation 3.8) and pressure-flow data of patients with croup.

2) X-rays of the larynx of patients with croup.

The orifice equation is widely used in the literature to describe flow in the larynges of adults where turbulent flow is known to predominate. In order to use this equation it is also necessary to assume that the air density changes in the subglottis are small, that the intrathoracic pressure closely reflects the static pressure in the subglottis and that the discharge coefficient Cd is known (see section 3.1.3 and 3.1.4). It is argued in this project that the static pressure inside the subglottis of a child with croup almost equals the intrathoraic pressure. This is based on the assumption that there is a lack of pressure recovery in the subglottis. It also follows that the air density changes in the subglottis are negligible and the discharge coefficient Cd = 1 (section 3.1.3). Thus, it is only the turbulence which remains to be established in order to use the orifice equation to calculate the area. Table 5.2 shows that if flow in the subglottis was laminar, then the pressure drop across the subglottis would be negligible when compared with the total pressure drop. However, this is not the case. In cases of severe croup the actual measured pressure drop across the subglottis far exceeds that which would occur if flow was laminar. For example the calculated pressure drop (assuming laminar flow equals 100ml/s) that would occur across the smallest airway that was found (using X-rays) is eleven times smaller than the average pressure drop that was measured. This suggest that flow is turbulent.

In addition to using the orifice equation the subglottal cross sectional areas of the airways using lateral and anterior-posterior views of the larynx (assuming that the airways are elliptical) was also calculated. However, it is not always a simple task to digitise anatomical structures from X-ray images because they do not have sharp outlines. This is particularly true of the lateral view of the larynx. For the cases

where the lateral view of the larynx was obscured, it was assumed that lateral width was equal to the average width of airway where one was able to obtain a lateral view. It is very difficult, in practice, to precisely relate the measured dimensions in the lateral view with those in the anterior-posterior view, even for the cases where X-rays of the larynx are well defined in the lateral view. It has been assumed that the geometry of the airway in the subglottis is elliptical. The standard deviation shown next to the average lateral width in Table 5.2 is small and one may assume that the major axis of the subglottis (length v in figure 5.2) is uniform. This is the worst case approximation because the average airway dimensions are much greater than the minimum (as demonstrated with laryngoscopy).

6.1.3 The lumped component model

The lumped component model introduced in this project is an alternative route which has been used to investigate flow limitation in patients with croup. The aim of this model is to investigate whether the flow in patients with croup is limited or just attenuated. This is important because in the upper airways, where flow is predominantly turbulent, the intrathoracic pressure is directly proportional to the square of the flow. This relationship may give an impression that flow is limited, when in fact it is attenuated.

Unfortunately, the lumped component model does not offer an improved method for calculating the subglottal cross sectional area. The assumption of turbulent flow in the larynx and lack of the pressure recovery in the subglottis during inspiration and expiration is still the basis for estimating the subglottal cross sectional area in children with croup. Therefore, the orifice equation (equation 3.8)

is still used to establish an average value for the subglottal cross sectional area. This orifice technique cannot be used with non-croup and intubated patients, since one is unable to assure lack of pressure recovery in these cases. However, the cross sectional area of the endotracheal tube is about 7 mm^2 for which value convective losses are negligible. Since intubated patients still have a larger linear resistance than the non-croup children (see Chapter 5) one could safely ignore the $Rb \cdot \dot{V}$ term in figure 3.4 for non-croup and intubated children.

In section 5.3.3 a linear resistance for children with croup was assumed to be $0.06 \cdot 10^8 \cdot [Pa \cdot s / m^3]$. This is an average value estimated from all non-croup and intubated cases. Although this value may vary from one child with croup to another, the effect of this linear resistance will be negligible when compared with the inertial pressure loss component (see section 3.2.1).

6.2 Results

This section discusses the results of:

1) the area calculations.

2) the maximum flow calculated from the wave speed equation.

3) the error analysis of lumped component models.

6.2.1 The area calculations

The areas calculated from X-rays are generally larger than areas calculated using equation 3.8. This is probably due to the fact that croup is a very dynamic disease. The child with croup may in fact improve within a short period of time, and so the X-ray data may not indicate the minimum airway area which occurred. The author specifically chose the pressure-flow graphs of very severe cases in order to ensure that the largest pressure drop occurs across the subglottis and that the condition of the lack of pressure recovery is still met. Another possibility is that the author might overestimate the value of the cross sectional area calculated from X-rays by assuming that the lateral view of the larynx is constant for all the patients. Finally, the orifice model does not include extra losses due to the effects of mucus secretion.

6.2.2 The maximum flow calculated from the wave speed equation

In Chapter 5 a number of graphs were presented which show the relationship between the measured flow and the calculated subglottal cross sectional area (figures 5.3-5.6). The measured and calculated maximum flows are shown in figures 5.7 and 5.8. In figure 5.7 the author estimated compliance, dA/dP, directly from the pressure flow graphs. However, this approach assumes that mucousal secretions have minimal effect. Figures 5.3-5.6 show various knees and plateaus which may well be caused by mucus flow. It is thus difficult to determine the point where flow limitation occurs. It is also difficult to estimate which samples to use to estimate the average compliance line in figures 5.3-5.6. As a rule of thumb the first two samples are disregarded because these samples are measured for pressures close to the ambient pressure and indicate flows at which there may be

significant pressure recovery. Also, those sections of the graph which are assumed to be beyond the flow limitation point are avoided. This is necessary because should the flow already be limited, equation 3.8 may no longer be used to calculate the subglottal cross sectional area.

Figure 5.8 shows the results of maximum flow calculated from an estimated compliance. This is a more objective analysis where compliance is no longer calculated from each individual graph. However, here it was assumed that the wall properties, such as Young's Modulus, and the dimensions of the airways in the subglottis will not significantly vary from one child with croup to another.

The result of the statistical correlation and the slope of the best-fit line for data shown in figure 5.7 is very close to that shown in figure 5.8. This may suggest that the wall properties of the subglottis are, on average, very similar among the patients. The high percentage of the statistical correlation and the slope of the best-fit line, which is almost one, is strong evidence that the patients are indeed flow limited. Statistically there is a relationship between the calculated and measured maximum flow which is significant at a 0.05 level (nonparametric Conover test) and this relationship is linear by the assumptions which underlie our test of a linear fit (Daniel and Terrell, 1989).

6.2.3 The error analysis of the lumped component model.

The difference between the calculated and measured flows during an inspiratory cycle have been expressed as a sum of squares. Figure 5.14 shows that this difference is relatively small in the case of non croup and intubated patients, which indicates that the model is able to fit the data relatively well in these cases. However in the case of patients with croup, the difference between the measured

flow and that predicted by the lumped component model is large. This indicates that the lumped component model is not able to fit the data adequately and that another mechanism is causing the deviation. This is consistent with lumped component model not being able to predict the flow accurately when there is flow limitation.

6.3 Implications in medicine

The findings of this project may influence the way croup will be investigated, diagnosed and treated in future.

The author was able to confirm that flow in patients with croup is turbulent. This means that the density and not viscosity has to be lowered in order to decrease the pressure losses in the larynx. Studies with a mixture of helium-oxygen (Duncan, 1979) show that it is possible to increase the flow in croup by decreasing the density of air in these patients. This may offer an alternative treatment for croup.

Further, there is strong evidence that the flow is limited by wave speed in the patients presented in this project. Equation 3.2 shows that the maximum flow will increase more markedly with the increasing cross sectional area than it would with decreasing compliance or density. Therefore, the paediatrician will only need to slightly increase the infant's subglottic cross sectional area in order to ensure a satisfactory flow.

Finally, the slit-like geometry of the cross sectional area in the subglottis may suggest that the design of the endotracheal tube should be more elliptical rather than circular in its cross section. In addition, it was found that the lateral views of the subglottis in patients with croup are relatively constant and thus the tubes' sizes should also follow this trend.

7. Conclusions

In this project the author has investigated the airflow changes which occur during infection in small children with croup. The author has had access to both anatomical data (X-rays of the subglottis and videos of the airways taken during laryngoscopic procedures), and functional data (pressure and flow during respiration). Unfortunately, for ethical reasons, it was not possible to obtain all of this data on each patient, and so each data set had to be analysed separately, and assumed that the response to infection in croup is uniform.

Thesearch revealed the following:

1. The videos which wereade during laryngoscopies showed that the infected region in croup children was severely narrowed in all of thetients. Due to movement of the structures relative to the lens during the breathing cycle, it was not possible to directly measure the areas of the infected airways using a laryngoscope. However the author was able to make the subjective observation that the area of the trachea was much larger than that of the subglottis, and was thus unlikely to contribute significantly to the total pressure drop. Although a small degree of tracheal collapse was observed, the resultant area of the trachea was still at least an order of magnitude larger than the area of the stenosed subglottis in croup.
2. The X-ray pictures of the subglottal region and extrathoracic trachea support the finding above, that the infected region is at least an order of magnitude smaller than that of the trachea, even during inspiration when the extrathoracic trachea collapses slightly. The lateral and anterior-posterior subglottal dimensions, in a group of twenty patients with severe croup, averaged **1.0 and 6.2 [mm]** respectively, with minimum of **0.3, and 4.8**

[mm] respectively. Most of the narrowing occurred in the lateral dimensions, while the anterior-posterior dimensions remained relatively constant.

3. The X-ray pictures also revealed that the length of the infected region was relatively short, and that the rate of change in the airway area with distance along the airway, both entering and leaving the infected subglottis, was very large. This finding is important because it means that there is a high degree of turbulence, and hence a large likelihood of a lack of pressure recovery downstream. The rate of change of airway area which was measured in our patient group was compared with literature reports which demonstrated a lack of pressure recovery in airways with a lower rate of change of area than it was shown in this project. From this it is possible to conclude that there is a high likelihood of a lack of pressure recovery in children with croup.

4. A lumped component, frequency independent, time invariant model of the airways is able to fit the pressure-flow data very well (i.e. with a low error between the measured flow and the flow which is predicted by the model with the measured pressure as the input) in cases of i) normal patients and ii) intubated patients. It is concluded from this that for these groups, flow and pressure area dependent, that an increase in pressure causes a corresponding increase in flow, which is predicted well by the model.

5. The same lumped component, frequency independent, time invariant model of the airway is unable to fit the inspiratory pressure-flow data well in the case of patients with severe croup. Here the error between the measured inspiratory flow curve and that predicted by the model with the measured inspiratory pressure input, is relatively large and that the error becomes larger as driving pressures increase. It is conclude from this that a mechanism not incorporated in the model is restricting the inspiratory flow.

The author believe that this mechanism is a wave-speed flow limitation, (see 6 below).

6. It was possible to calculate the infected airway area during inspiration by using the orifice equation. This allowed to calculate both the compliance of the walls and the speed of the gas molecules within the airway. The compliance of the walls dA/dP in turn allowed to calculate the speed of sound within the airway. The compliance of the walls dA/dP in turn allowed to calculate the speed of sound within the airway. As the result the plots of the calculated maximum flow (product of the speed of sound and the cross sectional area), using dA/dP, against the measured maximum flow of the gas molecules were produced, and an almost linear relationship and a strong correlation (the regression line had slope of **0.98 and p=0.05**) was observed. Even when a value for the compliance, dA/dP, was assumed based on the estimated Young's modulus of the tissue, a very strong correlation between the calculated maximum flow and the measured maximum flow of the gas molecules (the regression line had a slope of **1.05 and p=0.05**) was obtained. The theory of flow limitation predicts that the speed of gas molecules cannot be increased beyond the speed of sound by further decrease in negative downstream driving pressure. Since the gas molecules in patients with severe croup reach flows close to those of the calculated maximum flow within the airways during inspiration, it may be concluded that there is a high likelihood that this is the cause of inspiratory flow limitation in severe croup.

7. The calculated speed of sound (calculated maximum flows divided by the calculated cross sectional areas) in the patients with croup varied between **42 and 116.3 [m/s]** with a **median of 75 [m/s].**

By using the wave speed theory of flow limitation we found a significant correlation between the calculated maximum flow and the measured maximum flow in croup affected airways. We conclude that the mechanism by which flow becomes limited in croup children is most likely to be governed by wave-speed. This is further supported by the fact that the lumped component model, which does not incorporate flow limitation breaks down in the case of the inspiratory flow in croup patients. In addition we were able to confirm that the flow through the larynx of a croup child is turbulent. This means that it is the density of air and not the viscosity which needs to be lowered in order to increase the flow in croup patients who are not intubated or treated with steroids.

We also conclude that since the cross sectional area of the croup affected subglottis seems to decrease in one direction only (in width), the obstruction to flow due to this decrease is not as rapid as predicted by literature. However, lack of pressure recovery, which may exist in severe cases of croup, does cause large pressure losses and consequently it leads to significant decreases in flow.

8. Bibliography

Allen J. L., Castile R. G., Mead J., Positive effort dependence of maximal expiratory flow. Journal of Applied Physiology, 62(2): 718-724, 1987.

Baier H., Wanner A., Zarzecki S., Sackner A., Relationship among glottis opening, respiratory flow, and upper airway resistance in humans. Journal of Applied Physiology, 43(4): 603-611, 1977.

Benjamin B., *Diagnostic Laryngoscopy. Adults and Children.* United States: Saunders Company, 1990.

Bertram C. D., Raymond C. J., Measurements of wave speed and compliance in a collapsible tube during self-excited oscillations: a test of the chocking hypothesis. Medical and Bilogical Engineering and Computing, 29: 493-500, 1991.

Bickley C., Vocal-Fold Vibration in a Computer Model of a Larynx. *Vocal fold physiology: frontiers in basic science* (Edited by Titze I. R.). San Diego California: Singular Publisher Group, 1993.

Boonzaier D. A., Resonance Artefact in Intravascular Blood-pressure Measuring Systems: A Technique for On-line Digital Computer Correction. South African Journal of Science, 74: 250-255, 1978.

Bunn A. E., Guelke R. W. Mechanics of a Cochlea Model. Acustica, 53(5):237-249, 1983.

Chernick V., *Kendig's Disorders of the Respiratory Tract in Children.* Philadelphia: Saunders, 1990, page 338.

Coulson J. M., Richardson J. F., *Chemical Engineering Volume 1.* Oxford: Pergamon Press, 1988.

Dawson S. V., and Elliot E. A., Wave-speed limitation on expiratory flow - a unifying concept. Journal of Applied Physiology, 43: 498-515, 1977.

Daniel W. W., Terrell J. C., *Business Statistics for Management and Economics.* Fifth Edition, Boston: Houghton Mifflin Company, 1989, pages 701-703.

DuBois A. B., Brody A. W., Lewis D. H., Burgess B. F., Oscillation Mechanics of Lungs and Chest in Man. Journal of Applied Physiology, 8: 587-574, 1956.

Duncan P. G., Efficiacy of Helium - Oxygen Mixtures in the Management of Severe Viral and Post - Intubation Croup. Canadian Anaesthetists' Society Journal, 26(3): 206-212, 1979.

Elliot E. A., and Dawson S. V., Test of wave-speed theory of flow limitation in elastic tubes. Journal of Applied Physiology, 43: 517-522, 1977.

Fried M. P., *The Larynx. A multidisciplinary approach.* Second Edition, United States: Mosby-Year Book inc., 1996, pages 147-148

Fry D. L., Ebert R. V., Stead W. W., Brown C. C., The Mechanics of Pulmonary Ventilation in Normal Subjects and in Patients with Emphysema. American. Journal of Medicine, 16: 80-97, 1954.

Garel C., Contencin P., Polonovski J. M., Hassan M., Narcy P., Laryngeal ultrasonography in infants and children: a new way of investigating. Normal and pathological findings. International Journal of Pediatric Otorhinolaryngology, 23: 107-115, 1991.

Goodyer P. D., Fothergill J. C., Jones N. B., Hanning Ch. D., The Design of an Optical Fiber Pressure Transducer for Use in the Upper Airways. IEEE Transaction on Biomedical Engineering 43(6): 600-3, 1996.

Guelke R. W., Bunn A. E., The Propagation of Sound in Liquids Confined in Tubes with Compliant Walls. Acustica, 51(2):131-134, 1982.

Hall-Craggs E.C.B., *Anatomy as a Basis for Clinical Medicine.* Second Edition, Williams & Wilkins, 1990, pages 551-557.

Holmberg E. B., Hillman R. E., Perkell, J. S., Glottal airflow and transglottal air pressure measurements for male and female speakers in soft, normal, and loud voice. Journal of Acoustic Society of America, 84:511-529, 1988.

Hughes W. F., Brighton J. A., *Theory and Problems of Fluid dynamics.* Second Edition, Schaum's Series; McGraw-Hill, 1991; Chapter 1, 7 and Appendix G.

Hyatt R. E., Expiratory flow limitation. Journal of Applied Physiology, 55(1): 1-8, 1983.

Hyatt R. E., Wilson T. A., Bar-Yishay E., Prediction of maximal expiratory flow in excised human lungs. Journal of Applied Physiology, 48(6): 991-998, 1980.

Jackson A. C., Lutchen K. R., Modeling of respiratory system impedances in dogs. Journal of Applied Physiology, 62(2): 414-420, 1987.

John J. E., *Gas dynamics*. Boston: Allyn and Bacon, 1969, Chapter 2 and 3.

Jones J. G., Fraser R. B., Nadel J. A., Prediction of maximum expiratory flow rate from area-transmural pressure curve of compressed airway. Journal of Applied Physiology, 38(6): 1002-1011, 1975.

Klein M., Croup, epiglottitis and the febrile dysphagia syndrome. South African Journal of Continuing Medical Education, 4: 45-51, 1986.

Knudson R. J., Knudson D. E., Pressure-flow relationships in the isolated canine trachea. Journal of Applied Physiology, 35: 804-812, 1973.

Lambert R. K., Wilson T. A., Hyatt R. E., Rodarte J. R., A computational model of expiratory flow. Journal of Applied Physiology, 52(1): 44-56, 1982.

Lanteri C. J. and Sly P. D., Changes in respiratory mechanics with age. Journal of Applied Physiology, 74(1): 369-378, 1993.

Leiberman A., Cohen A., Tal A., International Journal of Paediatric Otorhinolaryngology, 12: 173-185, 1986.

Lutchen K. R., Costa K. D., Physiological interpretations based on lumped element models fit to respiratory impedance data: Use of forward-inverse modeling. IEEE Transactions on Biomedical Engineering, 37(11): 1076-1085, 1990.

Owczarek J. A., *Fundamentals of gas dynamics*. Scranton Pennsylvania: International Textbook Company, 1964, Chapter 1 and section 3.4.

Peslin R., Duvivier C., Gallina C., Total respiratory input and transfer impedances in humans. Journal of Applied Physiology, 59(2): 492-501, 1985.

Peslin R., Fredberg J., Oscillation Mechanics. *Handbook of Physiology*. Maryland: American Physiological Society 1986, pages 145-177.

Rayleigh J. W. S., *The Theory of Sound*. Second Edition, New york: Macmillan 1929, pages 195-196.

Rosler S., Strube H. W., Measurement of the glottal impedance with a mechanical model. Journal of the Acoustical Society of America, 86(5): 1708-16, 1989.

Scanlan C. L., Spearman C. B., Sheldon R. L., *Egan's Fundamentals of Respiratory Care*. Fifth Edition, St. Louis: Mosby, 1993 , pages 186-187.

Shapiro A. H., Steady flow in collapsible tubes. Journal of Biomechanical Engineering, 99: 126-147, 1977.

Solway J., Fredberg J. J., Ingram R. H., Pedersen O. F., Drazen J. M., Interdependent regional lung emptying during forced expiration: transistor model. Journal of Applied Physiology, 62(5) 2013-2025, 1987.

Stocks J., Sly P. D., Stepper R., Morgan W. J., *Infant Respiratory Function Testing.* Wiley-Liss, John Wiley and Sons, Inc. Publication, 1996, pages 241-268.

Swokowski E. W., *Calculus with Analytic Geometry*. Second Alternate Edition, Boston: PWS KENT Publishing Company, 1988, pages 521-527.

Thompson R. S., Stevens R. J., Mathematical model for interpretation of Doppler velocity waveform indices. Medical and Biological Engineering and Computing, 27: 269-276, 1989.

Van Den Berg Jw., Zantema T., Doornenbal P., On the Air Resistance and the Bernoulli Effect of the Human Larynx. The Journal of the Acoustical Society of America: 29(5) 626-631, 1957.

Warwick R., Williams P. L., *Gray's Anatomy.* 35th Edition, Edinburgh Norwich: Longman, 1973, pages 1181-1182

West B. J. (Editor), *Best and Taylor's Physiological Basis of Medical Practice.* 12th Edition, Baltimore: Williams & Wilkins, 1991, Chapter 39.

Wolfsdorf J., and Swift D.L. An Animal Model Simulating Acute Infective Upper Airway Obstruction of Childhood and its Use in the Investigation of Croup Therapy. Pediat. Res., 12: 1062-1065, 1978.

Wood L. D. H., Engel L. A., Griffin P., Despas P., Macklem P. T., Effect of gas physical properties and flow on lower pulmonary resistance. Journal of Applied Physiology, 41(2): 234-244, 1976.

Appendix A

Basic definitions and concepts of fluid dynamics

Perfect Fluid: A fluid which has negligible viscosity and heat conductivity (Owczarek, 1964, Chapter 1). This is a theoretical fluid which does not exist in practice. However, many fluids may closely resemble the behaviour of perfect fluid.

Adiabatic Flow: A flow in which there is no heat transfer between the fluid and its surroundings and there is no energy flow between a fluid element and its surroundings (Owczarek, 1964, Chapter 1).

Static Pressure: A normal force per unit area exerted across a surface at a point in a fluid at rest (Owczarek, 1964, Chapter 1).

$$P = \lim_{\Delta A \to 0} \frac{\Delta F}{\Delta A} \qquad (A.1)$$

where: P - the static pressure
F - the normal force
A - the area on which the normal force acts

The static pressure at a point in the fluid has the same value in all directions and therefore can be considered as a scalar point function.
Researchers also refer to the static pressure as the *lateral pressure*.

Total Pressure: The total pressure is the force per unit area which is able to bring the fluid to rest in the reversible adiabatic process. The total pressure of a moving column of fluid can be regarded as having a static component and a dynamic component (Owczarek, 1964, Chapter 1). If the fluid is at rest the total pressure equals the static pressure because the dynamic component of the total pressure is zero.

Dynamic Pressure: The difference between the total and the static pressure.

Kinetic Pressure (Convective Acceleration): The kinetic energy per unit volume of the fluid (Owczarek, 1964, Chapter 1).

$$Pca = \rho \cdot \frac{V^2}{2} \qquad (A.2)$$

where: Pca - the kinetic pressure

ρ - the density of fluid

V - the velocity of the fluid

When density changes are not significant, such as is the case when there is a lack of pressure recovery, the kinetic pressure equals the dynamic pressure.

Appendix B

Bernoulli equation from the line integral of Euler's momentum equation.

Equation B.1 represents an Euler's momentum equation (Owczarek, 1964, section 3.3)

$$\frac{\delta V}{\delta t} + V \cdot \nabla V + \frac{1}{\rho} \cdot \nabla P - f = 0 \qquad (B.1)$$

where: V - the velocity of the fluid flow
t - the time
P - the static pressure
ρ - the density of fluid
f - extraneous force per unit mass of the fluid (in our study this is the gravitational attraction on the flow and is, therefore, negligible).

Equation B.2 represents a line integral of Euler's momentum equation along a streamline in a field of conservative extraneous forces. For the derivation of equations B.1 and B.2 see Owczarek (1964, section 3.3 and 3.4)

$$\int \frac{\partial \cdot V}{\partial \cdot t} \cdot dr + \frac{V^2}{2} + \int \frac{dP}{\rho} + W = \text{constant} \qquad (B.2)$$

where: r - the position vector of the particle in space
W - the potential energy per unit mass

Equation B.2 is valid for an unsteady flow but only at a specific instant because at different times a streamline is made up of different fluid particles. Therefore, the integration of equation B.2 is possible only for the condition of steady and incompressible flow in which the density and the velocity remains constant. Thus equation B.2 becomes:

$$\frac{V^2}{2} + \int \frac{dP}{\rho} + W = \text{constant} \qquad (B.3)$$

For steady incompressible flow, equation B.3 reduces to:

$$\frac{V^2}{2} + \frac{P}{\rho} + W = \text{constant} \qquad \text{(B.4)}$$

Equation B.4 is known as Bernoulli's equation.

Let us consider a pipe of two different cross sectional areas (fig. B.1). If the flow in figure B.1 is steady, incompressible as well as reversible (frictionless) and adiabatic, equation B.4 will hold at any point in the tube.

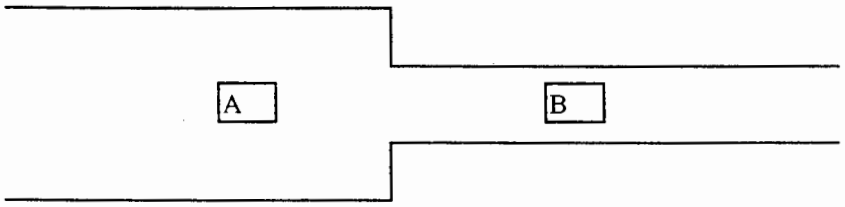

Figure B.1 Circular pipes with different cross sectional areas.

Therefore:

$$\frac{V_A^2}{2} + \frac{P_A}{\rho} + W_A = \frac{V_B^2}{2} + \frac{P_B}{\rho} + W_B = \text{constant} \qquad \text{(B.5)}$$

where subscript A and B indicate the conditions of the corresponding points in the tube.

Equation B.5 is often used to calculate the static pressures and the flows in channels of varying cross sectional areas. If there is a negligible difference in height between two points of interest, then the potential energy W in equation B.5 may be omitted.

Appendix C

C.1. Inertial pressure loss

Solway et al (1987) used the total pressure rather than the static pressure to represent the voltage in his electrical model of the flow limiting mechanism. He proposed that the static (lateral) pressure on its own would not provide a complete indication of the pressure losses. Figure C.1.1 shows the schematic diagram in which a tube, connected to the large chamber, opens abruptly into the atmosphere.

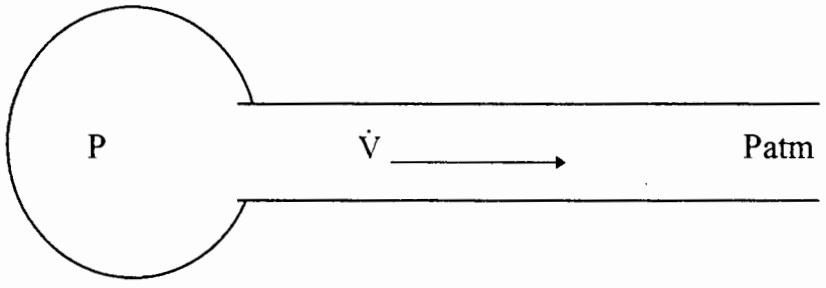

Figure C.1.1 The arrangement in which a rigid tube, connected to the large chamber, opens into the atmosphere. P is the pressure inside the chamber, Patm is the atmospheric pressure and $\dot{V}$ is the flow. The arrow indicates the direction of the flow. The diagram presented is often used to explain the mechanics of air flow in the alveolus.

If we were to make the incorrect assumption that the pressure drop (P-Patm) for a given flow is solely due to the tube resistance and if we further assume that the tube resistance in figure C.1.1 is negligible, then we will predict that the flow in the tube is infinite because from Ohms' law

$$\dot{V} = \frac{P - Patm}{(resistance)} \qquad (C.1.1)$$

It is true that a lossless tube is unrealistic because, according to Poiseuille, the tube resistance is directly proportional to the tube length. However, if we detach the tube from the chamber (figure C.1.2) and vent directly to the atmosphere, we will again mistakenly predict infinite flow across the nil airway resistance (no tube). The infinite flow is an impossible situation, therefore, something else must also contribute to the attenuation of the flow. To understand this, it is necessary to consider the kinetic energy of the fluid particles. Within the container where the velocity is low the kinetic energy is also low. However at the opening the velocity

is high and the kinetic energy is significant. Accelerating the fluid to this high velocity consumes energy and hence results in a pressure drop.

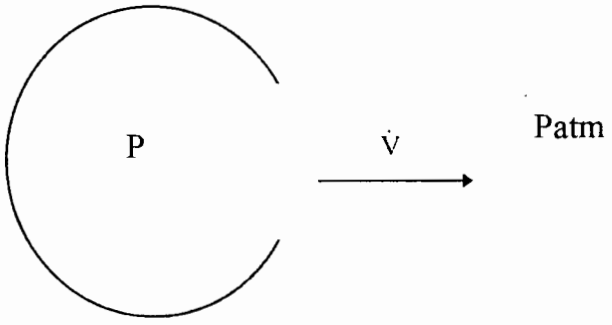

Figure C.1.2 A similar arrangement to the one shown in figure C.1.1 except that the tube is excluded. In this case there is no obvious resistive agent and, therefore, the flow should be infinite. Since the infinite flow is an impossible situation there must still be an additional mechanism which attenuates the flow.

This means that the flow will be turbulent and the pressure drop P-Patm will equal the kinetic component (also known as convective acceleration) of the total pressure. The value of this kinetic pressure is $\frac{1}{2} \cdot \rho \cdot \frac{\dot{V}^2}{A^2}$ where, $\dot{V}$ is the volume flow and A is the minimum cross sectional area.
It is now evident that these inertial losses will be prominent under the condition of high flows and large ratios of inlet to outlet areas.

C.2 Flow through a flat plate orifice

Figure C.2.1 shows a flat-plate orifice (Hughes and Brighton, 1991, Appendix G).

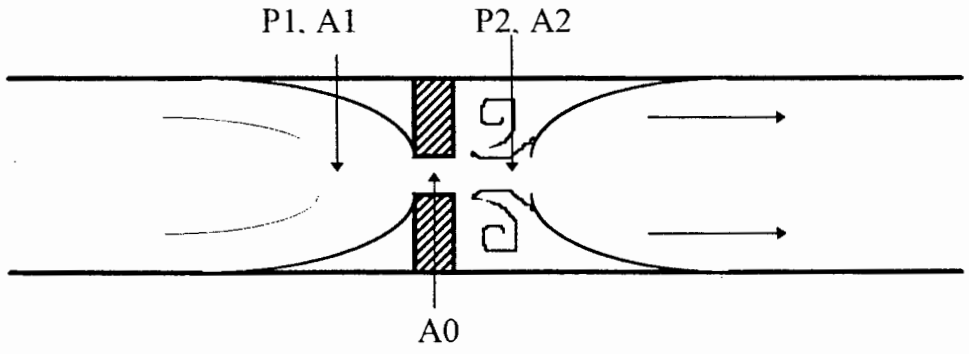

Figure C.2.1 The flat plate orifice. P1 and P2 are the static pressures at the indicated points. Similarly, A1 and A2 are the corresponding areas. It is important to note that areas are not determined by the tube walls but by the column of the fluid. In this case A2 is limited by the fact that the flow is separated from the tube wall. This results in eddy currents characteristic of turbulent flow

The Bernoulli equation between point 1 and 2 in figure C.2.1 for an incompressible fluid is

$$\frac{P1}{\rho} + \frac{V1^2}{2} = \frac{P2}{\rho} + \frac{V2^2}{2} \qquad (C.2.1)$$

where: P1 and P2 - static pressures at point 1 and 2
V1 and V2 - velocities of the fluid flow at point 1 and 2
ρ - the fluid density

The corresponding continuity equation is (refer to figure C.2.1)

$$\dot{V} = A1 \cdot V1 = A2 \cdot V2 = A0 \cdot V0 \qquad (C.2.2)$$

where: A1, A2, A0 - the cross sectional areas at the corresponding points
$\dot{V}$ - the fluid flow

Thus

$$V1 = V2 \cdot \frac{A2}{A1} \qquad (C.2.3)$$

Substitution of equation C.2.3 into C.2.1 yields

$$\frac{P1}{\rho}+\frac{V2^2\cdot(\frac{A2}{A1})^2}{2}=\frac{P2}{\rho}+\frac{V2^2}{2} \qquad (C.2.4)$$

Solving for V2

$$V2=\sqrt{\frac{2\cdot(P1-P2)}{\rho\cdot(1-(\frac{A2}{A1})^2)}} \qquad (C.2.5)$$

Therefore, the flow is

$$\dot{V}=C_v\cdot A2\cdot\sqrt{\frac{2\cdot(P1-P2)}{\rho\cdot(1-(\frac{A2}{A1})^2)}} \qquad (C.2.6)$$

where: C_v is the coefficient that corrects for the frictional losses in the Bernoulli equation. For industrial orifices this coefficient varies between 0.8 and 0.99.

Usually, the condition at point 0 in figure C.2.1 may be determined by the condition at point 2 with the aid of a discharge coefficient C_d which incorporates both the frictional losses and the area correction for vena contracta (Hughes and Brighton, 1991, Appendix G). Therefore, equation C.2.6 becomes

$$\dot{V}=C_d\cdot A0\cdot\sqrt{\frac{2\cdot(P1-P2)}{\rho\cdot(1-(\frac{A0}{A1})^2)}} \qquad (C.2.7)$$

For industrial orifices the value of the discharge coefficient, Cd, is in the range of 0.6 to 0.8. Both the discharge and the frictional coefficients are determined experimentally for a given orifice design. (Hughes and Brighton, 1991, Appendix G)

Usually, the cross sectional area A0 is very small compared to the area A1. Therefore, equation C.2.7 may further be simplified to obtain

$$\dot{V}=C_d\cdot A0\cdot\sqrt{\frac{2\cdot(P1-P2)}{\rho\cdot}} \qquad (C.2.8)$$

Appendix D

Velocity of sound

Let us assume the situation shown in figure D.1. An infinitesimal disturbance created by the piston causes a wave to propagate steadily with velocity of sound c relative to the compressible medium into which the wave is moving (John 1969 section 2.3).

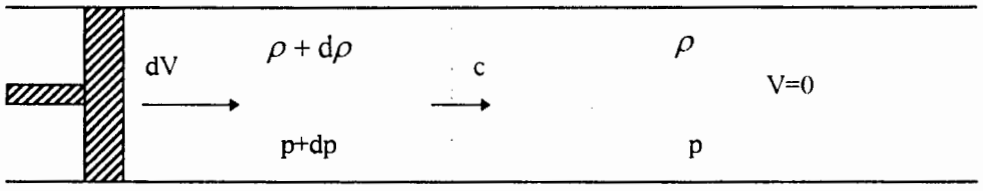

Figure D.1 The propagation of the sound wave.

The piston, in figure D.1, moves with a steady velocity dV to the right. To the left of the wavefront the fluid is compressed. This results in an increase in the pressure p and the density ρ. To the right of the wave the fluid is stationary. Here, both pressure and density remain unaffected by the movement of the piston. An observer moving with the wavefront sees the steady flow process as shown in figure D.2

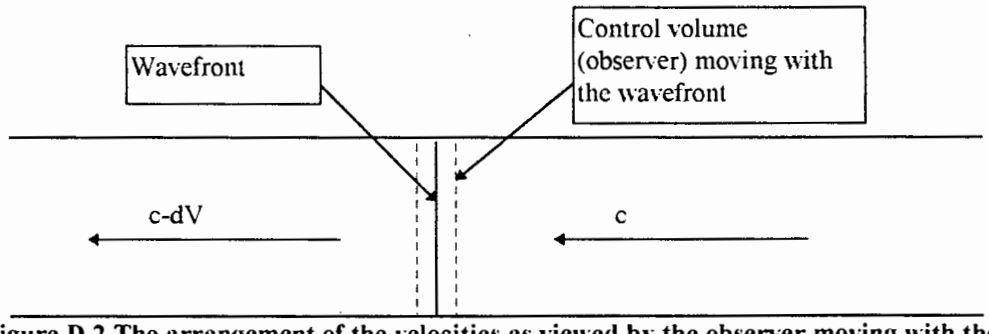

Figure D.2 The arrangement of the velocities as viewed by the observer moving with the wavefront.

Therefore, relative to the observer, the fluid enters the control volume at the sound velocity c. Then the fluid velocity becomes reduced (c-dV) which results in an increase in pressure and density.
There are two equations applicable to the problem presented in figure D.1 an D.2:

1) *The continuity equation for steady flow*

$$\rho \cdot A \cdot V = \dot{m} = \text{const} \qquad (D.1)$$

where:

ρ - the fluid density
A - the cross sectional area of the fluid
V - the velocity of the fluid flow
$\dot{m}$ - the fluid flow (mass flow)

2) *The momentum equation for steady flow with negligible body forces*

$$F_s = \int_{C.S} V \cdot \rho \cdot V \cdot dA \qquad (D.2)$$

where: F_s - the total surface force
C.S - the control surface over which the equation is integrated

Equation D.2 is valid because the control volume in figure D.2 is infinitesimally small (it approaches the volume of the wavefront). Therefore, the shear forces on the wall may be neglected.

The continuity equation for the steady flow (equation D.1) applied to the control volume of figure D.2 gives

$$c \cdot \rho \cdot A = (c - dV) \cdot (\rho + d\rho) \cdot A \qquad (D.3)$$

After dropping the second-order differentials and dividing out by the common area A, equation D.3 becomes

$$c \cdot d\rho = \rho \cdot dV \qquad (D.4)$$

The momentum equation for the arrangement shown in figure D.2 yields

$$(p + dp) \cdot A - p \cdot A = \rho \cdot c \cdot A \cdot [-(c - dV)] - \rho \cdot c \cdot A \cdot (-c) \qquad (D.5)$$

which, after simplification, gives

$$dp = \rho \cdot c \cdot dV \qquad (D.6)$$

Combining equation D.6 and D.4,

$$c^2 = \frac{dp}{d\rho} \qquad (D.7)$$

For a perfect gas undergoing an isentropic process, the pressure-density relation is

$$\frac{p}{\rho^k} = \text{constant} \tag{D.8}$$

where: k - ratio of specific heats (for air at sea level k = 1.402)

Taking the logarithmic differential, we get

$$\ln(p) - k \cdot \ln(\rho) = \ln(C) \tag{D.9a}$$

$$\frac{dp}{p} = k \cdot \frac{d\rho}{\rho} \tag{D.9b}$$

where: C - constant

Therefore

$$\frac{dp}{d\rho} = k \cdot \frac{p}{\rho} = c^2 \tag{D.10}$$

Appendix E

1. Maximum flow in a straight compliant tube under the condition of steady flow.

We present two different approaches for solving maximum flow under a steady flow condition:

- maximum flow with a constant pressure head; and
- maximum flow with a flow dependent pressure head.

1) *Maximum flow with a constant pressure head.* Figure E1 shows a simple model of a straight tube surrounded by a total pressure Pout. There is a pressure drop from point A (Pout) down to B (Pt) resulting in flow $\dot{V}$. Both Pout and Pt indicate total pressures at the indicated points. Plat is the static or lateral pressure component of Pt, while Pca is the kinetic component (see Appendix A). All pressures in figure E1 are expressed relative to Pout=0.

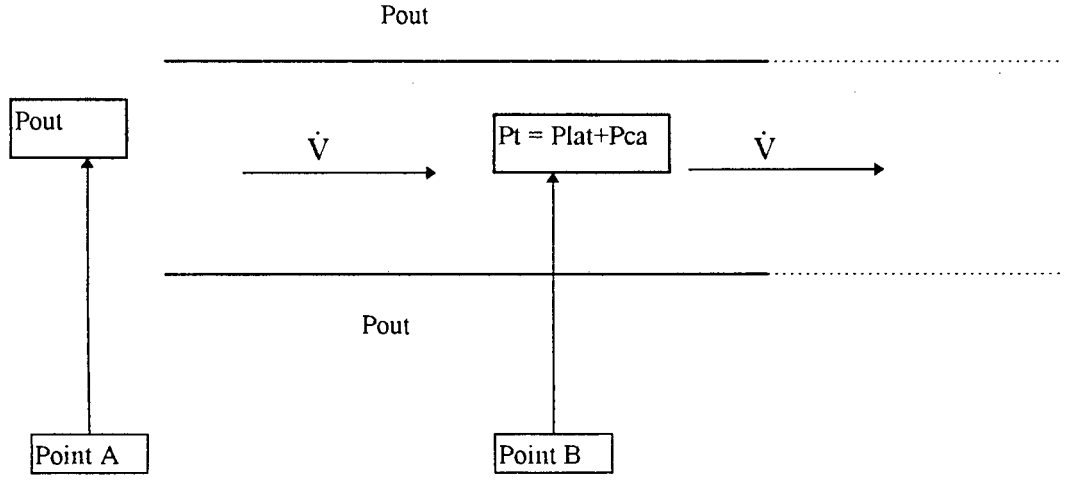

Figure E1 Pressure and flow distribution in the straight tube under the condition of steady flow $\dot{V}$. The tube is surrounded by the external pressure Pout. Pout and Pt are total pressures at indicated points. Plat and Pca are static and kinetic components of the total pressure Pt.

The situation at point B in figure E1 may be described by:

$$Pt = Plat + 0.5 \cdot \rho \cdot \frac{\dot{V}^2}{A^2} \qquad (E1)$$

where A - cross sectional area
$\dot{V}$ - flow
ρ - fluid density

Equation E1 is the Bernoulli's equation at point B and describes the pressure components of the total pressure Pt (see Appendix B).

The next relationship defines the transmural pressure Ptm which is the pressure difference between the static pressure inside and the static pressure outside the tube. Since Pout is the pressure in a very large chamber in which there is negligible flow, the value of the total pressure Pout is approximately the same as the value of the static component of Pout. Therefore, the solution for Ptm at point B is:

$$Ptm = Plat\text{-}Pout = Plat \qquad (E2)$$

Equation E3 shows another valid relationship at point B

$$J = Pt\text{-}Pout = Pt \qquad (E3)$$

J in equation E3 is often referred to as the pressure head, at the tip of the Pitot static probe, measured relative to Pout (Pedersen). J also describes frictional losses between Pout and Pt in figure E1.

Using equation E2 and E3, it may be shown that

$$J=Ptm+Pca \qquad (E4)$$

Substituting for Pca in equation E4 the flow $\dot{V}$ in figure E1 is

$$\dot{V} = A \cdot \left(\frac{2}{\rho} \cdot (J - Ptm)\right)^{0.5} \qquad (E5)$$

In an ideal situation the relationship between the transmural pressure and the flow will show a characteristic plateau . This means that the maximum flow will occur at the point where the gradient of flow with respect to the transmural pressure is zero. Mathematically this is represented by differentiating equation E5 with respect to Ptm and equating to zero.

$$\frac{d\dot{V}}{dPtm} = \frac{2}{\rho} \cdot A \cdot 0.5 \cdot (J - Ptm)^{-0.5} - \frac{2}{\rho} \cdot \frac{dA}{dPtm} \cdot (J - Ptm)^{0.5} = 0 \qquad (E6)$$

Equation E6 assumes that J is constant and A is a unique function of Ptm (this means that A and Ptm obey the 'tube law' - a term used by researchers to describe the airway compliance curve).

Solvig for (J-Ptm) we get

$$(J - Ptm) = 0.5 \cdot A \cdot \frac{dPtm}{dA} \qquad (E7)$$

Substitution of E7 in E5 gives

$$\dot{V}_{max} = \sqrt{(\frac{A^3}{\rho} \cdot \frac{dPtm}{dA})} \qquad (E8)$$

where: $\dot{V}max$ - maximum flow

The above derivation of maximum flow is often used by researchers in models of flow limitation in bronchial trees (Hyatt et al 1980). However, the model of lungs presented in the literature is more complicated than the model presented in figure E1 because the pressure surrounding the airways in the lungs (pleural pressure) is not constant. In the case of croup, the region of interest is above the intrathoracic region. This means that the pressure surrounding the flow limited airways is the atmospheric pressure which may be regarded as constant when compared with pressure changes in the airways.

We purposely avoided using Plat instead of Ptm and Pt instead of J in the derivation of equation E8. The reason for this is that the model shown in figure E1 represents a special case in which the pressure surrounding the tube is constant. In more complicated systems, such as models of lungs, Ptm is not the same as Plat and similarly, Pt is different from J.

2) *Maximum flow with a flow dependent pressure head.*

It is evident from the previous analysis that only wave speed determines the maximum flow in equation E8. In fact, researchers believe that maximum flow may either be a viscous or wave speed phenomenon, but not both (see Chapter 3). We intend to show, however, that the combination of viscosity and wave-speed may appear in the derivation of maximum flow if pressure losses (between A and

B in figure E1) are flow dependent (in our case the pressure losses in the extrathoracic airways are equivalent to pressure head J). In fact, it is unlikely that pressure losses will be flow independent. If the pressure gradient between point A and B in figure E1 is caused purely by viscous forces then

$$Pt\text{-}Pout = -R \cdot \dot{V} = J \tag{E9}$$

where: R - resistance caused by viscous forces. If flow is assumed to obey Pouseville's law $R = \frac{K \cdot l}{A^2}$ (K is constant, l is the airway's length and A is the airway's cross sectional area)

Equation E9 shows that the pressure head J in equation E4 now has to overcome additional viscous forces, thus

$$J = Ptm + Pca + R \cdot \dot{V} \tag{E10}$$

Therefore

$$R \cdot \dot{V} + Ptm + 0.5 \cdot \rho \cdot \frac{\dot{V}^2}{A^2} = 0 \tag{E11}$$

To solve $\dot{V}$ we obtain

$$\dot{V} = \frac{-R \pm \sqrt{(R^2 - 2 \cdot Ptm \cdot \frac{\rho}{A})}}{\frac{\rho}{A^2}} \tag{E12}$$

Equation E12 may further be simplified to

$$\dot{V} = -\frac{K \cdot l}{\rho} \pm \sqrt{(\frac{K^2 \cdot l^2 \cdot}{\rho^2} - 2 \cdot \frac{Ptm \cdot A^2}{\rho})} \tag{E13}$$

To find the maximum flow we ignore the negative solution and set $\frac{d\dot{V}}{dPtm} = 0$, that is

$$\frac{d\dot{V}}{dPtm} = 0.5 \cdot (\frac{K^2 \cdot l^2}{\rho^2} - 2 \cdot \frac{Ptm \cdot A^2}{\rho})^{-0.5} \cdot (-\frac{4 \cdot A \cdot \frac{dA}{dPtm} \cdot Ptm}{\rho} - 2 \cdot \frac{A^2}{\rho}) = 0 \tag{E14}$$

To avoid complex solutions or division by zero, the following must be satisfied in equation E14

$$0.5 \cdot \left(\frac{K^2 \cdot l^2}{\rho^2} - 2 \cdot \frac{Ptm \cdot A^2}{\rho}\right)^{-0.5} > 0 \qquad \text{(E15)}$$

This means that

$$\left(-\frac{4 \cdot A \cdot \frac{dA}{dPtm} \cdot Ptm}{\rho} - 2 \cdot \frac{A^2}{\rho}\right) = 0 \qquad \text{(E16)}$$

From E16 the transmural pressure Ptm is

$$Ptm = -0.5 \cdot A \cdot \frac{dPtm}{dA} \qquad \text{(E17)}$$

By substituting E17 into E13 and ignoring the negative solution, we obtain

$$\dot{V}max = -\frac{K \cdot l}{\rho} + \sqrt{\left(\frac{K^2 \cdot l^2}{\rho} + A^3 \cdot \frac{dPtm}{dA}\right)} \qquad \text{(E18)}$$

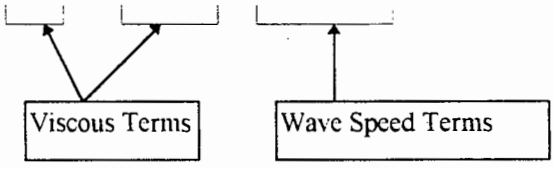

In order to derive equation E18 one does not have to assume that pressure losses between point A and B are purely viscous. In fact, the inclusion of convective losses will only change the value of the kinetic component of the total pressure Pt, but the form of equation E18 will remain unchanged.

Equation E18 may also be derived using a graphical interpretation. Let us again assume the situation shown in figure E1. Since the tube is compliant, the pressure drop Pout-Pt will tend to collapse the tube until the stretch in the wall resists the pressure. Now if the compliance of the tube is $C = \frac{dA}{dPtm}$, then

$$A = Ao - Ptm \cdot C \qquad \text{(E19)}$$

where Ao - initial area (when the tube is in an unstretched position)

A - area corresponding to pressure Ptm
Ptm - transmural pressure (refer to previous analysis)

Using equation E11 and substituting $\frac{K \cdot l}{A^2}$ for R, equation E19 becomes

$$A = Ao - (\frac{K \cdot l}{A} \cdot \dot{V} + 0.5 \cdot \rho \cdot \frac{\dot{V}^2}{A^2}) \cdot C \qquad \text{(E20)}$$

Multiplying E20 by A^2 and taking area terms to one side of equation E20, we obtain

$$A^3 - Ao \cdot A^2 = -K \cdot \dot{V} \cdot l \cdot C - 0.5 \cdot \rho \cdot \dot{V}^2 \cdot C \qquad \text{(E21)}$$

Equation E21 may be interpreted as a combination of two functions:

$$f1(A) = A^3 - Ao \cdot A^2 \qquad \text{(E22)}$$

and

$$f2(\dot{V}) = -K \cdot \dot{V} \cdot l \cdot C - 0.5 \cdot \rho \cdot \dot{V}^2 \cdot C \qquad \text{(E23)}$$

Equation E22 and E23 may be represented by figure E2

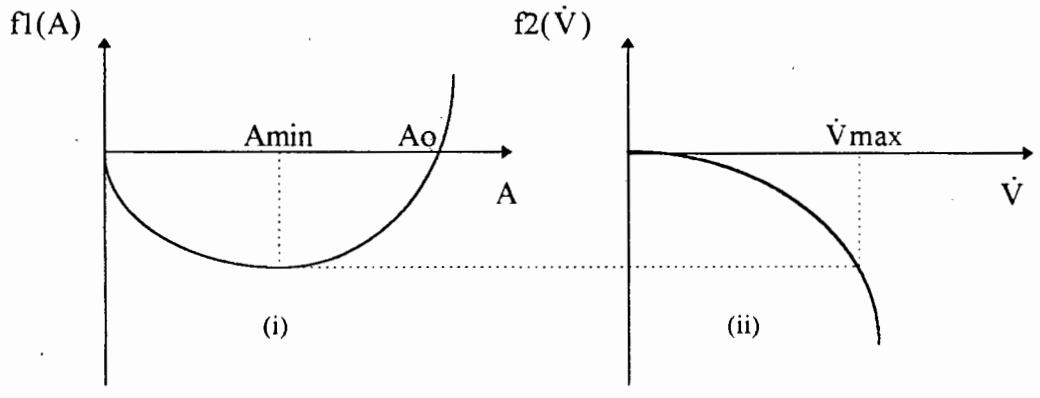

Figure E2 Two functions which represent equation E21. For each value of function f1(A) there is a corresponding value of f2($\dot{V}$). The value f1(Amin) marks the beginning of flow limitation (see text).

As flow, $\dot{V}$, is increased, so f2($\dot{V}$) decreases along the curve shown in figure E2 (ii). f2($\dot{V}$) will be equal to f1(A) (as per equation E21) at a specific value of A (assuming that A drops from Ao as $\dot{V}$ is increased). The minimum value for f2($\dot{V}$)

will thus also be the minimum value for f1(A) which occurs at Amin. The corresponding maximum flow is $\dot{V}max$.
Differentiating and setting to zero, equation E22 becomes

$$\frac{df1(A)}{dA} = 3 \cdot A^2 - 2 \cdot Ao \cdot A = 0 \qquad (E24)$$

Therefore area A at maximum flow is

$$A = \frac{2 \cdot Ao}{3} \qquad (E25)$$

Substituting E25 into E21

$$\frac{8 \cdot Ao^3}{27} - Ao^3 \cdot \frac{12}{27} = -\frac{4 \cdot Ao^3}{27} = -K \cdot l \cdot \dot{V} \cdot C - 0.5 \cdot \rho \cdot \dot{V}^2 \cdot C = 0 \qquad (E26)$$

To solve $\dot{V}$ (the maximum flow) we obtain

$$\dot{V} = -\frac{K \cdot l}{\rho} \pm \sqrt{\left(\frac{K^2 \cdot l^2}{\rho^2} + \frac{8}{27} \cdot \frac{Ao^3}{\rho \cdot C}\right)} \qquad (E27)$$

To solve Ao in equation E25 and substituting $\frac{dA}{dPtm}$ for C, equation E27 becomes (ignoring the negative solution):

$$\dot{V} = -\frac{K \cdot l}{\rho} + \sqrt{\left(\frac{K^2 \cdot l^2}{\rho} + A^3 \cdot \frac{dPtm}{dA}\right)} \qquad (E28)$$

Equation E28 and E18 are identical.

Appendix F

Programs

```
function y=maxflow(stage)
%function
%
%This is a a flow limitation MATLAB programme
%
%stage - breathing cycle
%//////////////////////////////////////////////////



%////this section loads patient's data/////////////

load('c:\\patientfile');
fil_n=patientfile;

%//////////////////////////////////////////////////



%//////////constants//////////////////

q=1.2047; %air density
t=0.02; %sampling time
w=90.3; %the resonant angular frequency of catheter
b=23.11;%damping constant of catheter
p5(1)=0;%initialisation of first recoil pressure sample
p5(2)=0;%initialisation of second recoil pressure sample

%//////////////////////////////////////



%//////find begin and end of cycle/////////////

i=0;
for n=1:length(fil_n)
```

```
 if fil_n(n,2) == 0,
  i=i+1;
  pos(i)=n;
 end
end

bgin=pos(2*stage);
endi=pos(2*stage+2);

%//////////////////////////////////////////////


%//////////get static pressures inside orifice//////////

 for d=bgin:endi
  p(d)=fil_n(d,3);
  p5(d)=fil_n(d,3)-fil_n(d,5);

%get alias for flow
  f5(d)=fil_n(d,2);

%Boonzaier correction algorithm
  K=1-2*exp(-b*t)*cos(w*t)+exp(-2*b*t);
  z(d)=(p5(d)-2*exp(-b*t)*cos(w*t)*p5(d-1)+exp(-2*b*t)*p5(d-2))/K;

end;

%//////////////////////////////////////////////


%//////////plot pressure versus flow//////////////

d=bgin:endi;
 plot(p5(d),fil_n(d,2),'w+');

%//////////////////////////////////////////////


%//////////choose maximum sample/////////////////
```

```
[x1,y1]=ginput(1);
for d=bgin:endi
 if(abs(x1)<=abs(p5(d))),
  d_n=d,break;
 end
end;

%//////////////////////////////////////////////////

%////////////get cross sectional area////////////////

for d=bgin:endi
A2(d)=abs(f5(d)*10^(-6))/( ( (2/q)*abs(p5(d))*98 )^0.5);
end;

%//////////////////////////////////////////////////

%//plot pressure versus flow and pressure versus
%//area

d=bgin:endi;
clg;

subplot(211),plot(p5(d),f5(d),'w+');
grid;
subplot(212),plot(p5(d),A2(d),'r+');
grid;

%get average stiffness
[x2,y2]=ginput(1);
[x3,y3]=ginput(1);
[xa,ya]=ginput(1);
Stiff=98*(x3-x2)/(y3-y2);

%get area
Area=ya
```

```
%get flow
flow=10^(6)*ya*(abs(xa*98)*2/q)^0.5

%calculate flow from wave-speed
Vmax=10^(6)*( ((ya^3)/q)*abs(Stiff) )^0.5;

%find difference
dmax=abs(Vmax)-flow

%display compliance
Compl=1/Stiff

%//////////////////////////////////////////////



end;
```

----------END----------

```
function y=lumped(bgin,endi,ai,bi,ae,be)
%function
%
%This is a lumped component model MATLAB programme
%
%bgin - begin sample number
%endi - finsh sample number
%ai   - inspiratory linear resistor constant
%bi   - inspiratory inertial pressure loss constant
%ae   - expiratory linear resistor constant
%be   - expiratory inertial pressure loss constant
%//////////////////////////////////////////////

%///////This section loads patient's data///////

load('c:\ \patientfile');
fil_n=patientfile;

%//////////////////////////////////////////////
%//////////////Constants/////////////////////////
```

```
t=0.02;         %sampling time
w=90.3; %the resonant angular frequency of catheter
b=23.11;%damping constant of catheter
p(1)=0; %initialisation of first pressure sample
p(2)=0; %initialisation of second pressure sample

%////////////////////////////////////////////////

%////Loading pressure and flow from patient's data//

 for d=bgin:endi
  p(d)=(98*((fil_n(d,3))));
  pn(d)=((fil_n(d,3)));
  f(d)=10^(-6)*fil_n(d,2);
  fn(d)=fil_n(d,2);

%Boonzaier correction algorithm
  K=1-2*exp(-b*t)*cos(w*t)+exp(-2*b*t);
  y_b(d)=(p(d)-2*exp(-b*t)*cos(w*t)*p(d-1)+exp(-2*b*t)*p(d-2))/K;
  y_b(d)=p(d);
 end;

%////////////////////////////////////////////////

%///////Picture of circuit model////////////////
%
%p(d)-/\/\/\---oooo---[     ]-----  pc(d)
%      R        L        Rb*I(d)     |
%                                    |
%                                  -----
%                                  -----  C
%                                    |
%                                    |
%////////////////////////////////////////////////

%///////Variables to change//////////////////////

q=1.204; %air density
u=16*10^(-6); %air viscosity
A=7*10^(-6);  %subglottal cross sectional area
C=1*10^(-7);  %compliance
z=0.01; %subglottal distance
```

```
%//////////////////////////////////////////////

%//Initialisation for recoil pressure pc(d)///

Rb=-bi*0.5*q/(A^2); %inertial losses
R=ai*98*10^6;          %Linear resistance

%initialisation of 1st and 2nd recoil pressure
pc(bgin)=0;
pc(bgin+1)=0;

%Coefficients of quadratic equation (solving for recoil pressure)
Ae=Rb*C^2/(t^2);
Be=((R*C/t) - (2*pc(bgin+1)*Rb*C^2/(t^2)) + (L*C/(t^2)) + 1);
Ce=( (-R*C*pc(bgin+1)/t) + (Rb*C^2*(pc(bgin+1))^2)/(t^2) + (-
2*pc(bgin+1)*L*C/(t^2)) + (pc(bgin)*L*C/(t^2)) - (y_b(bgin+2)) );

pc(bgin+2)=((-Be+(Be^2-4*Ae*Ce)^(0.5))/(2*Ae));

%//////////////////////////////////////////////////

%//////////Loop for all chosen samples/////////////

for d=bgin+3:endi

%Check for positive and negative solution
if pc(d-1)-pc(d-2)<=0 %if flow<0
 k=-1;
 Rb=k*bi*0.5*q/(A^2);
 R=ai*98*10^6;
end
if pc(d-1)-pc(d-2)>0 %if flow>0
 k=1;
 Rb=k*be*0.5*q/(A^2);
 R=ae*98*10^6;
end

%pc calculation for each sample
 Ae=Rb*C^2/(t^2);
 Be=((R*C/t) - (2*pc(d-1)*Rb*C^2/(t^2)) + (L*C/(t^2)) + 1);
```

```
 Ce=( (-R*C*pc(d-1)/t) + (Rb*C^2*(pc(d-1))^2)/(t^2) + (-2*pc(d-1)*L*C/(t^2)) +
(pc(d-2)*L*C/(t^2)) - (y_b(d)) );
 pc(d)=((-Be+(Be^2-4*Ae*Ce)^(0.5))/(2*Ae));

end;

%//////////////////////////////////////////////////

%///////////////Flow calculation/////////////////////

for d=bgin+2:endi
 pc(bgin)=0;
 pc(bgin+1)=0;

l(d)=(C*(pc(d)-pc(d-1))/(t));
end;

%//////////////////////////////////////////////////

%////////////Plots/////////////////////////////////

d=bgin+2:endi;
pc(bgin)=0;
pc(bgin+1)=0;

clg;
plot(d,(f(d)),'y');
hold;
grid;
plot(d,5*((fil_n(d,3)-pc(d)'/98))*10^(-6),'r');
plot(d,5*pc(d)*10^(-6)/98,'w');
plot(d,5*(fil_n(d,5))*10^(-6),'g');
plot(d,0.1*(p(d))*10^(-6),'r');
plot(d,(I(d)),'b');

%//////////////////////////////////////////////////

end;
```

----------END----------

Appendix G

Flow calculation from the intrathoracic pressure using a modified three element DuBois model

We present a solution to the flow from a modified three element DuBois model.

Figure G.1 shows a modified three element DuBois model.

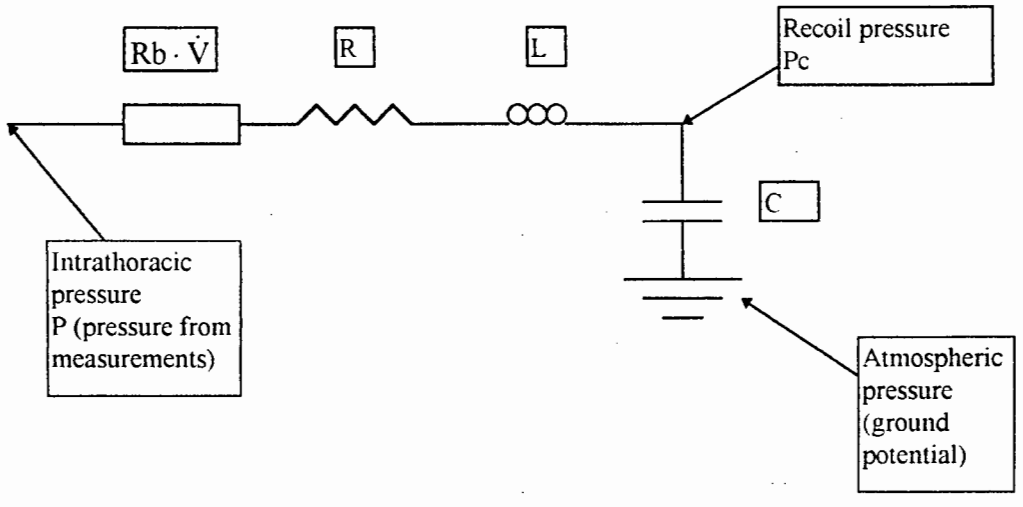

Figure G.1 The modified three element DuBois model. R, L and C are the airways resistance, the lung wall inertance and the lung wall compliance respectively. The $Rb \cdot \dot{V}$ represents inertial losses where $\dot{V}$ is the air flow.

The following equations apply to the model shown in figure G.1:

$$\text{Pressure drop across R} = \dot{V}(d) \cdot R \qquad \text{(G.1)}$$

where d represents a current sample number.

$$\text{Pressure drop across inertial loss component} = \dot{V}^2(d) \cdot Rb \qquad \text{(G.2)}$$

$$\text{Pressure drop across L} = L \cdot \frac{\dot{V}(d) - \dot{V}(d-1)}{\Delta t} \qquad \text{(G.3)}$$

where Δt is the sampling time and d-1 is the previous sample.

$$\dot{V}(d) = C \cdot \frac{Pc(d) - Pc(d-1)}{\Delta t} \qquad (G.4)$$

Therefore, the intrathoracic pressure P is

$$P(d) = R \cdot \dot{V}(d) + Rb \cdot \dot{V}^2 + L \cdot \frac{\dot{V}(d) - \dot{V}(d-1)}{\Delta t} + Pc(d) \qquad (G.5)$$

Substitution of G.4 into G.5 gives:

$$P(d) = R \cdot C \cdot \frac{Pc(d) - Pc(d-1)}{\Delta t} + Rb \cdot C^2 \cdot \frac{Pc(d)^2 - 2 \cdot Pc(d) \cdot Pc(d-1) + Pc(d-1)^2}{\Delta t^2} + \\ + L \cdot C \cdot \frac{Pc(d) - 2 \cdot Pc(d-1) + Pc(d-2)}{\Delta t^2} + Pc(d) \qquad (G.6)$$

If one estimates (fits) R, Rb, C and L (see Chapter 3 and 4) then G.6 is a quadratic equation with only one unknown - the recoil pressure Pc(d). This means we can solve for Pc(d) in equation G.6 and substitute this value into equation G.4. Then equation G.4 calculates the flow $\dot{V}$.

This method of the flow calculation is used in the MATLAB programme (see Appendix F).

Appendix H

Performance of the pressure and the flow measurement equipment

Figure H.1 represents a response of the catheter, used in our study, to a step input.

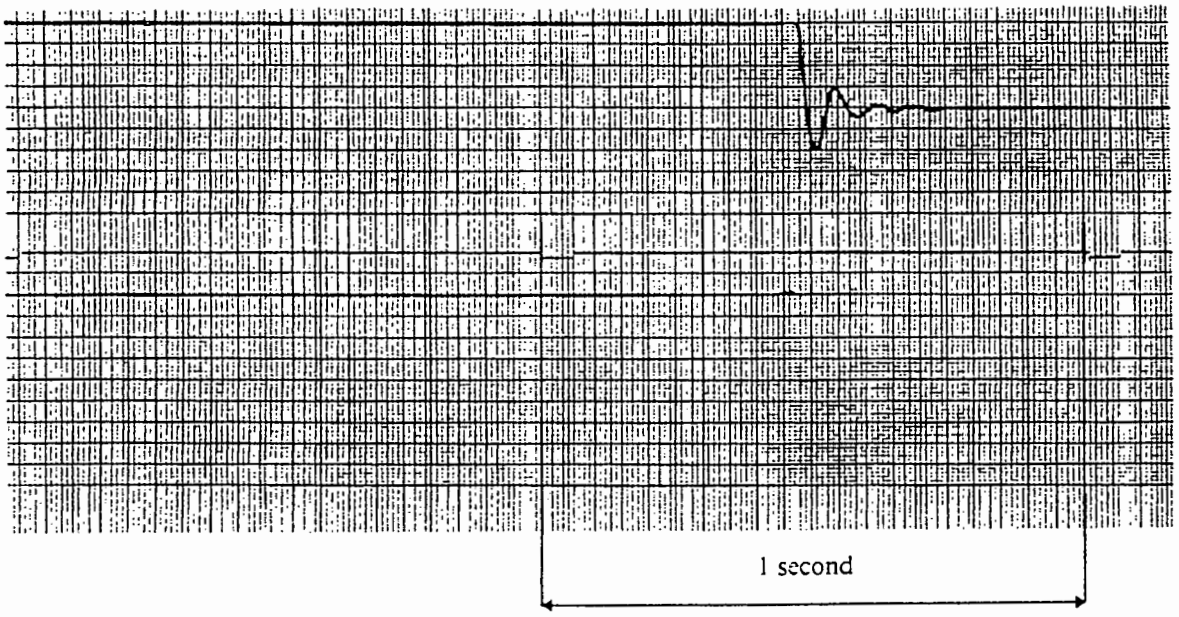

Figure H.1 Response of the catheter to a step input.

In order to eliminate the catheter's effect on pressure measurements, we employed the Autoregressive Digital Technique for Pressure Restoration developed by Boonzaier (1978). Equation 5.1 (see section 5.1.3 and Boonzaier, 1978) extracts the true pressure y from the pressure x which is measured with the catheter inserted in oesophagus.

$$y(n) = (x(n) - 2 \cdot e^{(-\beta \cdot T)} \cdot \cos(\omega \cdot T) \cdot x(n-1) + e^{(-2 \cdot \beta \cdot T)} \cdot x(n-2)) / K \qquad (5.1)$$

where y - true signal

x - measured signal

n, n-1, n-2 - current and previous sample numbers

T - one sampling interval (0.02 [s])

ω - resonant angular frequency (90.3 [rad/s])

β - dumping constant (23.11 [rad/s])

K - DC value $= 1 - 2 \cdot e^{(-\beta \cdot T)} \cdot \cos(\omega \cdot T) + e^{(-2 \cdot \beta \cdot T)}$

Figures H.2-H.5 represent the pressure and the flow traces obtained with the setup shown in figure 5.1. Using reflex microscope (Prior S2000), we found that the peak flow corresponds to the peak pressure .

The following equations are used to calculate the parameters of equation 5.1 from figure H.1 (see Boonzaier, 1978).

$$f = \frac{\sqrt{4 \cdot \pi^2 + (\ln(d1/d3))^2}}{2 \cdot \pi \cdot T_c} \qquad (H.1)$$

where f - frequency of oscillations (14.3[Hz])
d1 - initial value (when catheter is pressurised)
d3 - first positive peak (after depressurisation). The ratio d1/d3 is 5.29.
T_c - period of catheter oscillations (0.072[s]).

$$\omega = 2 \cdot \pi \cdot f \qquad (H.2)$$

where: ω- resonant angular frequency of oscillations (90.3[rad/s])

$$\beta_f = \frac{\ln(d1/d2)}{\sqrt{4\cdot\pi^2 + (\ln(d1/d3))^2}} \qquad \text{(H.3)}$$

where: β_f - dumping factor (0.256)

$$\beta = \omega \cdot \beta_f \qquad \text{(H.4)}$$

where: β - dumping constant (23.11 [rad/s])

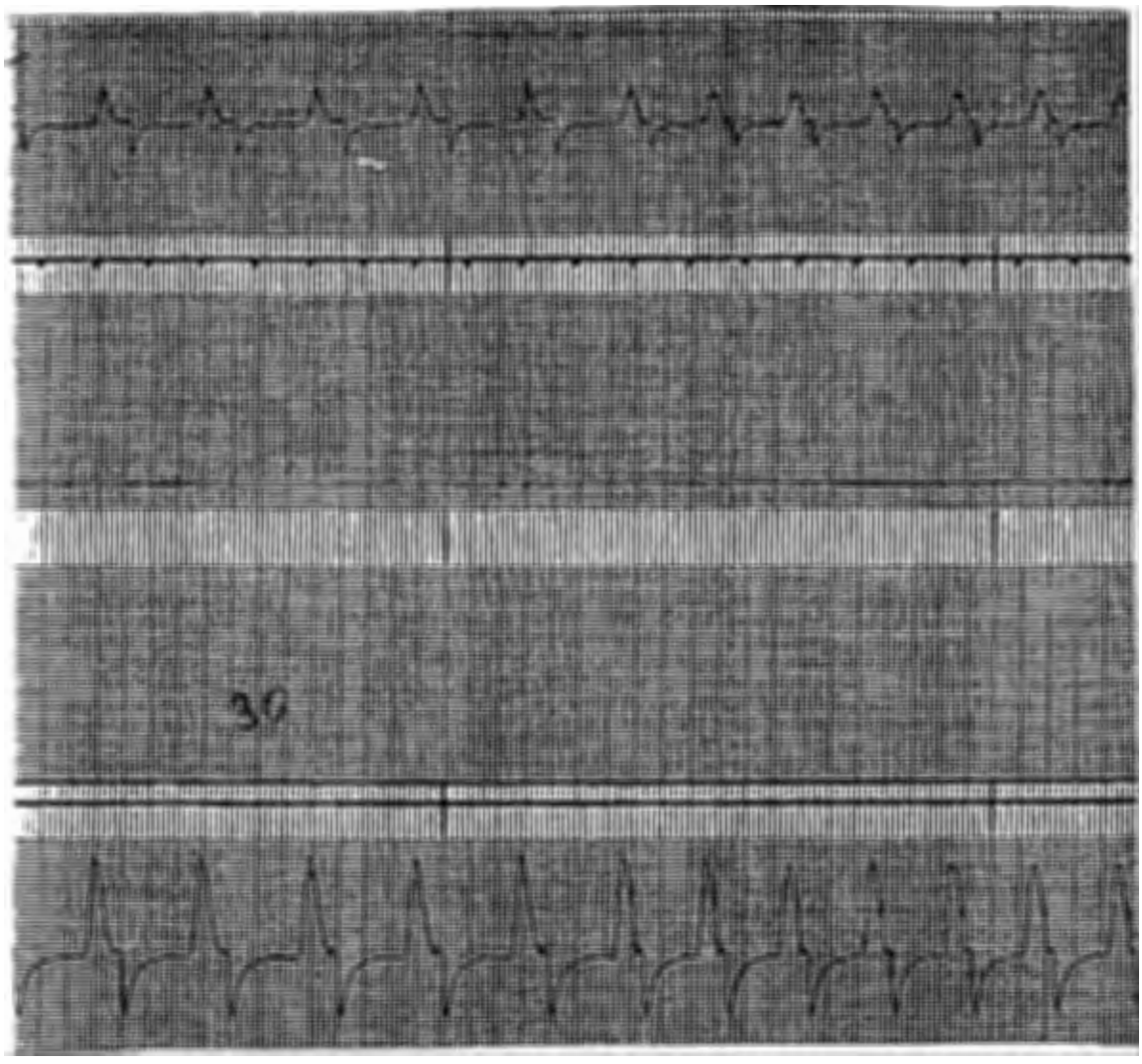

Figure H.2 The pressure (upper traces) and the flow (lower traces) taken for phase measurements (see Chapter 5). This graph represents 30 beats per minute.

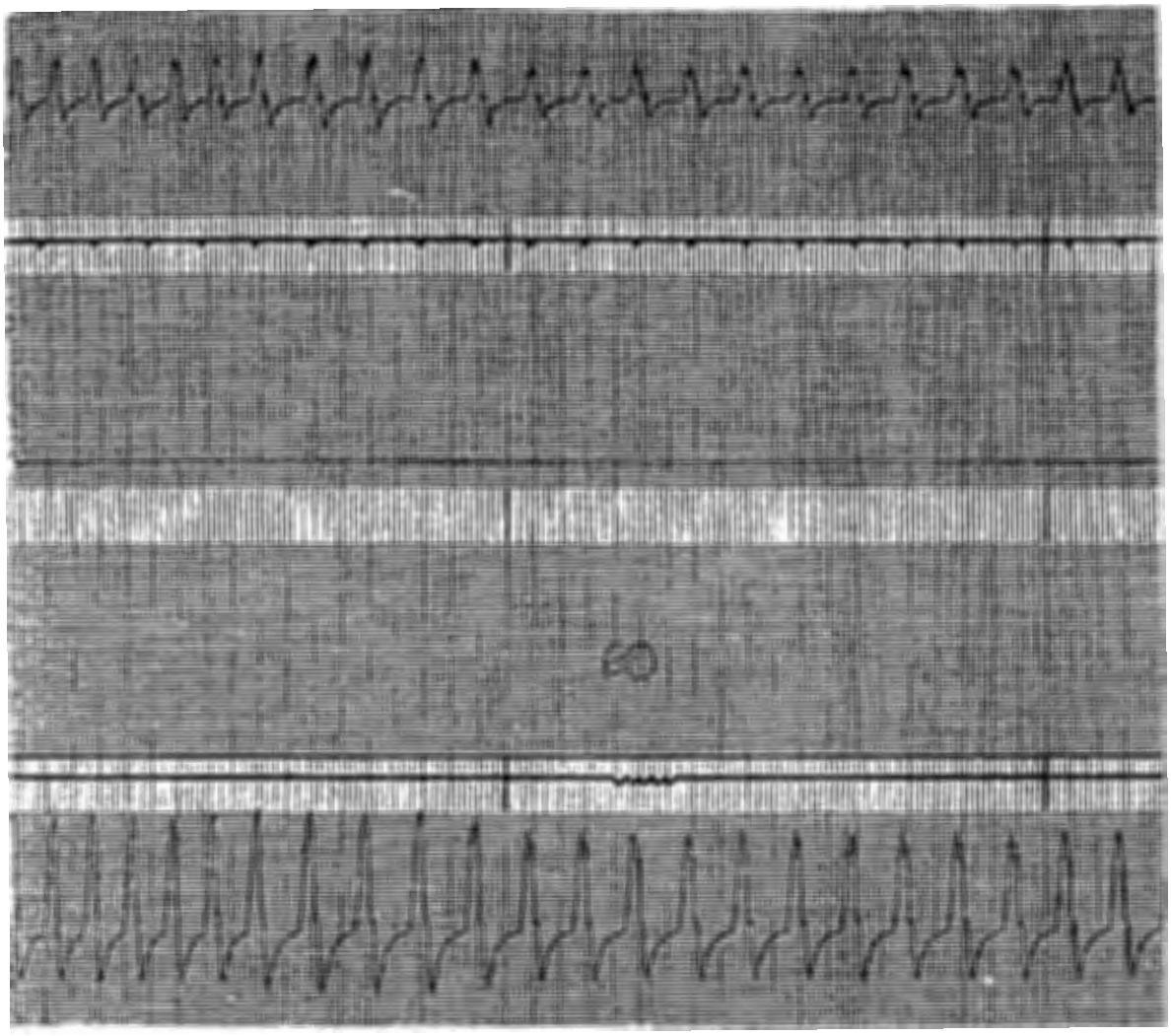

Figure H.3 The pressure (upper traces) and the flow (lower traces) taken for phase measurements (see Chapter 5). This graph represents 60 beats per minute.

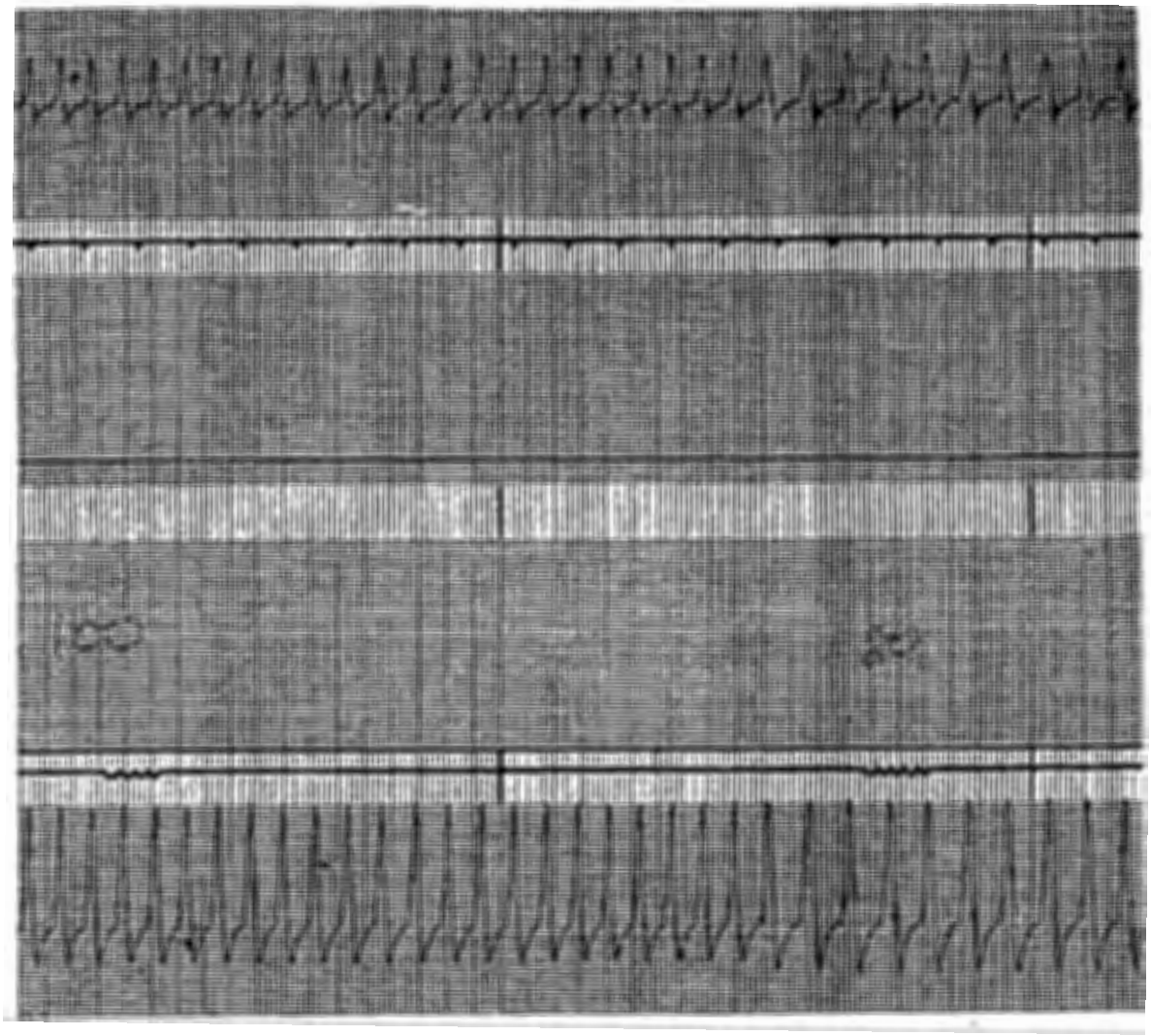

Figure H.4 The pressure (upper traces) and the flow (lower traces) taken for phase measurements (see Chapter 5). This graph represents 80 and 100 beats per minute.

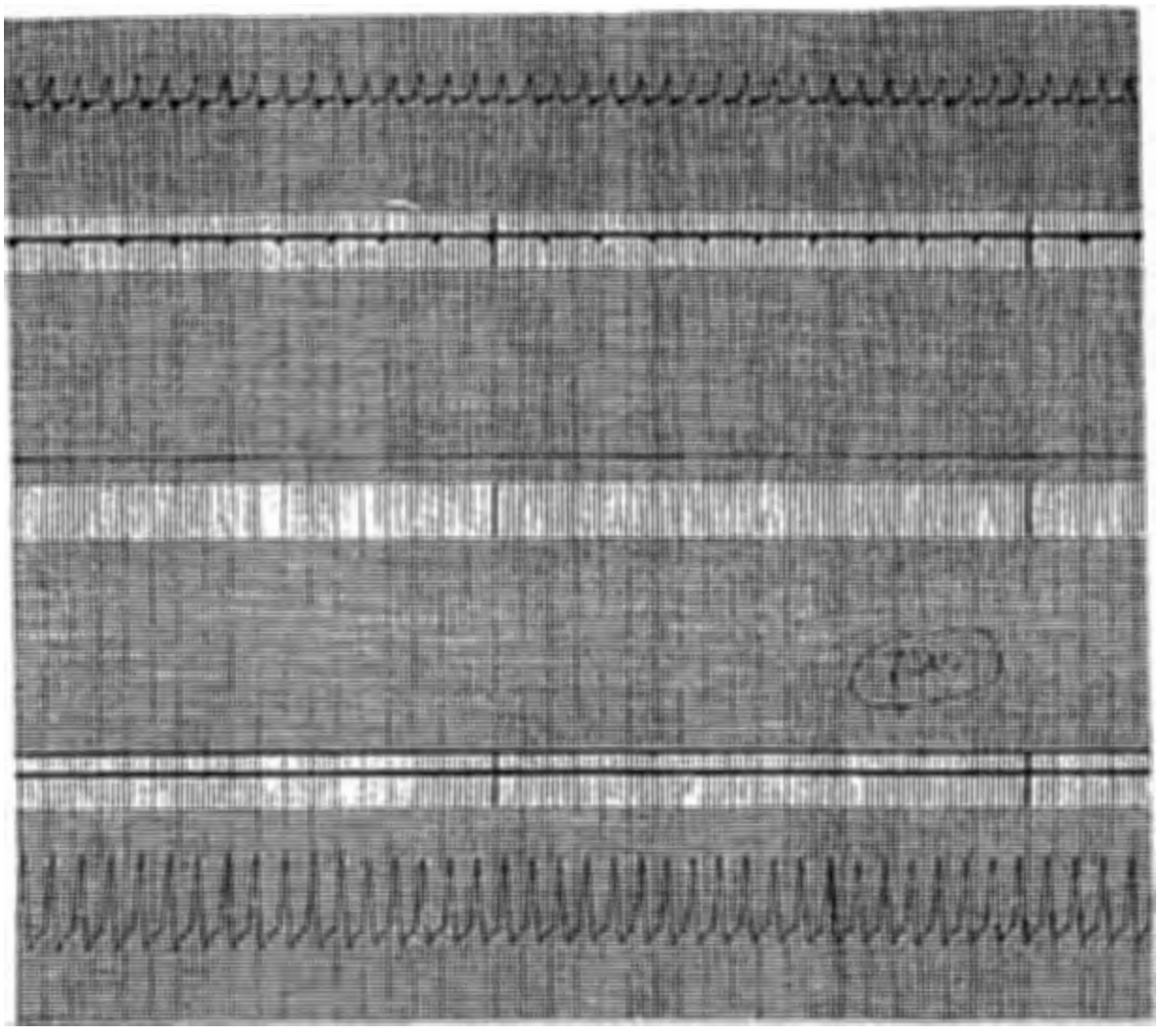

Figure H.5 The pressure (upper traces) and the flow (lower traces) taken for phase measurements (see Chapter 5). This graph represents 120 beats per minute.